

POLITECNICO DI TORINO

Master of Science course
in Mechanical Engineering

Master of Science thesis

Investigation about dimensional accuracy, shrinkage and distortion
in Selective Laser Sintering



Supervisor
Prof. Luca Iuliano
Co-supervisors
Prof. Flaviana Calignano
Prof. Paolo Minetola

Candidate
Catherine Martinez Freire

Academic year 2018/2019

Contents

Abstract.....	4
List of figures	5
List of tables	8
List of acronyms	9
Scope and Motivation.....	10
Introduction	11
Methodology.....	19
Results and Discussion.....	28
Conclusions	81
References	83

Abstract

Selective Laser Sintering is one of the many technologies that can be applied to produce a 3D model. This additive manufacturing process is not only used for rapid prototyping but as well for final goods, so the quality of the component is very important. The aim of this study is to analyze the dimensional tolerances of different prototypes printed using the selective laser sintering technology, employing a benchmark process, comparing the dimensions of the geometries as well as their measures, by means of the IT Grades and the ISO basic sizes.

Many geometries were studied: cylinders, cones, planes, tilted planes, angular planes, polygons, etc. in order to get for each of them, the best position, horizontally or vertically, and if it is better to be in the bottom, in the middle or in the top of the building volume of the Formiga Velocis P110.

Overall, horizontally printed samples show a better behavior for all vertical features, and vertically printed ones are better for horizontal geometries. The found differences in the same height of the building volume are due to a non-constant heat distribution, so the scale factor, actually, should not be constant neither. The non-homogeneous heat diffusion is then, a key factor to get better tolerances and less shrinkage.

List of figures

Figure 1. Schematic description of SLS	14
Figure 2. Description of the geometries present on the sample.....	20
Figure 3. Description of the geometries present on the sample.....	20
Figure 4. Description of the geometries present on the sample.....	21
Figure 5. Description of the geometries present on the sample.....	21
Figure 6. Formiga Velocis P110.....	23
Figure 7. Distribution of the samples inside the printer.	24
Figure 8. Divided distribution of the samples inside the printer.	24
Figure 9. Top view of the building volume with the samples inside.....	25
Figure 10. Bottom view of the building volume with the samples inside.....	25
Figure 11. Comparison between the 3 measurements of sample O1 in terms of IT grades and the ISO Basic sizes.	28
Figure 12. Comparison between the 3 measurements of sample O1 in terms of flatness, parallelism, perpendicularity and coaxiality versus its deviation without outliers.....	29
Figure 13. Comparison between the 3 measurements of sample O2 in terms of IT grades and the ISO Basic sizes.	30
Figure 14. Comparison between the 3 measurements of sample O2 in terms of flatness, parallelism, perpendicularity and coaxiality versus its deviation without outliers.....	31
Figure 15. Comparison between the 3 measurements of sample O3 in terms of IT grades and the ISO Basic sizes.	32
Figure 16. Comparison between the 3 measurements of sample O3 in terms of flatness, parallelism, perpendicularity and coaxiality versus its deviation without outliers.....	33
Figure 17. Comparison of sphericity of samples O1, O2 and O3, first measurement for both.	34
Figure 18. Comparison of cylindricity of samples O1, O2 and O3, first measurement for both.	35
Figure 19. Comparison of conicity of samples O1, O2 and O3, first measurement for both.	36
Figure 20. Average deviation of Convex (light blue) and Concave (dark blue) geometries for O1-1.	36
Figure 21. Average deviation of Convex (light blue) and Concave (dark blue) geometries for O2-2.	37
Figure 22. Average deviation of Convex (light blue) and Concave (dark blue) geometries for O3-2.	37
Figure 23. Convex (light blue) and Concave (dark blue) geometries for sample O1-1.	38
Figure 24. Convex (light blue) and Concave (dark blue) geometries for sample O2-1.	38
Figure 25. Convex (light blue) and Concave (dark blue) geometries for sample O3-1.	39
Figure 26. Comparison between the 3 measurements of sample V1 in terms of IT grades and the ISO Basic sizes.	40

Figure 27. Comparison between the 3 measurements of sample V1 in terms of flatness, parallelism, perpendicularity and coaxiality versus its deviation without outliers.....	41
Figure 28. Comparison between the 3 measurements of sample V2 in terms of IT grades and the ISO Basic sizes.	42
Figure 29. Comparison between the 3 measurements of sample V2 in terms of flatness, parallelism, perpendicularity and coaxiality versus its deviation without outliers.....	43
Figure 30. Comparison between the 3 measurements of sample V3 in terms of IT grades and the ISO Basic sizes.	44
Figure 31. Comparison between the 3 measurements of sample V3 in terms of flatness, parallelism, perpendicularity and coaxiality versus its deviation without outliers.....	45
Figure 32. Comparison between the 3 measurements of sample V4 in terms of IT grades and the ISO Basic sizes.	46
Figure 33. Comparison between the 3 measurements of sample V4 in terms of flatness, parallelism, perpendicularity and coaxiality versus its deviation without outliers.....	47
Figure 34. Comparison between the 3 measurements of sample V5 in terms of IT grades and the ISO Basic sizes.	48
Figure 35. Comparison between the 3 measurements of sample V5 in terms of flatness, parallelism, perpendicularity and coaxiality versus its deviation without outliers.....	49
Figure 36. Comparison between the 3 measurements of sample V6 in terms of IT grades and the ISO Basic sizes.	50
Figure 37. Comparison between the 3 measurements of sample V6 in terms of flatness, parallelism, perpendicularity and coaxiality versus its deviation without outliers.....	51
Figure 38. Comparison between the 3 measurements of sample V7 in terms of IT grades and the ISO Basic sizes.	52
Figure 39. Comparison between the 3 measurements of sample V7 in terms of flatness, parallelism, perpendicularity and coaxiality versus its deviation without outliers.....	53
Figure 40. Comparison of sphericity between samples V1, V3 and V5, first measurement for all three.....	54
Figure 41. Comparison of cylindricity between samples V1, V3 and V5, first measurement for all three.....	55
Figure 42. Comparison of conicity between samples V1, V3 and V5, first measurement for all three.	55
Figure 43. Convex (light blue) and Concave (dark blue) geometries for sample V1-1.	56
Figure 44. Convex (light blue) and Concave (dark blue) geometries for sample V3-1.	56
Figure 45. Convex (light blue) and Concave (dark blue) geometries for sample V5-1.	57
Figure 46. Average deviation of Convex (light blue) and Concave (dark blue) geometries for V1-1.	57
Figure 47. Average deviation of Convex (light blue) and Concave (dark blue) geometries for V3-1.	58
Figure 48. Average deviation of Convex (light blue) and Concave (dark blue) geometries for V5-1.	58
Figure 49. Comparison of sphericity between samples V4, V2 and V6.	59
Figure 50. Comparison of cylindricity between samples V4, V2 and V6.....	60

Figure 51. Comparison of conicity between samples V4, V2 and V6.	60
Figure 52. Co Convex (light blue) and Concave (dark blue) geometries for sample V4-1.	61
Figure 53. Average deviation of Convex (light blue) and Concave (dark blue) geometries for V4-1	61
Figure 54. Convex (light blue) and Concave (dark blue) geometries for sample V2-1.	62
Figure 55. Average deviation of Convex (light blue) and Concave (dark blue) geometries for V2-1	62
Figure 56. Convex (light blue) and Concave (dark blue) geometries for sample V6-3	63
Figure 57. Average deviation of Convex (light blue) and Concave (dark blue) geometries for V6-3	63
Figure 58. Comparison of sphericity between samples V1 and V7, first measurement for both.	64
Figure 59. Comparison of cylindricity between samples V1 and V7, first measurement for both.	65
Figure 60. Comparison of conicity between samples V1 and V7, first measurement for all three.	66
Figure 61. Convex (light blue) and Concave (dark blue) geometries for sample V7-1.	67
Figure 62. Average deviation of Convex (light blue) and Concave (dark blue) geometries for V7-1	67
Figure 63. Comparison of sphericity between samples O1 and V3, second and third measurement respectively.....	68
Figure 64. Comparison of cylindricity between samples O1 and V3, second and third measurement respectively.....	69
Figure 65. Comparison of conicity between samples O1 and V3, second and third measurement respectively.....	69
Figure 66. Convex (light blue) and Concave (dark blue) geometries for sample O1-2.	70
Figure 67. Convex (light blue) and Concave (dark blue) geometries for sample V3-3.	70
Figure 68. Average deviation of Convex (light blue) and Concave (dark blue) geometries for O1-2.	71
Figure 69. Average deviation of Convex (light blue) and Concave (dark blue) geometries for V3-3.	72
Figure 70. Sample V3.....	77
Figure 71. Sample V2.....	78
Figure 72. Sample V4.....	79
Figure 73. Sample V6.....	80

List of tables

Table 1. Comparison of different additive manufacturing technologies.....	12
Table 2. 3D Printer Machine description.....	22
Table 3. Ranges of ISO basic sizes and corresponding tolerance factor i	26
Table 4. Classification of IT grades according to ISO 286-1:1988.....	27
Table 5. Comparison of the characteristics of the spheres on V3-1 and on V5-1.....	73
Table 6. Comparison of the characteristics of the cylinders on V3-1 and on V5-1.....	74
Table 7. Comparison of the characteristics of the spheres on V4-1 and on V6-3.....	74
Table 8. Comparison of the characteristics of the cylinders on V4-1 and on V6-3.....	75
Table 9. Comparison of the characteristics of the spheres on V1-1 and on V2-1.....	76
Table 10. Comparison of the characteristics of the cylinders on V1-1 and on V2-1.....	76

List of acronyms

AM- Additive Manufacturing

RP- Rapid Prototyping

PBF- Powder Bed Fusion

EBM- Electron Beam Melting

SLM- Selective Laser Melting

SLS- Selective Laser Sintering

STL- Stereolithography

PA11- Polyamide 11

PA12- Polyamide 12

PEEK- Polyetheretherketone

PEBA- Polyether Block Amide

TPU- thermoplastic polyurethane

PA6- Polyamide 6

PCL- Polycaprolactone

CMM- Coordinate Measuring Machine

Scope and Motivation

The scope is to know the dimensional tolerances for this particular AM process, by means of a benchmarking analysis, obtaining the best positioning inside the printing chamber, and the inclination of the sample, depending on the tolerances that one wants to achieve and the geometry that prevails over the others in a particular component that will be produced with this technology. The dimensional accuracy has been defined using the ISO IT grades.

The great motivation of this thesis is the non-existence, until today, of studies that correlate position-heat-geometric factor for the SLS process.

Chapter 1

Introduction

1.1 Additive Manufacturing

Additive manufacturing allows the production of very versatile forms, adding material layer by layer. AM can also be explained as a process that creates 2D layers, and the sum of all of these layers create the final feature in 3D.

Conventional processes are not as good as this technology under many points of view, for example with AM one can perform rapid prototyping or create cooling channels, with no ends, that can be very difficult to achieve or even impossible to build, by machining. The materials implemented the most for 3D printing are by far polymers, because they have mechanical properties that make them great for this procedure, as low melting point and high viscosity. [1]

Additive manufacturing is used in many areas of production, so there are many production techniques that can broadly be divided in seven major ones, depending on how the layer is being produced: photopolymerization, extrusion, sheet lamination, beam deposition, direct write and printing, powder bed binder jet printing, and powder bed fusion. [2]

The applications can vary from the aerospace field to the medical one, since the advantages that this kind of technology shows, can help in many ways, from the versatility in shapes, to the diversity in materials, to create the desired piece.

1.2 Comparison of different additive manufacturing technologies

To determine the best technology to be applied on a case study, is necessary to compare the characteristics of each of them, considering which material suits best the application, and the advantages and disadvantages that will be present during the production as observed in Table 1.

Technology	Processes	Materials	Advantages	Disadvantages	Applications
Binder jetting	<ul style="list-style-type: none"> —Ink-jetting —S-Print —M-Print —3D Printing [3] 	<ul style="list-style-type: none"> —Metals: Stainless steel —Polymers: ABS, PA, PC —Ceramics: Glass [4] 	<ul style="list-style-type: none"> —Range of different colours —Many materials —Is a faster process with respect to the others —The two material method allows for a large number of different binder-powder combinations and various mechanical properties [4] 	<ul style="list-style-type: none"> —Needs a binder material so it's not good for structural parts —Additional time due to finishing operations [4] 	<ul style="list-style-type: none"> 3D print figurines and topographical maps, thanks to the low cost [5]
Directed energy deposition	<ul style="list-style-type: none"> —Directed light fabrication —Electron beam direct manufacturing —Direct metal deposition —Direct laser deposition —Laser engineered net shaping [6] 	<ul style="list-style-type: none"> —Metals, in the form of either powder or a wire. —Also polymers and ceramics [7] 	<ul style="list-style-type: none"> —Grain structure can be controlled, getting high quality —Great speed [8] 	<ul style="list-style-type: none"> —Finishing or post processing may be needed —Limited material use —Fusion process does not have a mainstream positioning [8] 	<ul style="list-style-type: none"> The main used is in industrial remanufacturing and repairing, for example restoring the configuration of some turbine blades or propellers, also suitable for repairing and remanufacturing automotive and aerospace components [9]
Material extrusion	<ul style="list-style-type: none"> —Fused deposition modeling —Fused filament fabrication —3D bioprinting 	<ul style="list-style-type: none"> —Polymers: ABS, Nylon, PC, PC, AB —Paste-like materials such as ceramics, concrete and chocolate [10] 	<ul style="list-style-type: none"> —A lot of materials to choose from —Easily understandable printing technique —Low costs —Comparable faster print time for small and thin parts —No supervision required —Small equipment [11] 	<ul style="list-style-type: none"> —Visible layer lines —The extrusion head must continue moving, or else material bumps up —Supports may be required —Poor part strength along Z-axis (perpendicular to build platform) —Finer resolution and wider area increases print time —Toxic and susceptible to warping [11] 	<ul style="list-style-type: none"> —Plastic prototypes —Also produce functional prototypes from engineering materials [12]
Material jetting	<ul style="list-style-type: none"> —Inkjet printing —Thermojet —Polyject 	<ul style="list-style-type: none"> —Photopolymer —Wax [3] 	<ul style="list-style-type: none"> —Smooth parts with surfaces comparable to injection molding —Very high dimensional accuracy. —Homogeneous mechanical and thermal properties. —"The multi-material capabilities of MJ enables the creation of accurate visual and haptic prototypes" [13] 	<ul style="list-style-type: none"> —Poor mechanical properties (low elongation at break). —The materials used are photosensitive and their mechanical properties degrade over time. —High cost [13] 	<ul style="list-style-type: none"> —Non-functional prototypes —Prototypes used for visual and form/fit testing. —Casting patterns in the medical, dental and jewellery industry [14]
Powder bed fusion	<ul style="list-style-type: none"> —Selective laser sintering —Selective laser melting —Electron beam melting 	<ul style="list-style-type: none"> —Metal —Polymer —Ceramic [3] 	<ul style="list-style-type: none"> —No support structures are required for SLS (EBM might need them and SLM needs them) —Superior mechanical properties [15] 	<ul style="list-style-type: none"> —Expensive —Few compatible materials —Rough or grainy surface [15] 	<ul style="list-style-type: none"> —Biomedical field —Electronics —Aerospace —Lightweight structures
Sheet lamination	<ul style="list-style-type: none"> —Laminated object manufacturing —Ultrasonic additive manufacturing 	<ul style="list-style-type: none"> —Hybrids —Metallic —Ceramics [3] 	<ul style="list-style-type: none"> —Speed, low cost, ease of material handling —The strength and integrity of models is reliant on the adhesive used. —Cutting can be very fast due to the cutting route only being that of the shape outline, not the entire cross sectional area [16] 	<ul style="list-style-type: none"> —Finishes can vary depending on paper or plastic material but may require post processing to achieve desired effect —Limited materials [16] 	<ul style="list-style-type: none"> —Paper manufacturing —Foundry industries —Electronics —Smart structures [15]
Vat photopolymerization	<ul style="list-style-type: none"> —Stereolithography —Digital light processing —Two-photon polymerization 	<ul style="list-style-type: none"> —Photopolymer —Ceramic [3] 	<ul style="list-style-type: none"> —High resolution to build time ratio —Good durability [15] 	<ul style="list-style-type: none"> —Relatively expensive due to requirement for vat change —Need of support material —Cannot create parts with enclosed volumes due to liquid environment 	<ul style="list-style-type: none"> —Medical modeling —All types of prototyping, as well as mass production. —Parts with fine details and a smooth surface finish, like jewelry, investment casting or dental applications [17]

Table 1. Comparison of different additive manufacturing technologies.

1.3 Powder Bed Fusion

Powder Bed Fusion (PBF), is mainly used for printing parts with complex geometries. The process is simple, a heat source (laser or electron beam) melts and fuses the powder to build one layer and then it does it again for another layer of powder, building in this way, the part. [18]

The Powder Bed Fusion process includes the following commonly used printing techniques: Electron beam melting (EBM), Selective laser melting (SLM) and Selective laser sintering (SLS).

For SLS and for SLM a laser beam scans the specific positions of the powder bed and fuses the powder attaching it to the solid material, by either complete melting (SLM) or partial melting (SLS). The powder bed goes down by the amount defined as the layer thickness and then a new layer of powder is dropped and levelled after laser radiation in one layer is completed. The process will be repeated until the component is fully built. [19]

For Electron Beam Melting (EBM), the heat source is a high-power electron beam, that's why this technology can only use conductive metals as materials. EBM process typically has lower resolutions and higher surface roughness in comparison with SLM. [3]

1.4 Selective Laser Sintering

Generally, the SLS process can be seen as in Figure 1. To be straight forward, the powder rests in a bed, which has down to it, an elevator that lifts the correct amount of powder, above the build plate, then the recoater (which is mostly a roller) is in charge of spreading the thin layer all over it. [20]

On top of the build surface, the powder can also be supplied there, using a hopper. Commonly, the layer of powder doesn't go beyond the 100 μm but neither less than 10 μm .

After this happens, a focused laser passes by the correct zones, sintering or melting the desired parts, across all the surface.

For a deeper explanation of the process is important to highlight that a focused laser beam is the one in charge to consolidate the powder in selected areas. The sintering of the powder happens thanks to a raise in temperature, above a certain softening temperature.

Also, many types of lasers such as the CO₂ laser, lamp or diode pumped Nd:YAG laser are used. For plastic parts that are wanted for rapid manufacturing a disk or fiber laser have been used.

Galvano mirror is used for scanning, following the CAD model of the component. The SLS machine preheats the powder present in the bed, below its melting point, to assist the laser to raise the temperature of the specific regions to the melting point. Then a roller will drop a layer of fresh powder, which will be sintered to the accordingly STL file. The build platform will get down before applying a new layer of powder over the build area. To get the completed part, the process will repeat as many times as layers will be present. [21]

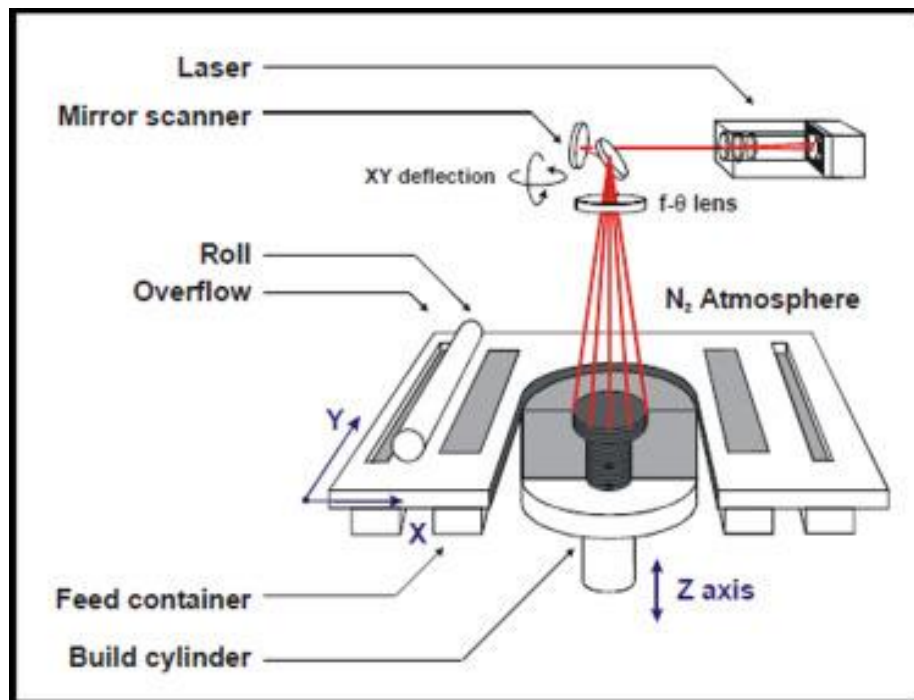


Figure 1. Schematic description of SLS

1.5. Materials in SLS

This technique employs a huge amount of different kind of materials, and the last studies show that any material can be put together with another material, with low melting point, that will act as glue.

Some materials make SLS superior to other techniques, like wax, ceramics, metal-polymer powders, nylon/glass composite, polymers, nylon, cermet, and carbonate. [22]

Polymers used in SLS

There are not so many polymers that can be used in SLS. The most used one is PA12. PA 2200, the one actually used for the development of these thesis, is the PA12- based commercialized polymer characterized by higher crystallinity and melting point which is considered biocompatible and to have a stable processing along with repeatable properties of manufactured parts. Another one that is used in SLS is PA11.

All the other materials are some rare ones, for example PEEK, PEBA and TPU and another polyamide like PA 6. [22]

PEBA is implemented when needing impact protection or grips in the medical field. PEEK is great when needing to put an implant without resorbable capacity. PCL is in the other hand, bioresorbable, so it is used for bone repairing or even cartilage. [23]

1.6 Applications of SLS

At the beginning SLS was a technology used only for RP, but now also final products are being produced, with great quality as well. Nowadays SLS materials can handle direct functional applications, even when specific requirements must be met, like chemical resistance, high temperatures, wear and abrasion, flexibility, thin walls, internal/external surface pressures.

Rapid Manufacturing:

-Aerospace and military hardware.

-Unmanned air systems hardware plus underground and normal vehicle hardware.

-Medical (huge development).

Rapid Prototypes:

-Functional proof of concept prototypes.

-Design evaluation models (form, fit & function).

-Product performance & testing.

-Engineering design verification.

-Wind-tunnel test models.

Tooling and Patterns:

-Tooling and manufacturing estimating visual aid.

-Investment casting patterns.

-Jigs and Fixtures. [24]

SLS applications in Biomedical Engineering

This technology got a great growth in the last 20 years, with applications in surgical planning, surgical guides in orthopedics and dental reconstructions, manufacturing of skeletal prostheses and tissue engineering. [25]

For surgical planning, the model is 3D printed, allowing a nice simulation, because some human organs are very difficult to reproduce with other technologies, so the surgeon gets to be in touch with a very similar prototype, before any real intervention takes place. These models can be done super specific, following the real anatomic shape of one patient, as well as having the mechanical properties of the real tissue. The RP models are very well suited for use in the diagnosis and the precise preoperative planning of skeleton modifying interventions. Also, for customized implants it is used SLS.

1.7 Accuracy and tolerances in SLS

When trying to measure a nominal geometry, there are many factors involved in the final shape of the product, so the deviation can be caused by many things.

For this reason, on the product blueprint engineers indicate the admissible tolerance interval for critical dimensions. But additive manufacturing is a non-common manufacturing process in which only one machine is needed in order to create thousands of shapes and products.

Thanks to its capacity to get a very good finish (by building very fine layers one over the other), there is no need to improve the final product with polishing operations, the superficial roughness can stay as produced by the SLS machine. [26]

1.8 Scale factor

SLS prototypes should have high accuracy in order to satisfy functional requirements. Shrinkage is one of the major factors which influence the accuracy of the SLS parts. To compensate for shrinkage, the material scale factor is to be calculated in each direction and is to be applied to the STL file. The amount of shrinkage encountered is found to be governed by the process parameters during processing and cannot be kept constant. [27]

1.9 Benchmarking process

“Application of benchmarking focuses on the understanding in details your own processes, and then compare your own performance with that of others analyzed”. [28]

When doing the comparison, it’s important to realize which feature is the one fulfilling the specifications from already studied and carried experiments, the one that respects the admitted tolerances.

The main idea is to comprehend the limitations of the process, without forgetting to optimize each process in an iteratively way. A good way to choose the optimal parameters, is doing a loop of benchmark tests. The benchmark procedure needs the variables to be constant, so that the machine, the powder and the process parameters can’t change, allowing one to

analyze the mechanical properties and accuracy of the sample. When speaking about offset and scaling values for example, that in general are used to compensate the distortions due to heat and the changes in dimensions because of the laser beam spot size, can be perk up using an in iterative process based on the analyses of the dimension of the printed benchmark parts.
[29]

Chapter 2

Methodology

2.1 Description of the sample

The part analyzed in this thesis, seen on Figure 2, is designed in order to be printed 10 times into the building volume, of the printer Formiga Velocis P110 (Figure 6), the designed dimensions of the sample are 110 x 110 x 33 mm. It's important to highlight that the part does not require support structures for its production. For the dimensional inspection, the presence of simple classic geometries allows for the analyses of form errors and geometrical tolerances. The description of these shapes are as follows:

- A set of seven rectangular blocks from PL1 to PL7.
- A set of seven rectangular slots from SLOT1 to SLOT7.
- A set of seven steps from PR1 to PR7.
- Two couples of coaxial truncated cones (CON1, CON2 and CON3, CON4).
- Two sets of coaxial cylinders (CIL13 to CIL16 and CIL9 to CIL12).
- Two sets of hemicylinders (CIL1 to CIL4 and CIL5 to CIL8).
- Four sets of quarters of spheres (SFERA1, SFERA2; SFERA3, SFERA4; SFERA5, SFERA6 and SFERA7, SFERA8).
- Three sets of tilted planes (from PL_ANG1 to PL_ANG10, from PL_ANG18 to PL_ANG21 and from PL_ANG22 to PL_ANG26).
- Several other vertical or horizontal planes, that are parallel or orthogonal to the square base of the reference part (for example PIANO8).

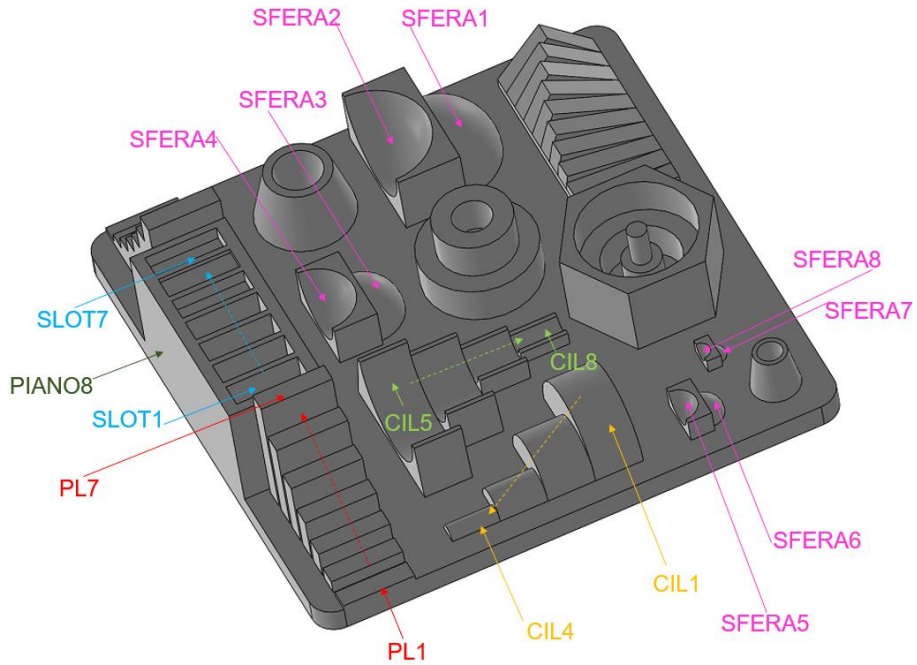


Figure 2. Description of the geometries present on the sample

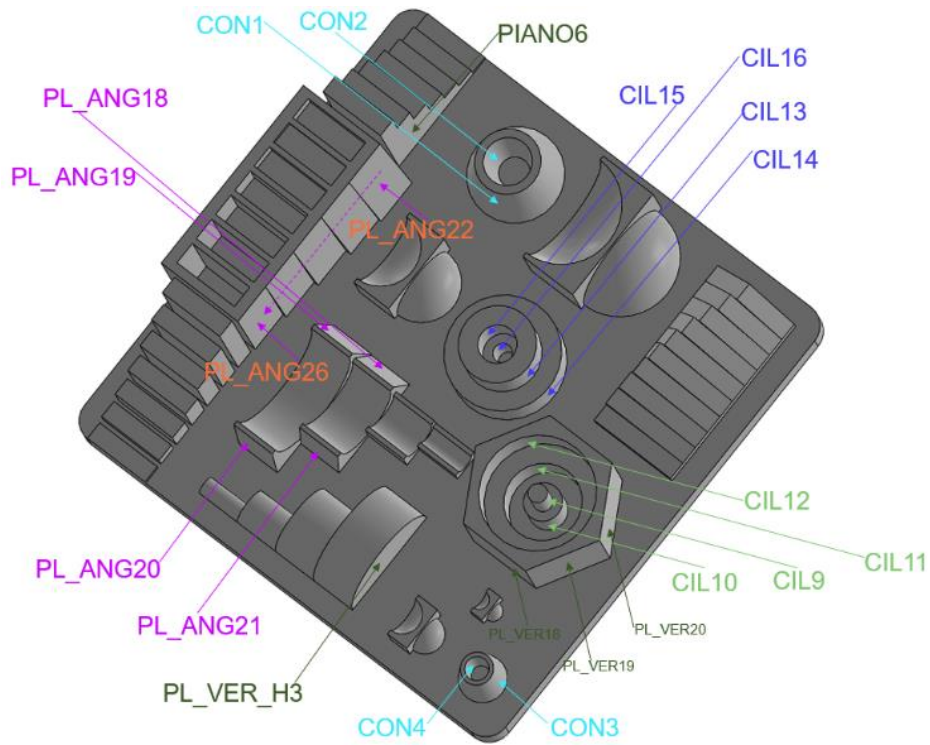


Figure 3. Description of the geometries present on the sample

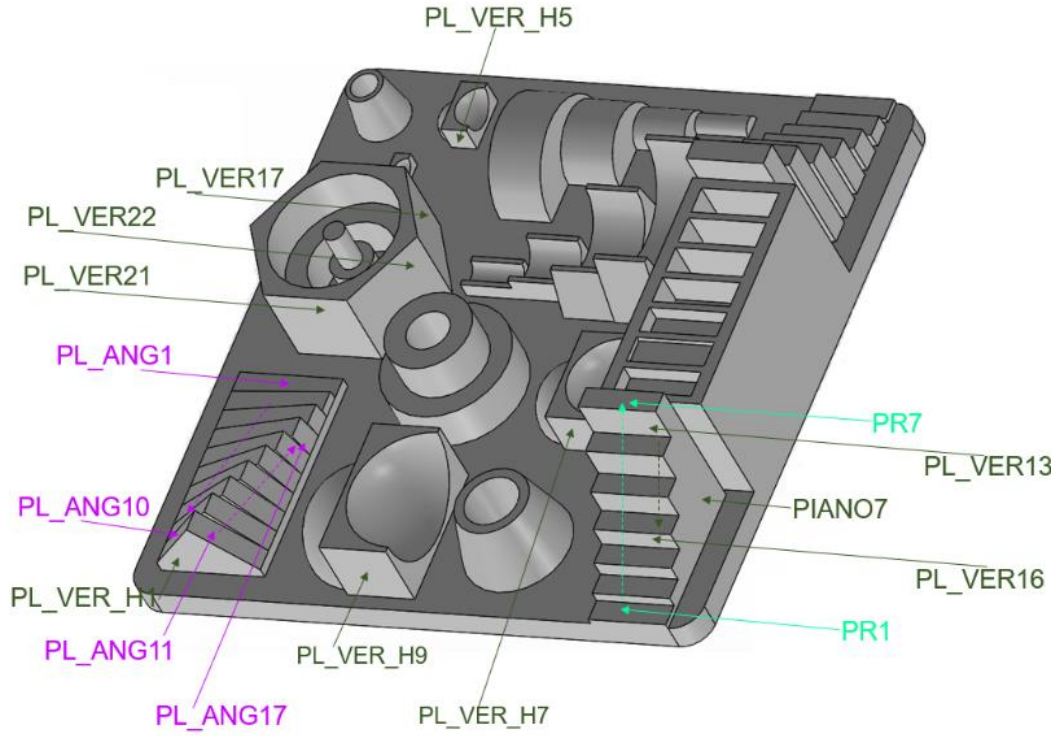


Figure 4. Description of the geometries present on the sample

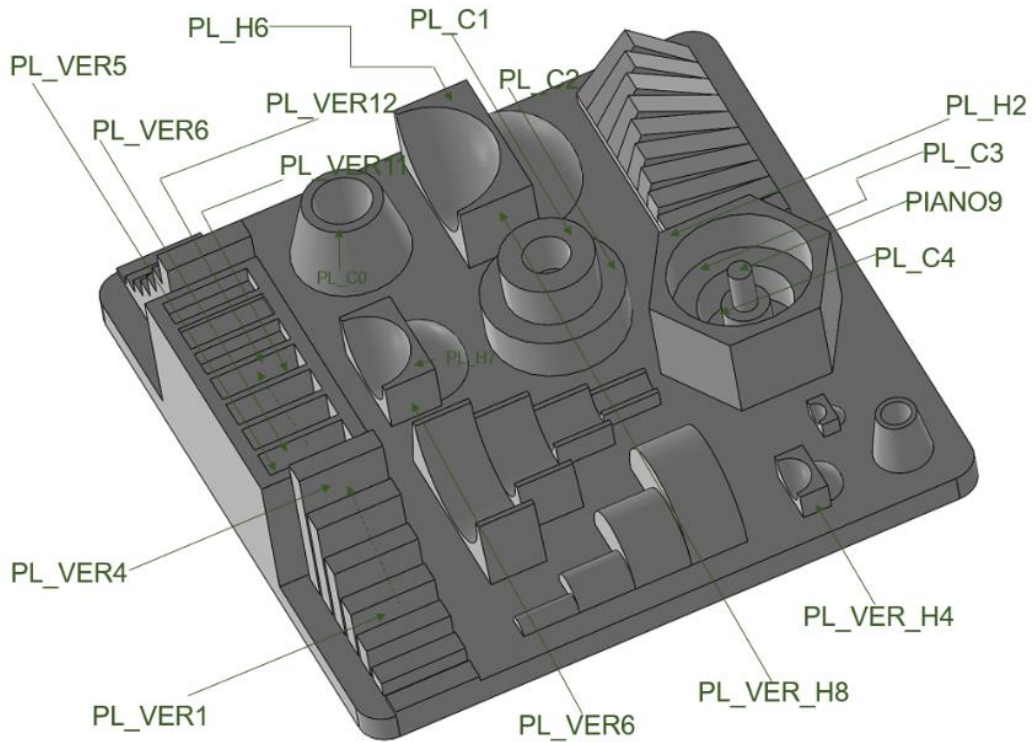


Figure 5. Description of the geometries present on the sample

2.2 Description of the printer

The printer, a Formiga P 110 Velocis of Figure 6, is described on Table 1.

FORMIGA P 110 Velocis	
Building volume	250 x 250 x 330 (7.9 x 9.8 x 13 in)
Laser type	CO ₂ , 30 W
Building rate	up to 1,2 l/h
Layer thickness (depending in material)	0,06 mm - 0,10 mm - 0,12 mm (0.0024 in - 0.0039 in - 0.0047 in)
Precision optics	F-theta lens; high-speed-scanner
Scan speed during building process	up to 5 m/s (16.4 ft/s)
Power supply	16 A
Power consumption	Typical 3 kW; maximum 5 kW
Dimensions (W x D x H) System	1,320 x 1,067 x 2,204 mm (51.97 x 42.01 x 86.77 in)
Recommended installation space	min. 3.2 x 3.5 m x 3.0 m (126 x 138 x 118 in)
Weight	Approximately 600 kg (1.323 lb)
Software	EOS ParameterEditor, EOS RP Tools, PSW 3.6
Material	PA 2200
Optional accessories	Mixing station, unpacking and sieving station, blasting cabinet

Table 2. 3D Printer machine description.

The building platform is heated at 156 °C, while the building chamber has a working temperature of about 170 °C. The hot build volume helps to retain the volumetric shrinkage of the material during the SLS process. However, the upper part of the volume is hotter because of the thermal gradient induced by the colder build platform. [26]

The slicing software EOS PSW 3.6.91 takes in account the thermal gradient by applying a different scaling factor for shrinkage compensation that ranges from 2.6% at the bottom of the build volume to 2.0% at the top in the build direction (Z-axis). [26]



Figure 6. Formiga Velocis P110

2.3 Distribution inside the 3D printer

Ten of these samples were 3D SLS printed and knowing that heat plays a huge role, a benchmarking process is going to be made in order to select the best position for every single geometry, varying only that, because the material, the parameters and the printer will be the same for all of the samples.

All “V” samples were printed vertically and all “O” samples horizontally, as shown on Figure 7 and Figure 8. A view from the top of the printer, in order to later account for changes in tolerances due to different heat gradients, are available on Figure 9 and a view from the bottom can be seen on Figure 10.

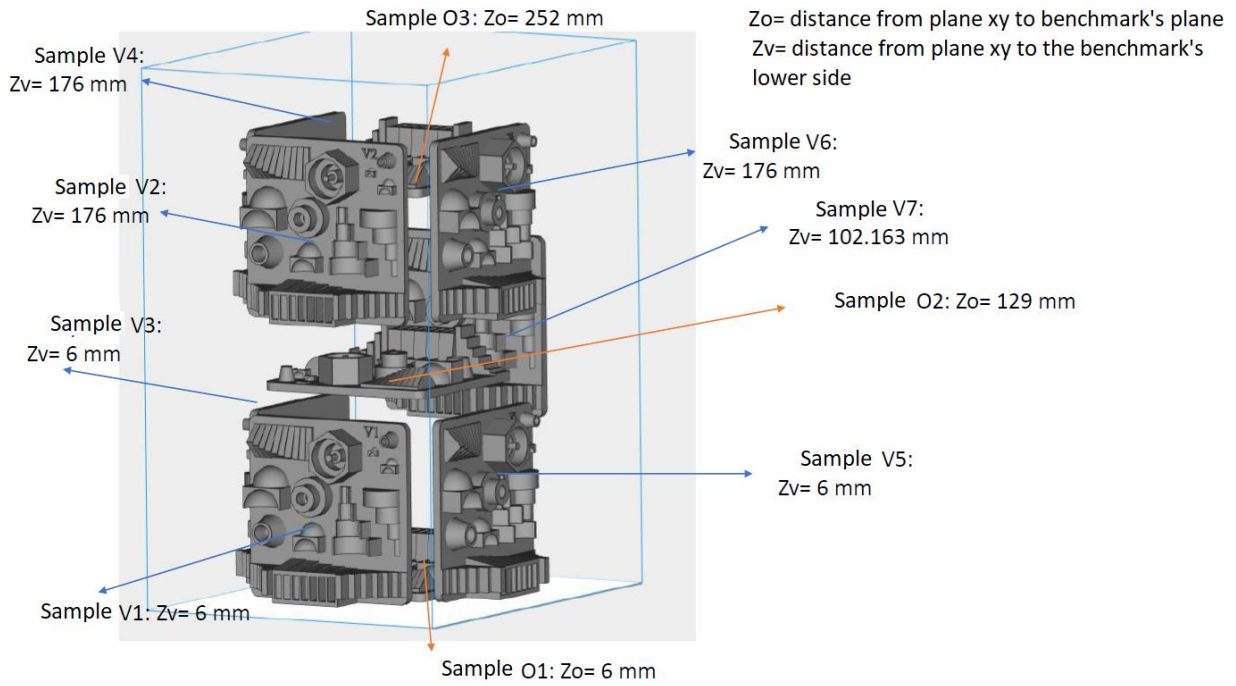


Figure 7. Distribution of the samples inside the printer.

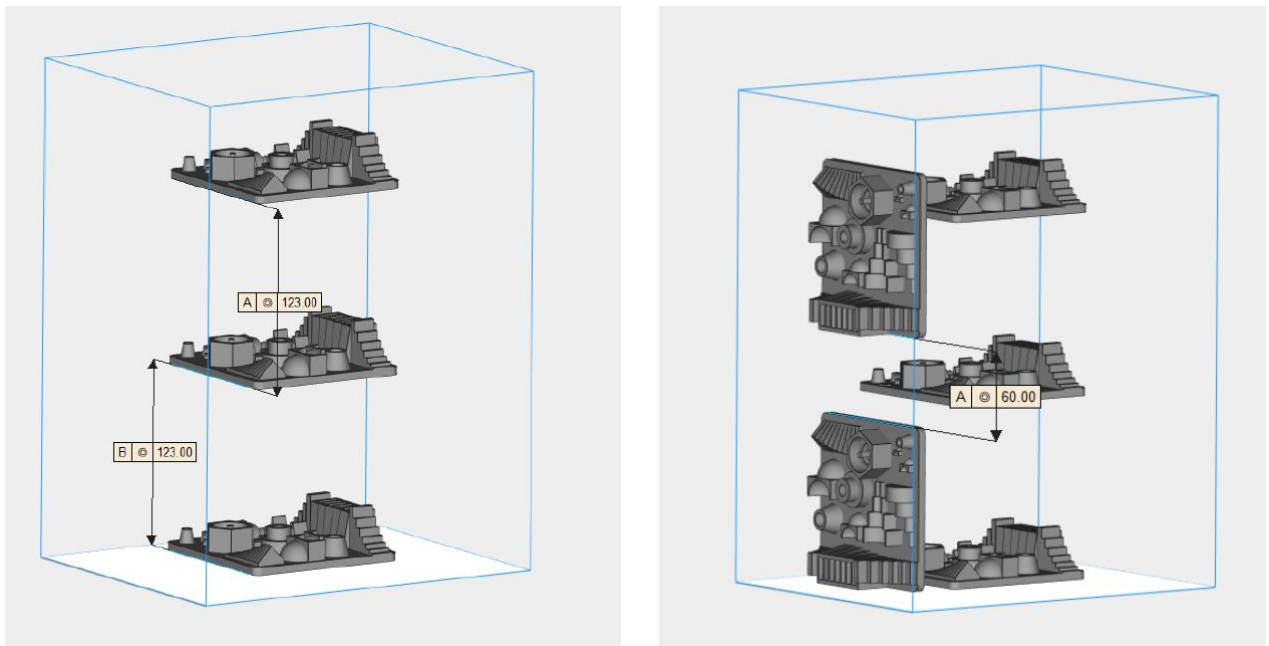


Figure 8. Divided distribution of the samples inside the printer.

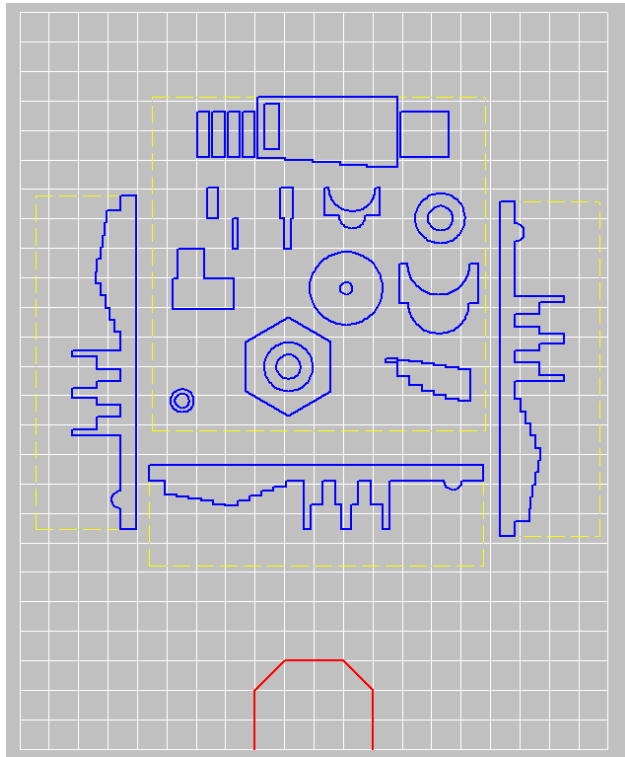


Figure 9. Top view of the building volume with the samples inside.

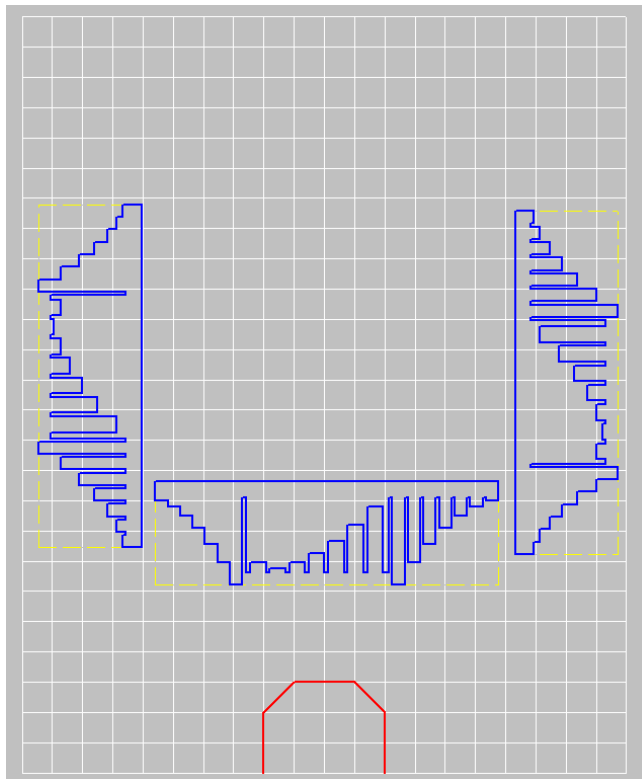


Figure 10. Bottom view of the building volume with the samples inside.

After printing, the samples were cleaned up with compressed air, no polishing or finishing process were applied, to actually evaluate the real tolerances during the measuring process.

Every sample was inspected by means of a CMM machine by DEA model IOTA. The measurements were replicated three times.

All the data obtained from the CMM was used to compare the results of the three replications for each sample, in terms of the ISO IT grades.

2.4 Description of the approach used to classify each measure into an IT grade

The measurements made by the CMM machine were used, to compare the dimensional accuracy of each sample by means of the ISO IT grades. [30]

The values of standard tolerances corresponding to IT5 – IT18 grades for nominal sizes up to 500 mm are evaluated through the standard tolerance factor i [μm] by the following formula:

$$i = 0.45\sqrt[3]{D} + 0.001 \cdot D$$

D is the geometric mean of the range of nominal sizes [mm]

$$D = \sqrt{D_1 \cdot D_2}$$

Range	Basic sizes								
Above	D_1 [mm]	1	3	6	10	18	30	50	80
Up to and including	D_2 [mm]	3	6	10	18	30	50	80	120
Standard tolerance factor	i [μm]	0.542	0.733	0.898	1.083	1.307	1.561	1.856	2.173

Table 3. Ranges of ISO basic sizes and corresponding tolerance factor i .

The IT grades are classified according to the number n of times that the tolerance factor i fits into the dimensional deviation. For example, the grade IT13 corresponds to a minimum of $250i$ with $n = 250$, as seen in Table 4.

Range		IT9	IT10	IT11	IT12	IT13	IT14	IT15	IT16	IT17
Above 1 mm	Up to 500 mm	$40i$	$64i$	$100i$	$160i$	$250i$	$400i$	$640i$	$1000i$	$1600i$

Table 4. Classification of IT grades according to ISO 286-1:1988

“ISO IT grades are used to summarize the machine accuracy and refers to the International Tolerance Grade of an industrial process defined in ISO 286. This grade identifies what tolerances a given process can produce for a given dimension”. [31]

D is the key dimension in the part and a required tolerance in that key dimension will be in relation with the IT grade assigned to it. The larger the IT value, the looser the tolerance.

The number n_j of tolerance units will be computed for every key measure in its respective range of ISO sizes using this formula:

$$n_j = \frac{1000 |D_{jn} - D_{jm}|}{i}$$

D_{jn} generic nominal dimension

D_{jm} the corresponding measured dimension

A certain distribution of numbers of units is so obtained for each ISO range for every replica. Within each range the n value corresponding to the 95th percentile of the distribution is assumed as the maximum dimensional error.

Chapter 3

Results and Discussion

3.1 Horizontal samples

3.1.1 Horizontal bottom sample O1

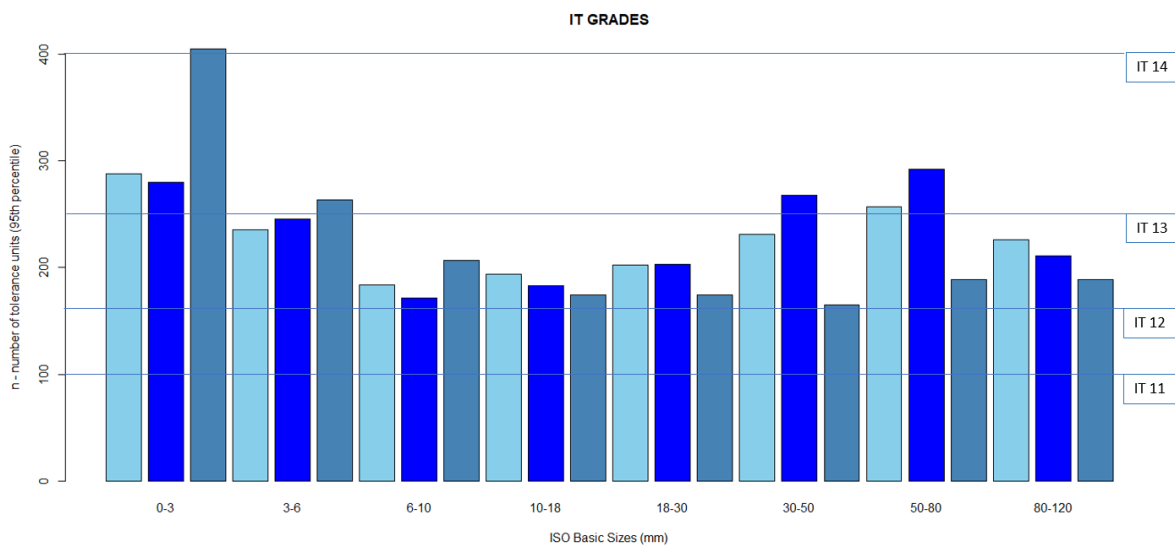


Figure 11. Comparison between the 3 measurements of sample O1 in terms of IT grades and the ISO Basic sizes.

Remembering that these are all measures of the same O1 sample, Figure 11 should look like an almost constant graph for every basic size. At least it can be seen that many ranges of sizes are below the IT13; the smallest one, (from 0 to 3 mm as key dimension) has its third measurement with a lower tolerance, being IT14. This is because of the geometry called CIL16 with a diameter of 4 mm, which had some powder attached to its borders, lowering the quality of the tolerance. Being so small and surrounded by such a great amount of material because of the greater cylinders around, makes it very hard for the heat to leave the region, so the powder gets stuck in the middle.

The box plots representing the levels of flatness, parallelism, perpendicularity and coaxiality of coaxial features can be observed in Figure 12, are all within the normal ranges of deviation, being the flatness of the tangential and horizontal planes the better ones with around 0.07 and 0.06 mm of maximum deviation each. For perpendicularity the maximum error is 0.14 mm and 0.4 mm for coaxiality, the first one on the second measure and the other on the third measure.

Thus, the third measurement of the O1 sample is the one with the greatest irregularities, the first and the second one, are more alike, so they should be considered more accurate, with results closer to the real measured obtained at the end of the process.

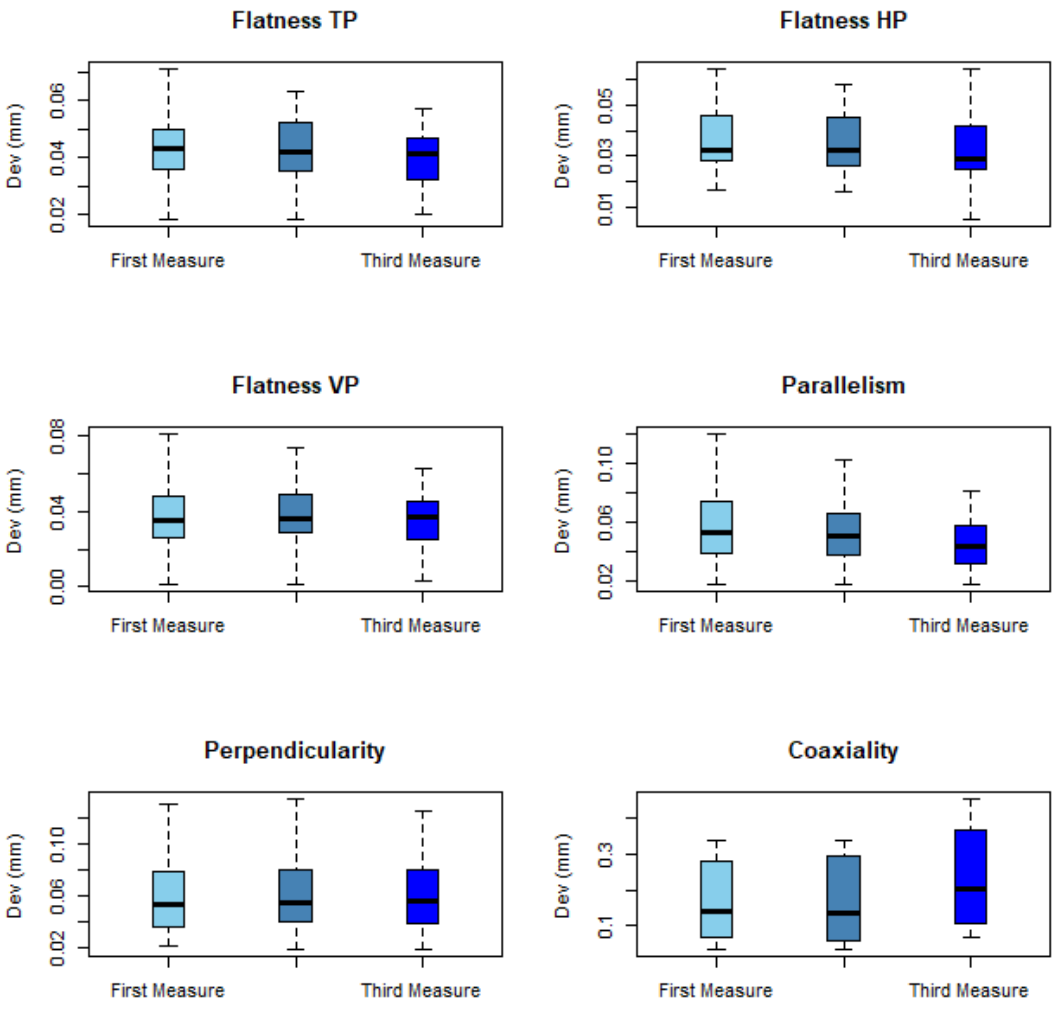


Figure 12. Comparison between the 3 measurements of sample O1 in terms of flatness, parallelism, perpendicularity and coaxiality versus its deviation without outliers.

3.1.2 Horizontal middle sample O2

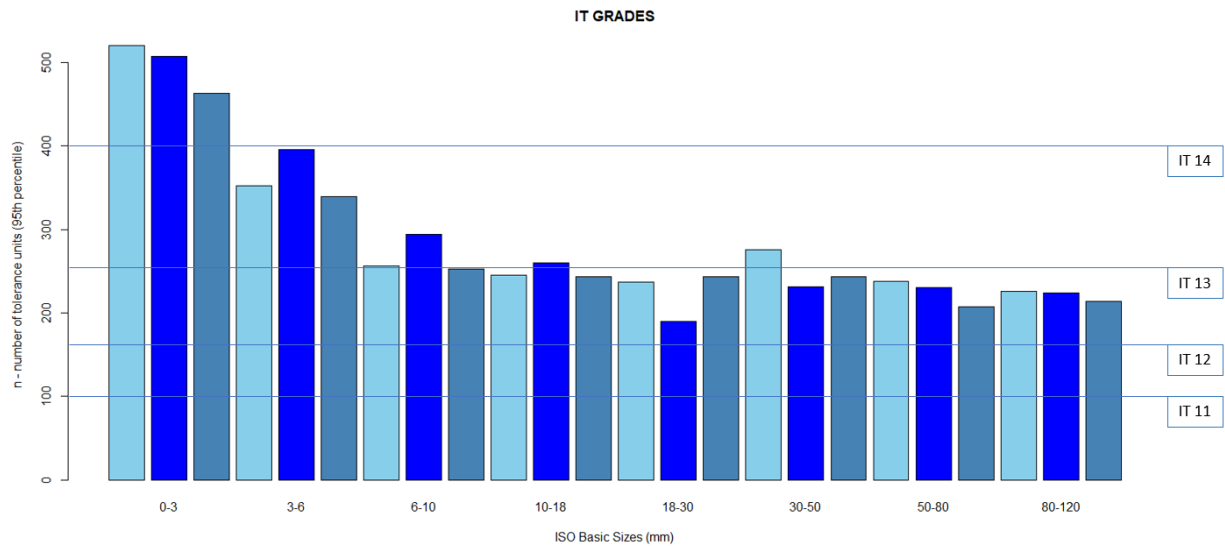


Figure 13. Comparison between the 3 measurements of sample O2 in terms of IT grades and the ISO Basic sizes.

All of the measures of Figure 13, for O2 sample are similar within every basic size. Most of the ranges have a quality below IT13, but the one from 0 to 3 mm as key dimension, belongs totally to a grade IT14. This is again because of the geometry called CIL16, as well as the other small geometries in which the heat transfer was stopped by the presence of more material around it.

In Figure 14, the box plots representing the levels of flatness, parallelism, perpendicularity and coaxiality of coaxial features, show that the second replication has worse accuracy in the flatness of tilted planes, with 0.25 mm of maximum deviation, but the best one for flatness in the horizontal planes with 0.06 mm.

The other two measures are very similar, so they seem to be more reliable than the second one for the flatness of tilted planes.

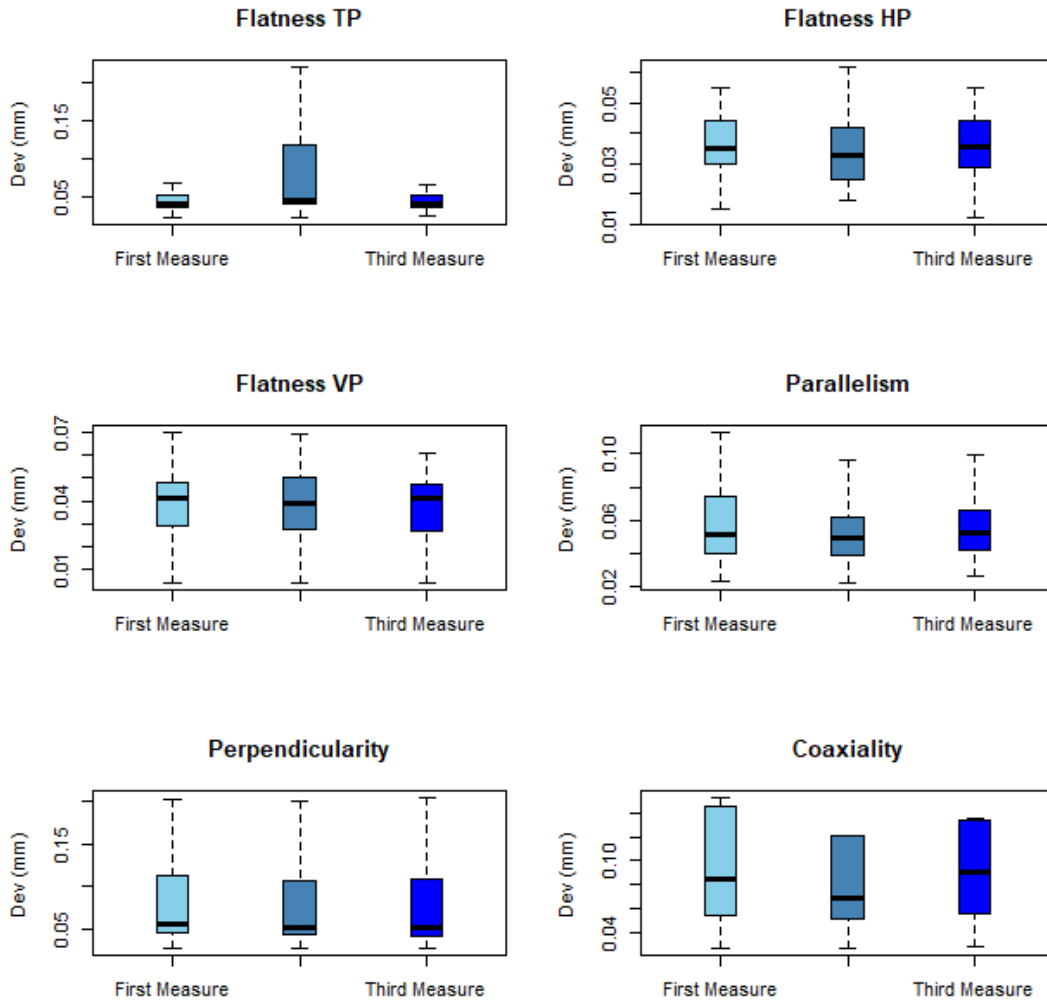


Figure 14. Comparison between the 3 measurements of sample O2 in terms of flatness, parallelism, perpendicularity and coaxiality versus its deviation without outliers.

3.1.3 Horizontal Top sample O3

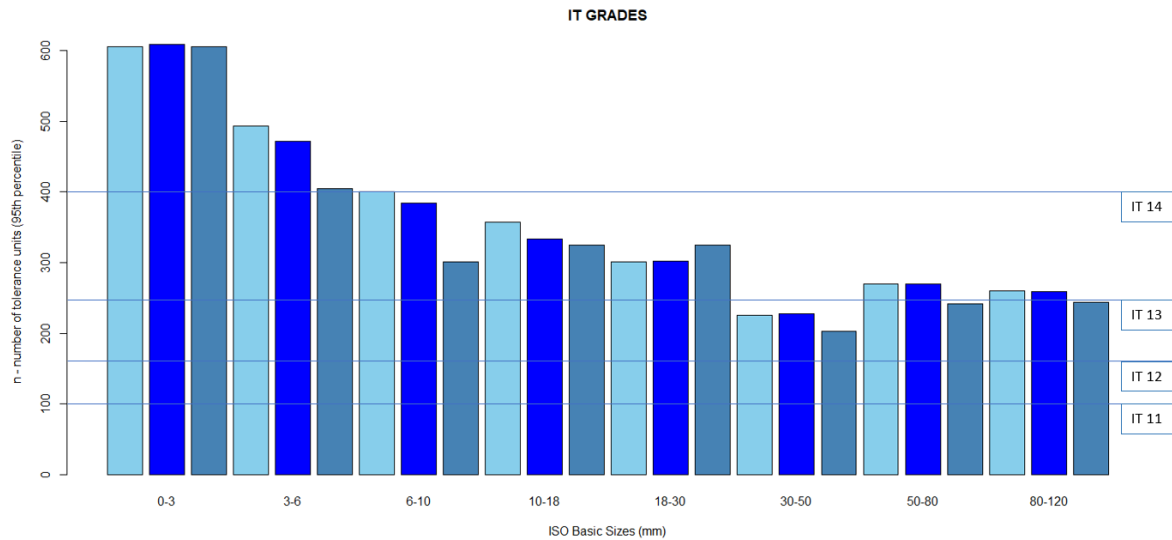


Figure 15. Comparison between the 3 measurements of sample O3 in terms of IT grades and the ISO Basic sizes.

When looking at the number of tolerance units (95th percentile), for the smallest ISO basic size range (0-3 mm), it is detected the highest number of 600 units, in comparison with the other two horizontal samples, which had their peaks at 400 and 500 units respectively.

As observed in Figure 15, the first two ranges belong to IT grade 14, then all others fall inside the IT grade 13, with the exception of range 30-50 mm, in which the three measures gave an IT grade of 12. The shape of the graph is as expected, but the tendency to get smaller IT grades for the greater ranges of sizes is not met.

At the comparison of the features, by the box plots of Figure 16, one can see that the 3 measures are much alike. For flatness in tangential planes the maximum deviation is 0.35 mm, for horizontal planes is 0.06 mm, and 0.08 mm for vertical planes. Perpendicularity and parallelism have their peaks at 0.15 mm of deviation, while coaxiality is the worst of these features, having 0.2 mm of maximum deviation, for the first two measures.

For all the forward analysis it would be wise to use measurement one or two, because of the similarities between them.

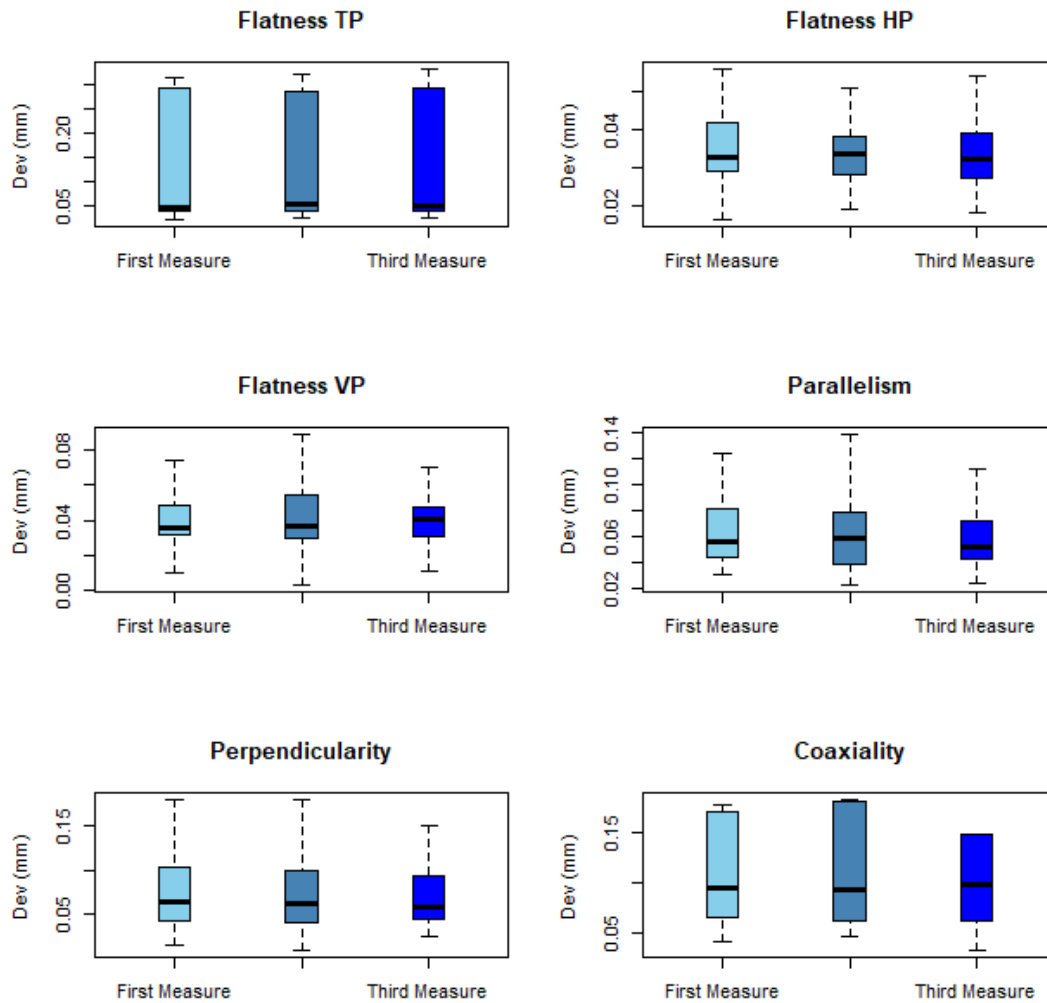


Figure 16. Comparison between the 3 measurements of sample O3 in terms of flatness, parallelism, perpendicularity and coaxiality versus its deviation without outliers.

3.1.4 Comparison of samples O1, O2 and O3

All three samples, O1, O2 and O3 were printed horizontally, O1 on the bottom, O2 in the middle and O3 on the top of the printing volume, so we need to compare them to evaluate if the scale factor used by the printer is the correct one. The measurement number one will be considered for all samples because is the one inside the media in each case, representing the whole 3 measures.

Analyzing Figure 17 can be seen that O1 shows the worst results for concave features, O2 also but with lower mistakes, recalling that the convex spheres are 1, 3, 7 and 6 (as seen on Figure 2) and the concave ones 2, 4, 8 and 5. So for sphericity seems better to print the part in the middle of the printing volume. O3 showed a better behavior for concave spheres, with only 0.01 mm of difference though. Both outliers are on the sphere 2, showing that the error is on the sample itself due to the printing operation and not due to measuring operation.

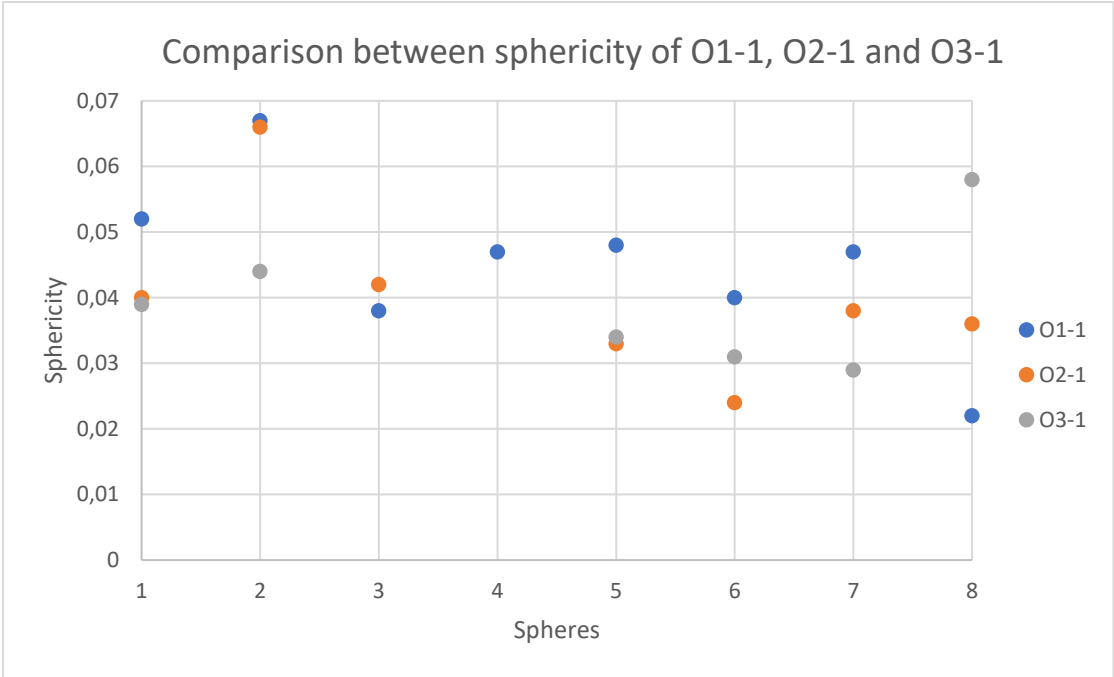


Figure 17. Comparison of sphericity of samples O1, O2 and O3, first measurement for both.

Taking into account cylindricity, in Figure 18, it can be obtained the second outlier on cylinder 16, which is probably due to measurements as well as the printing procedure. During the measurements with the CMM, the probe can hardly enter in the cavity because of some residual dust, and the small length of the cavity, not allowing the heat to be dissipated so the powder gets partially sintered anyway. Sample O1 shows better results for cylindricity than O2, thus for cylinders it will be better to position them on the bottom part of the printing volume. From Figure 3 it can be seen that cylinders 16 and 9, are the smallest ones present

in the sample. O3 is mostly in the middle of deviation, and it is the worst among concave horizontal cylinders (from 5 to 8), getting a maximum deviation of 0.2 mm.

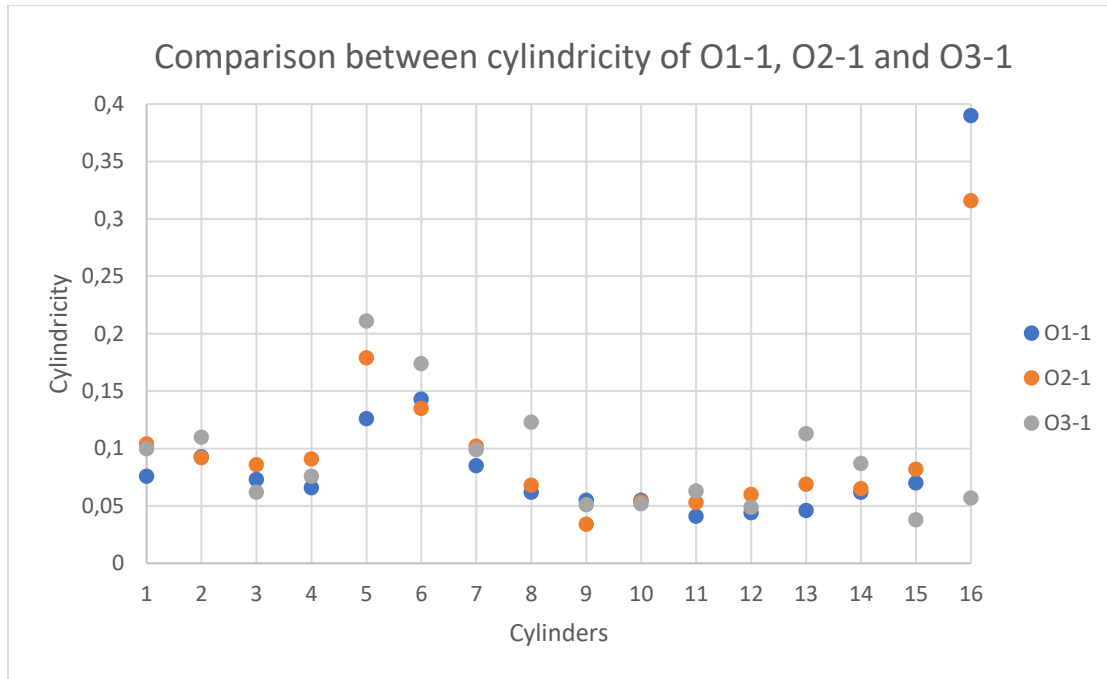


Figure 18. Comparison of cylindricity of samples O1, O2 and O3, first measurement for both.

The conicity (Figure 19) is the one feature that doesn't show an outlier, being this a great sign of no mistakes in the measuring or printing process. The O2 sample has in all four cones better values, so it's better the position them in the middle of the chamber, but the absolute best is at the top with O3. Cones 1 and 3 are external shapes and 2 and 4 internal ones.

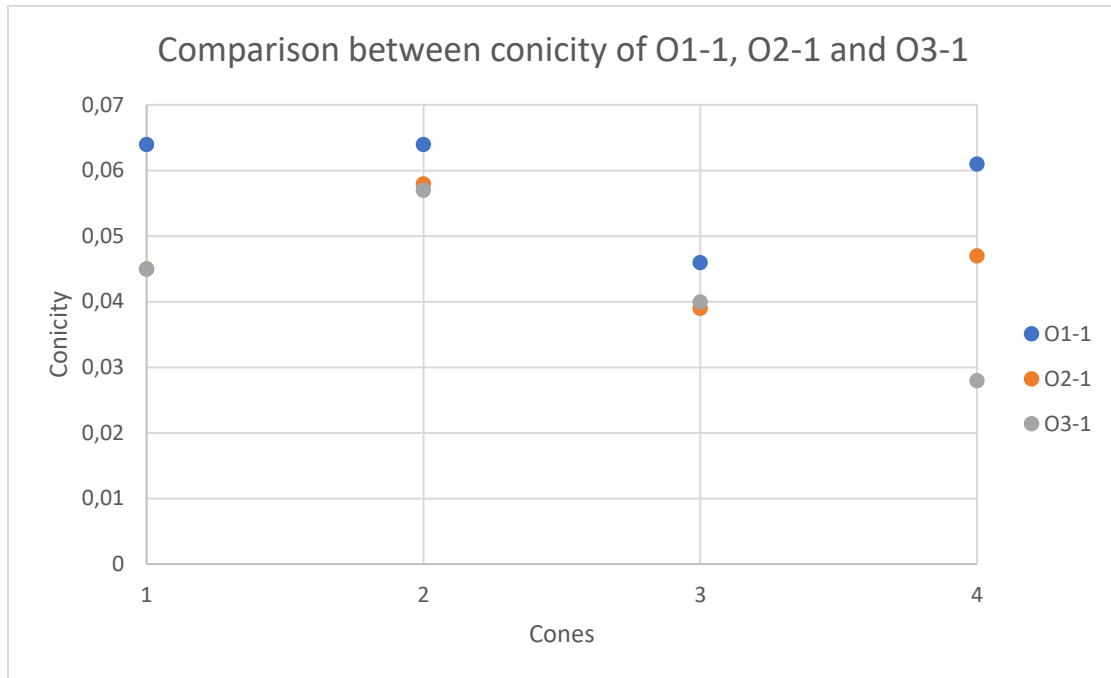


Figure 19. Comparison of conicity of samples O1, O2 and O3, first measurement for both.

In order to be better understand these results, another comparison will be considered to investigate which of the samples showed better behavior for the features of concavity and convexity.

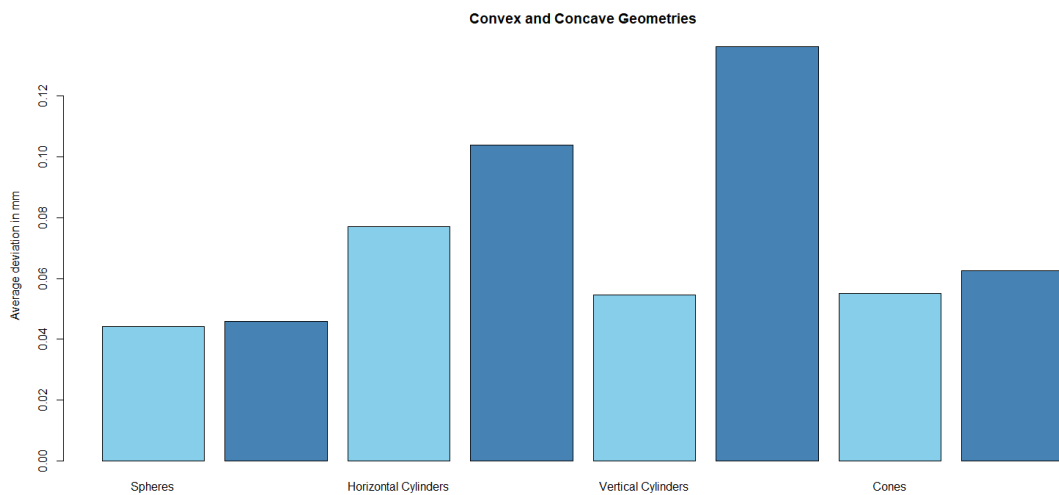


Figure 20. Average deviation of Convex (light blue) and Concave (dark blue) geometries for O1-1.

In general, as evidenced in Figure 20, 21 and 22, the convex features had a lower deviation in comparison with the concave ones. For example, the vertical cylinders, in the case of O1-1, have an average deviation of 0.04 for convex cylinders and 0.12 for concave ones, concluding that the layer thickness and temperature have minor effects on to the XY planar dimensional accuracy. These results are consistent with the ones obtained in Figure 18.

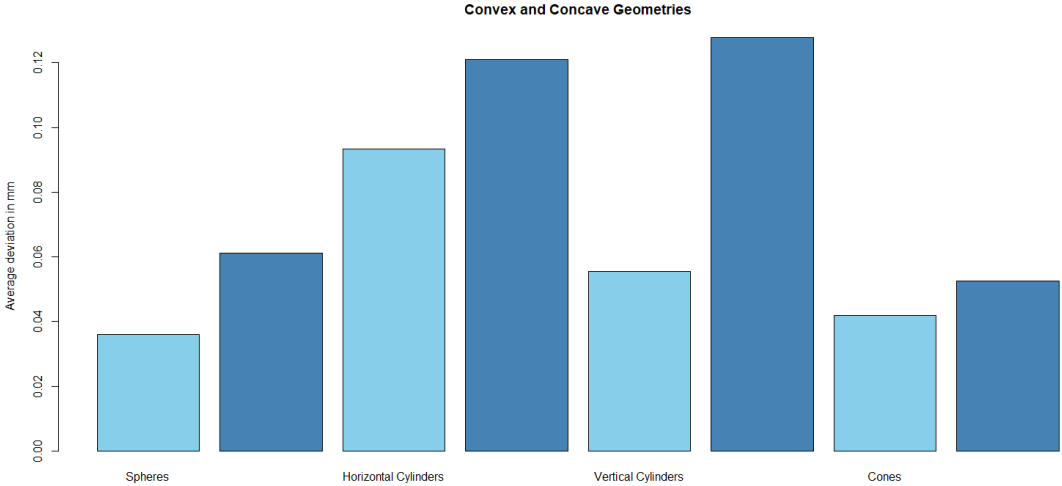


Figure 21. Average deviation of Convex (light blue) and Concave (dark blue) geometries for O2-2.

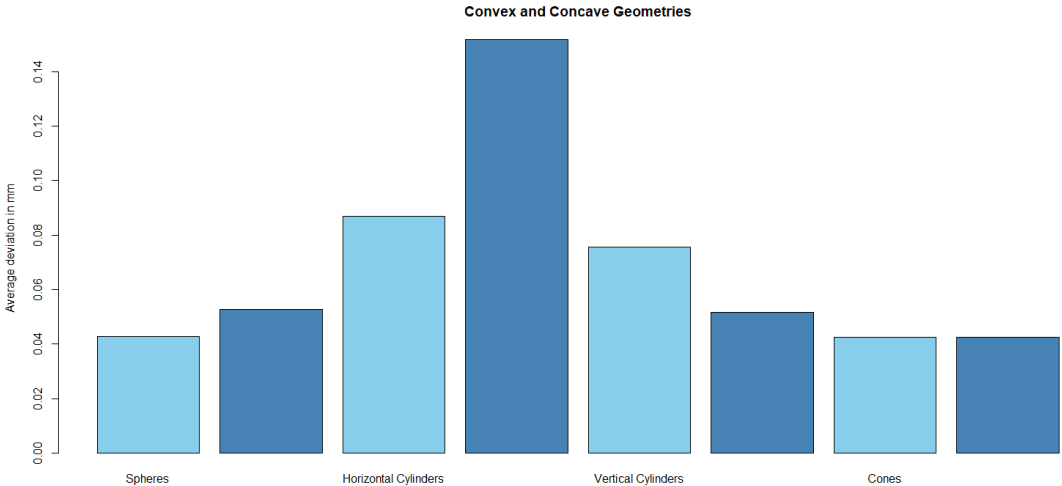


Figure 22. Average deviation of Convex (light blue) and Concave (dark blue) geometries for O3-2.

Figure 23, 24 and Figure 25 show that conicity for sample O2-1 it's better, having all its mean values around 0.04, while O1-1 has them around 0.06. Concave vertical cylinders (from 5 to 8) are not very accurate in neither of the samples. The spheres have better accuracy when convex for O1-1, and much better for O2-1. Cones have lower shape errors for O3-1.

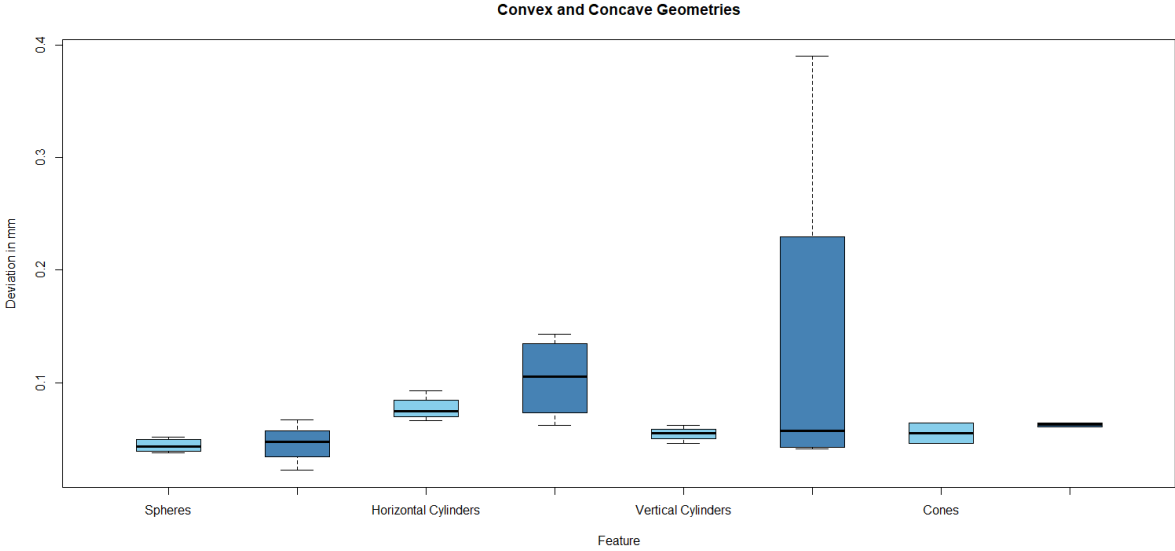


Figure 23. Convex (light blue) and Concave (dark blue) geometries for sample O1-1.

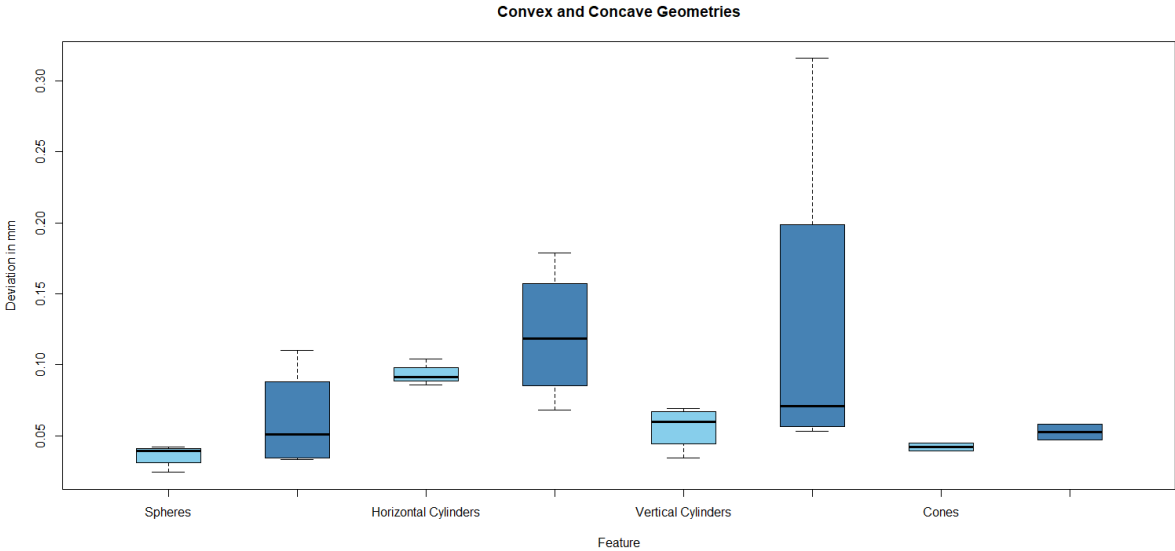


Figure 24. Convex (light blue) and Concave (dark blue) geometries for sample O2-1.

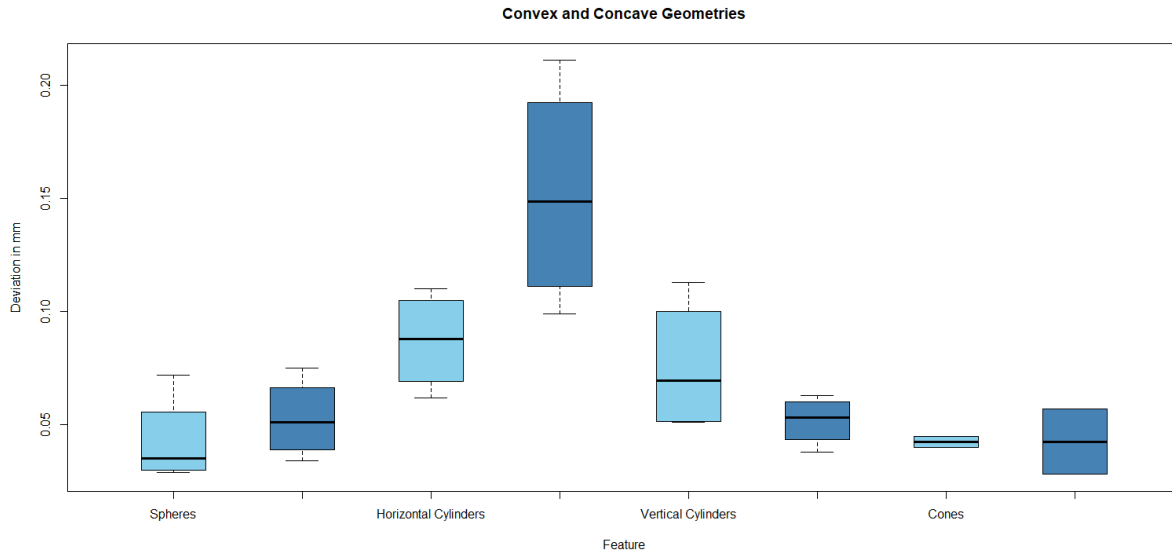


Figure 25. Convex (light blue) and Concave (dark blue) geometries for sample O3-1.

3.2 Vertical samples

3.2.1 Vertical frontal bottom sample V1

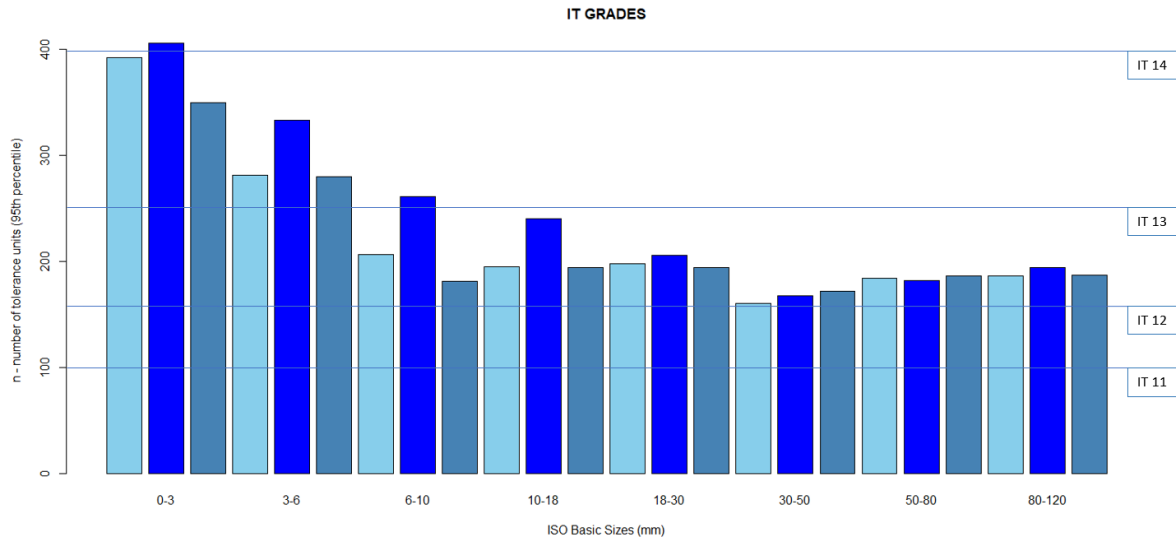


Figure 26. Comparison between the 3 measurements of sample V1 in terms of IT grades and the ISO Basic sizes.

This V1 sample has better dimensional accuracy than the first O1, O2 and O3 parts already. Almost all measures from the third range of sizes until the one fit into the IT12 class. The grade IT14 is achieved for the second measurements of the smallest range of ISO basic sizes (Figure 26), indicating that vertical positioning could be better than horizontally.

The Figure indicates a decreasing behavior, again because the greater the ISO basic size, usually, the better the dimensional accuracy, so the lower its IT grade.

The box plots in Figure 27, shows that the errors of flatness, parallelism, perpendicularity and coaxiality of coaxial features, are consistent among the 3 measurements. The greatest change, is observed for the coaxiality of the second measurement getting a deviation of 0.2 mm, while in the third measurement coaxiality reaches the maximum of 0.6 mm. The maximum GD&T deviation is observed for the perpendicularity with 0.12 mm.

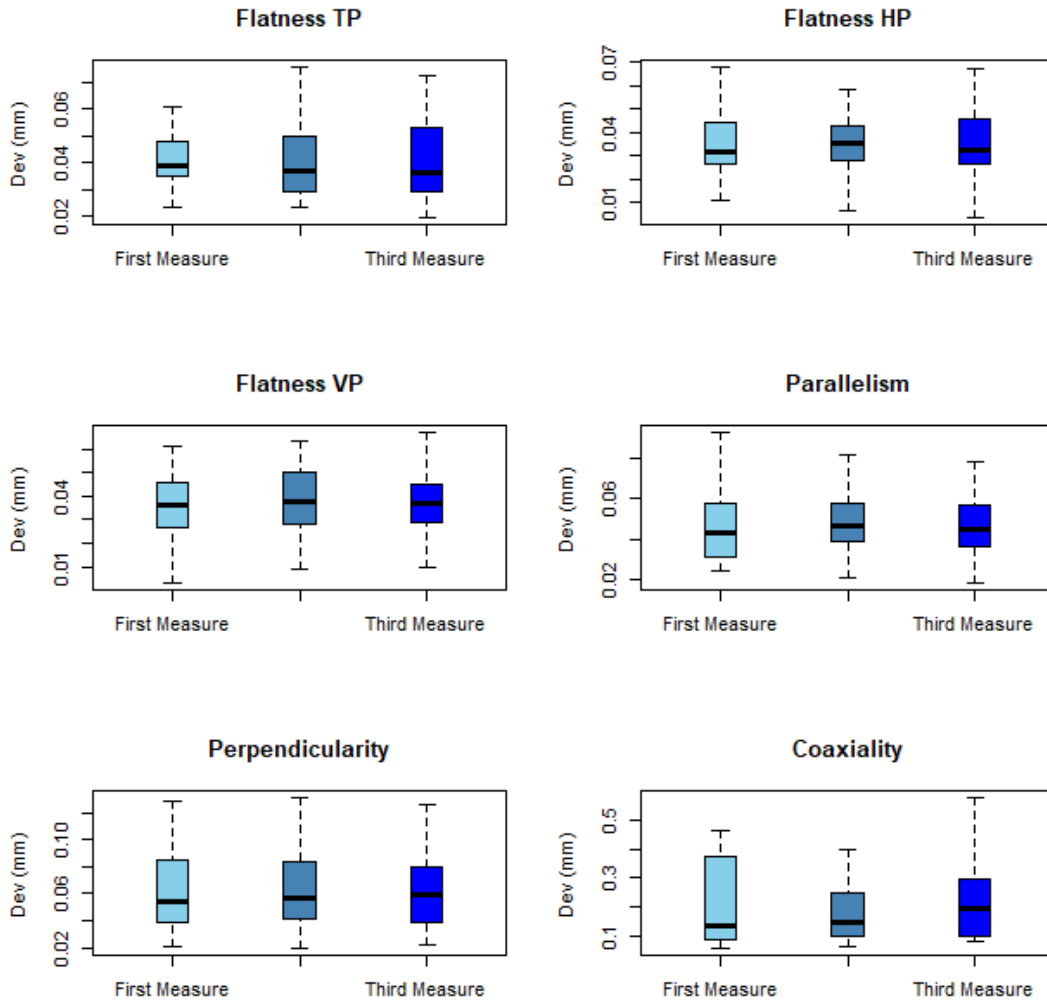


Figure 27. Comparison between the 3 measurements of sample V1 in terms of flatness, parallelism, perpendicularity and coaxiality versus its deviation without outliers.

3.2.2 Vertical frontal top sample V2

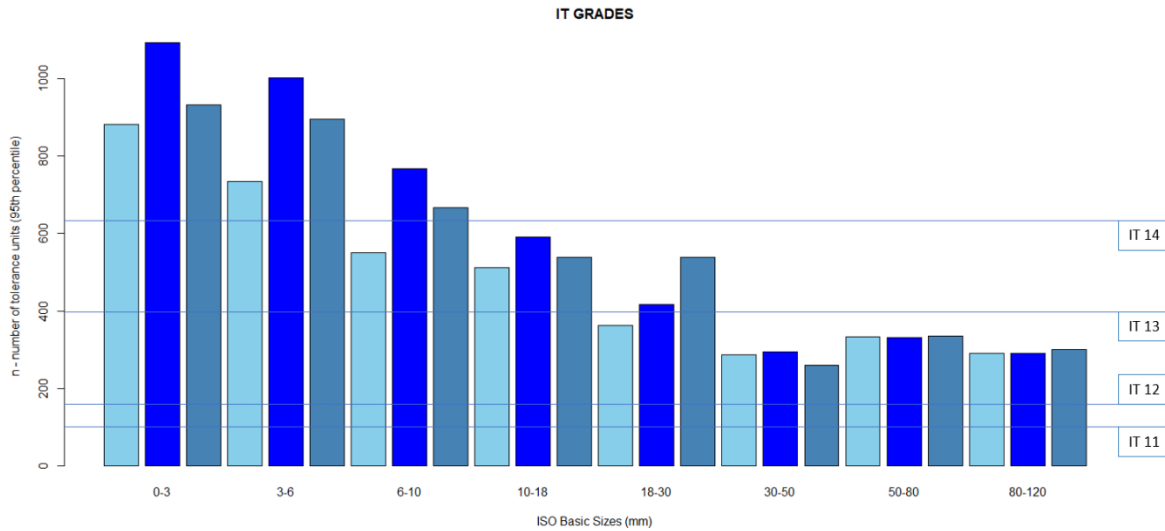


Figure 28. Comparison between the 3 measurements of sample V2 in terms of IT grades and the ISO Basic sizes.

As regards V2 sample, Figure 28 shows that the results of the second and third measurement are more similar than that of the first one. Grade IT14 is met by the first three ranges of ISO basic sizes, then IT13 for intermediate sizes 10-18 mm and 18-30 mm, the remaining ones fit into the IT12 class. The sample V2 in its second measure exceeds 1000 tolerance units for the smaller ISO basic size 0-3 mm. Such a high value, was never measured for the horizontal samples.

The box plot, of Figure 29 for the V2 sample shows a common tendency to the maximum values for all three measurement replications. The maximum values are detailed here below:

- Flatness of the tangential plane: 0.25 mm;
- Flatness of the horizontal plane: 0.1 mm;
- Flatness of the vertical plane: 0.6 mm the first one and 0.5 mm the other two;
- Parallelism: 0.35 mm;
- Perpendicularity: 0.7 mm;

-Coaxiality: 1.2 mm.

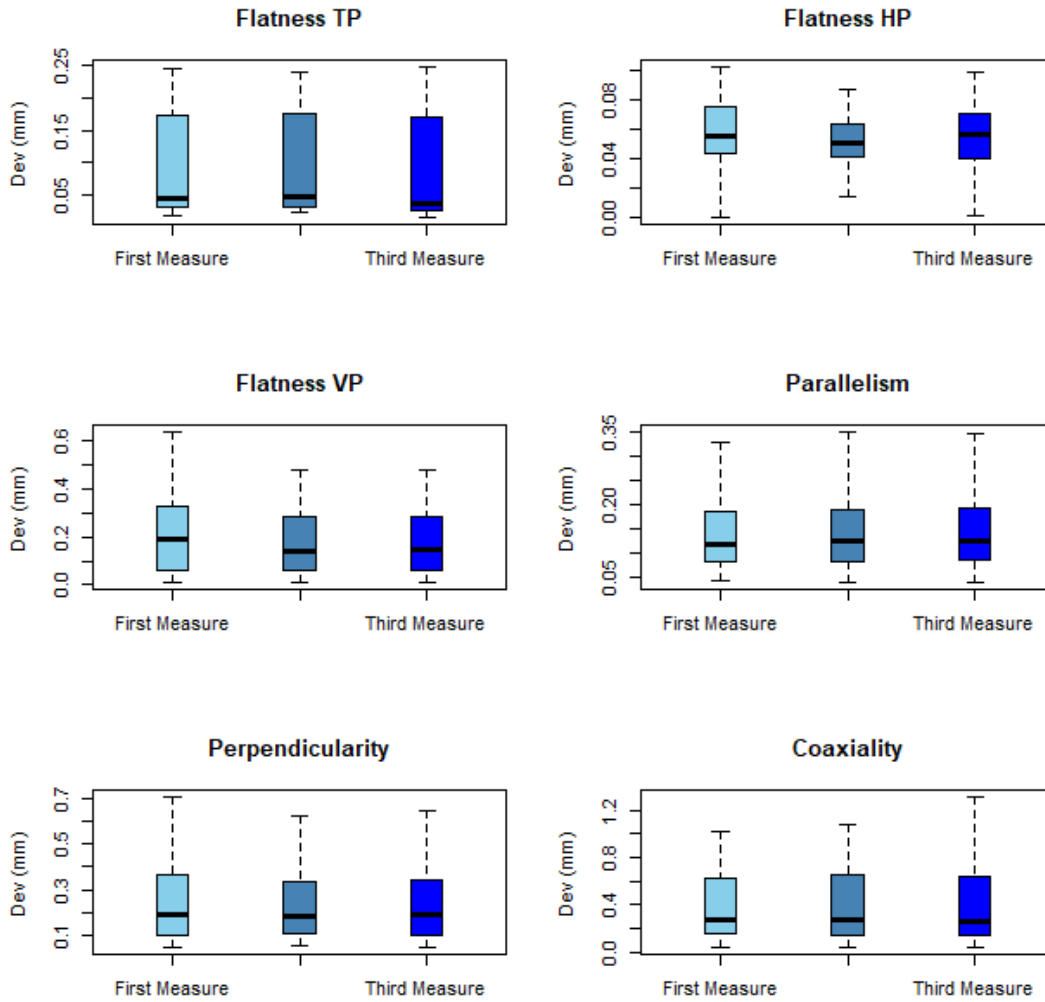


Figure 29. Comparison between the 3 measurements of sample V2 in terms of flatness, parallelism, perpendicularity and coaxiality versus its deviation without outliers.

3.2.3 Vertical lateral bottom sample V3

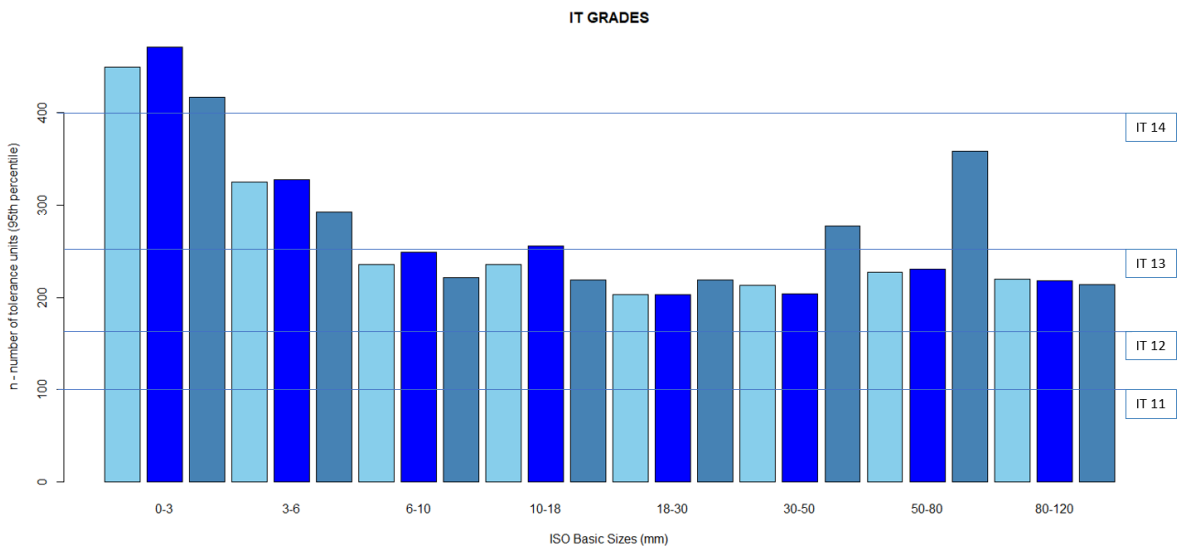


Figure 30. Comparison between the 3 measurements of sample V3 in terms of IT grades and the ISO Basic sizes.

The results of the dimensional accuracy of V3 sample are similar to those of V1 sample. However, the accuracy of the V3 sample is worse than that of the V1 sample. For the smallest range of ISO basic sizes, IT14 class is achieved and the third measure in the ranges from 30-50 and 50-80 fit into the IT13 class.

The Figure indicates a decreasing behavior, again because the greater the ISO basic size, usually, the better the dimensional accuracy, so the lower its IT grade.

The graphs of Figure 31, representing once again that the errors of flatness, parallelism, perpendicularity and coaxiality of coaxial features, indicate the good repeatability of the three measurements. The greatest difference among the replications is registered for the flatness in the tangential plane, which has the lowest maximum at 0.065 mm on the third measurement, while the other two measurements have it at 0.08 mm.

The maximum error of the horizontal flatness is 0.06 mm, one of the vertical flatness is 0.07 mm. Parallelism peak is of 0.08 mm and perpendicularity has a maximum value of 0.14 mm. Coaxiality is by far the less accurate feature once again, with almost 0.3 mm of maximum deviation.

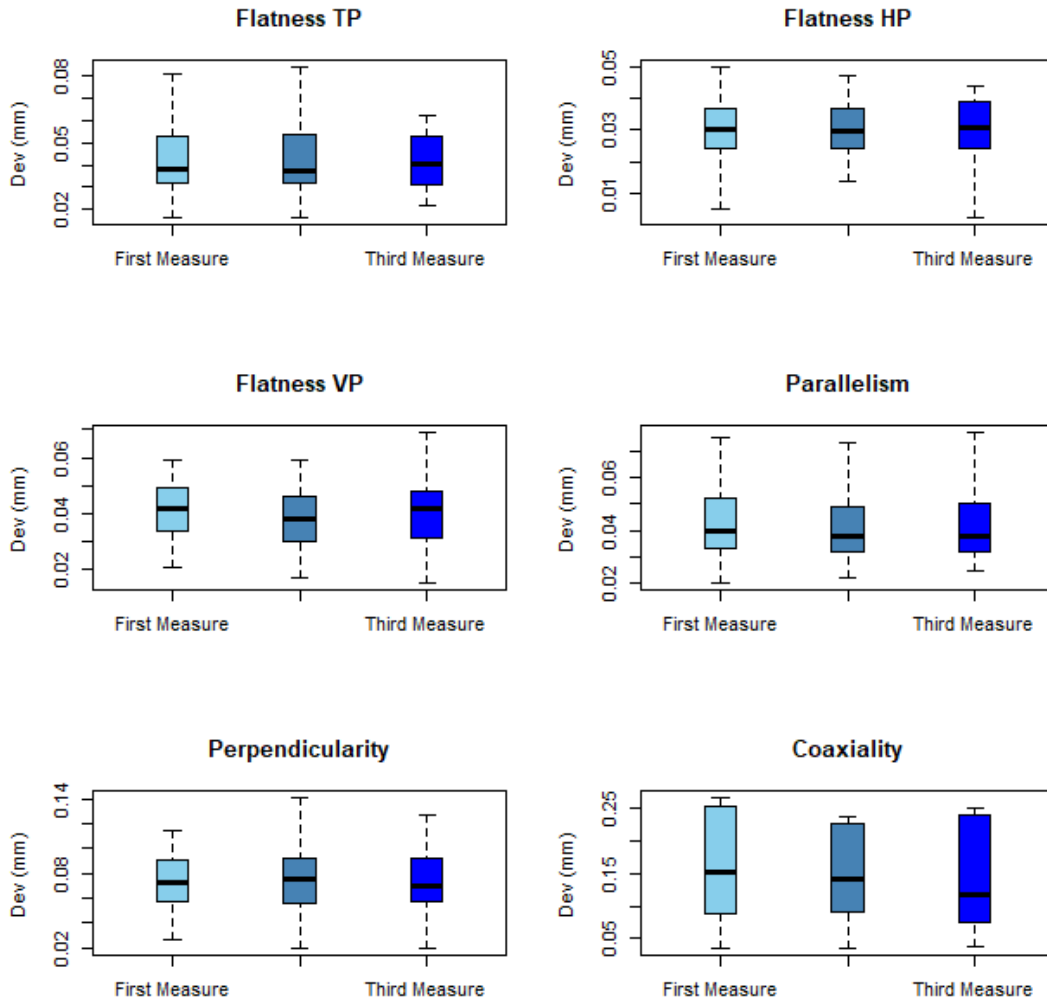


Figure 31. Comparison between the 3 measurements of sample V3 in terms of flatness, parallelism, perpendicularity and coaxiality versus its deviation without outliers.

3.2.4 Vertical lateral top sample V4

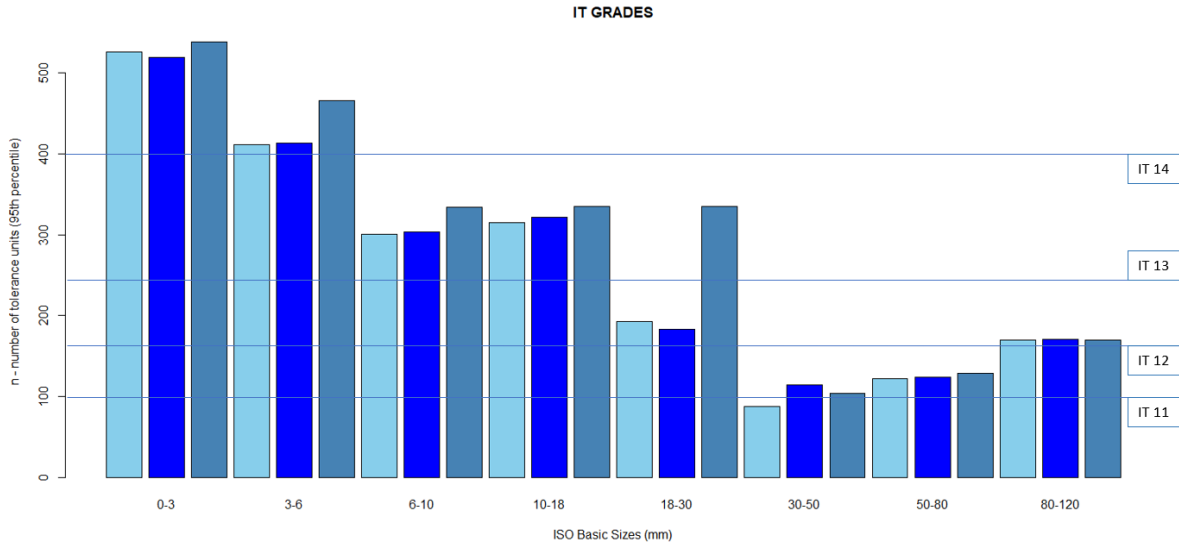


Figure 32. Comparison between the 3 measurements of sample V4 in terms of IT grades and the ISO Basic sizes.

In the case of V4 sample (Figure 32), the maximum number of tolerance units is around 500 for the first range of 0-3 mm. This is a much better improvement with respect to V2, but 100 units higher than V1 and V3. A further analysis regarding these differences will be carried out later, to better understand how a difference in the position and the size of the geometry can induce a huge change in the final result. Belonging to grade IT14 are the first two ranges of sizes, the following three belong to IT13. Range 30-50 and 50-80 mm are IT11, but range 80-120 mm is IT12.

The values of all the features of sample V4, reported in Figure 33 are all consistent within the three replications of the measurements. Maximum deviations are listed here below:

-Flatness of tilted planes: 0.06 mm, better than the previous samples;

-Flatness of horizontal planes: 0.06 mm;

-Flatness of vertical planes: 0.07 mm;

-Parallelism: 0.08 mm;

-Perpendicularity: 0.14 mm;

-Coaxiality: 0.35 mm, similar to sample V3, and better than sample V2.

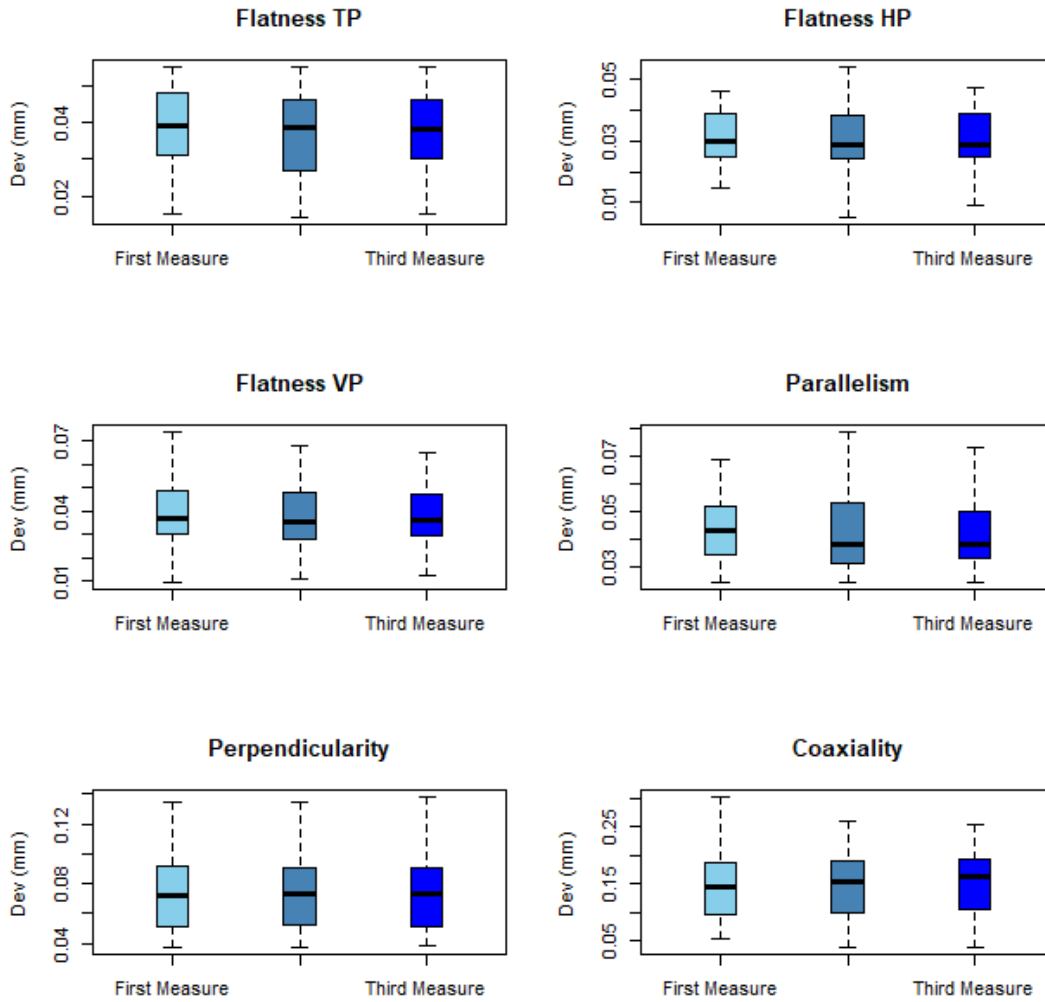


Figure 33. Comparison between the 3 measurements of sample V4 in terms of flatness, parallelism, perpendicularity and coaxiality versus its deviation without outliers.

3.2.5 Vertical lateral bottom sample V5

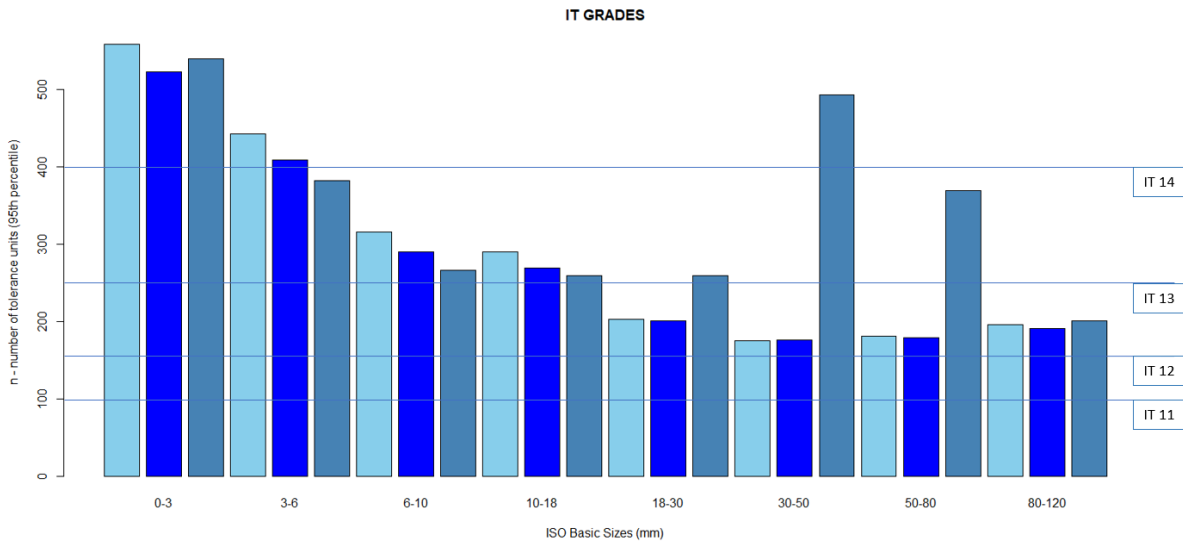


Figure 34. Comparison between the 3 measurements of sample V5 in terms of IT grades and the ISO Basic sizes.

The V5 sample has the lowest deviations to the ideal shape as can be seen in Figure 34. Nevertheless, the third replication of the measurements in the ISO ranges 30-50 mm and 50-80 mm seems to be affected by a systematic error. The highest-grade IT 14 is registered for the smaller sizes 0-3 mm and 3-6 mm. The dimensional accuracy gets better as the size increases going through IT13 until 18-30 as basic size becomes IT12. Once again, the results suggest that vertical positioning could be better than horizontally.

In Figure 35, the box plots resuming the errors of flatness, parallelism and perpendicularity for sample V5 are shown. The errors are within the normal ranges of deviation, with a maximum deviation for coaxiality feature of 0.3 mm, the highest one. The maximum value for the flatness of tilted planes is 0.12 mm, while the one of horizontal planes is 0.06 mm.

With the exception of parallelism, the results of the three replications of the measurements are consistent. In the case of parallelism, a maximum error of 0.15 mm is registered in the first measurement, whereas the error in the second and third measurements is 0.10 mm.

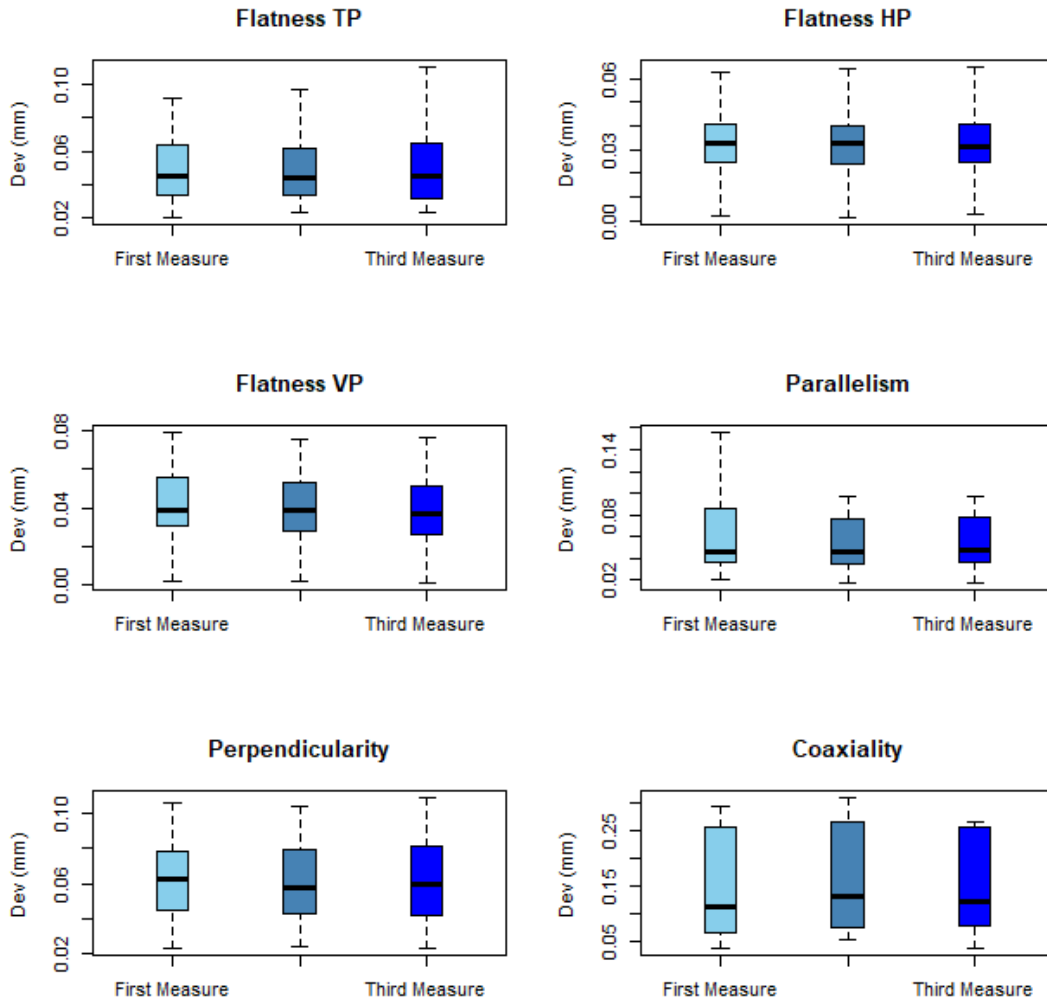


Figure 35. Comparison between the 3 measurements of sample V5 in terms of flatness, parallelism, perpendicularity and coaxiality versus its deviation without outliers.

3.2.6 Vertical lateral top sample V6

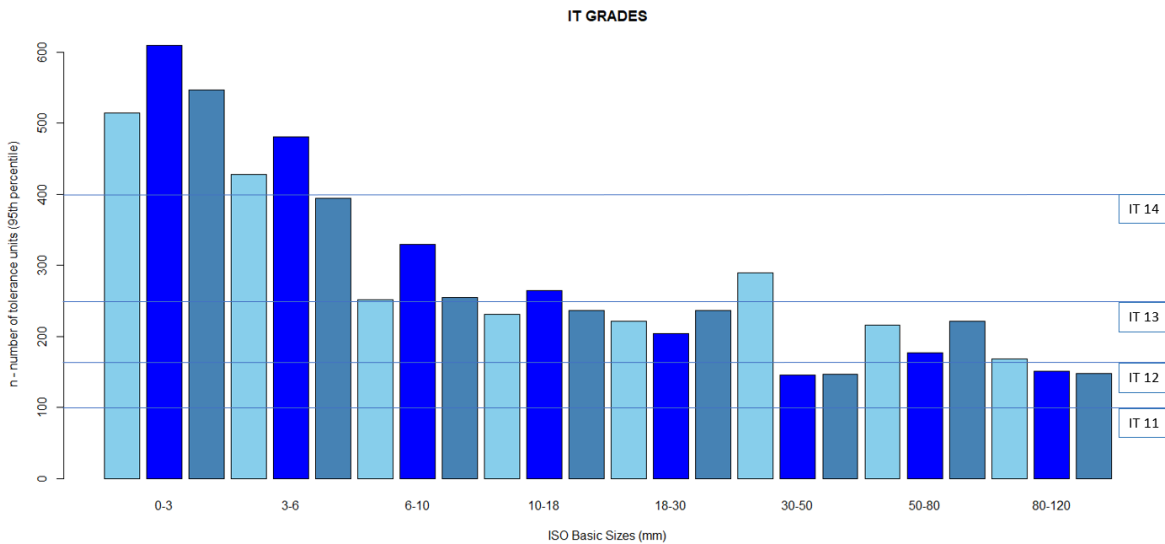


Figure 36. Comparison between the 3 measurements of sample V6 in terms of IT grades and the ISO Basic sizes.

As regards sample V6, the maximum number of tolerance unit for the smaller range of ISO basic sizes is 600 as shown in Figure 36. This result is still better than the one of V2 sample, but worst than those of samples V1, V3 and V4. IT14 is the grade for the first two 0-3 mm and 3-6 mm, IT13 for the third range 6-10 mm, while IT12 is achieved for other ranges.

Without considering the outliers, in the box plots of geometrical tolerances, the average values of the three replications of the measurements vary. In terms of each feature:

- Flatness of tilted planes: there's a small change in the first measure 0.1 mm as deviation, having its maximum value at 0.07 mm and its minimum 0.04, the other two have their values as 0.03 and 0.08 as minimum and maximum respectively;

- Flatness of horizontal planes: maximum of 0.05 mm and minimum of 0.01mm;

- Flatness of vertical planes: maximum of 0.1 mm and minimum of 0.01 mm;

- Parallelism: maximum of 0.08 mm and minimum of 0.01mm;

- Perpendicularity: maximum of 0.20 mm and minimum of 0.05mm;

- Coaxiality: maximum of 0.45 mm and minimum of 0.05mm.

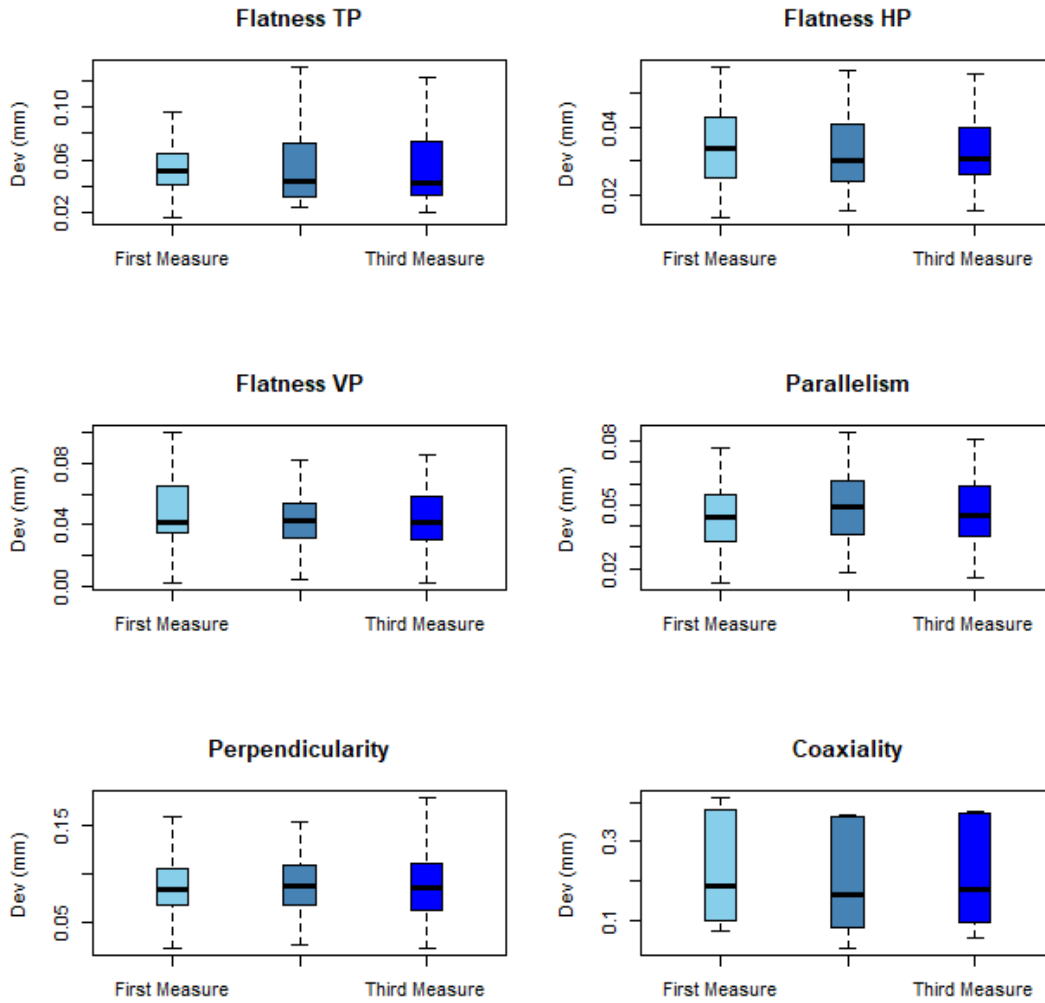


Figure 37. Comparison between the 3 measurements of sample V6 in terms of flatness, parallelism, perpendicularity and coaxiality versus its deviation without outliers.

3.2.7 Vertical lateral bottom sample V7

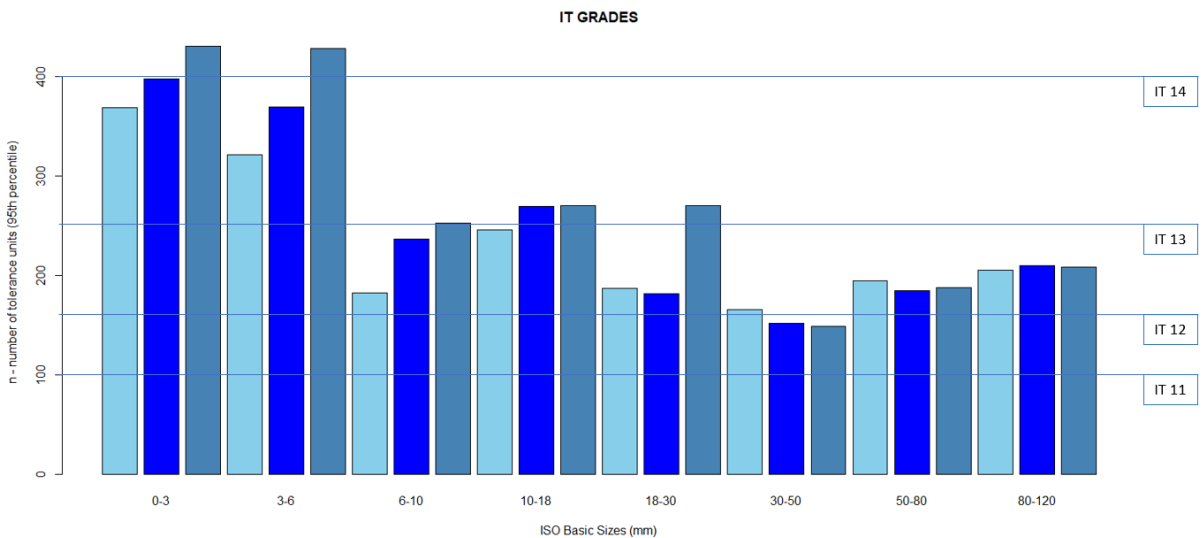


Figure 38. Comparison between the 3 measurements of sample V7 in terms of IT grades and the ISO Basic sizes.

Figure 38 shows that the dimensional accuracy of sample V7 achieves a grade IT14 for the first two ranges of ISO Basic sizes, in the third replication of the measurements. Grade IT13 is achieved in some replications in the next three ranges and then a grade IT12 is registered for all the measures in the last three ranges, some reaching even IT11 for the ISO Basic sizes of 30-50. The dimensional accuracy of V7 sample is not as good as the one of the other vertical samples, but still better than that of the horizontal samples.

The box plots on Figure 39, shows that the levels of flatness, parallelism, perpendicularity and coaxiality of coaxial features, are pretty much equal considering the 3 measurements, and they are all in the normal range of deviation. The obtained values as maximum and minimum for each feature, are listed as follows:

- Flatness of tilted planes: 0.08 mm and 0.02;
- Flatness of horizontal planes: 0.06 mm and 0.01 mm;
- Flatness of vertical planes: 0.08 mm and 0.01 mm;
- Parallelism: 0.1 mm and 0.02 mm;

-Perpendicularity: 0.14 mm and 0.02 mm;

-Coaxiality: 0.23 mm and 0.05mm.

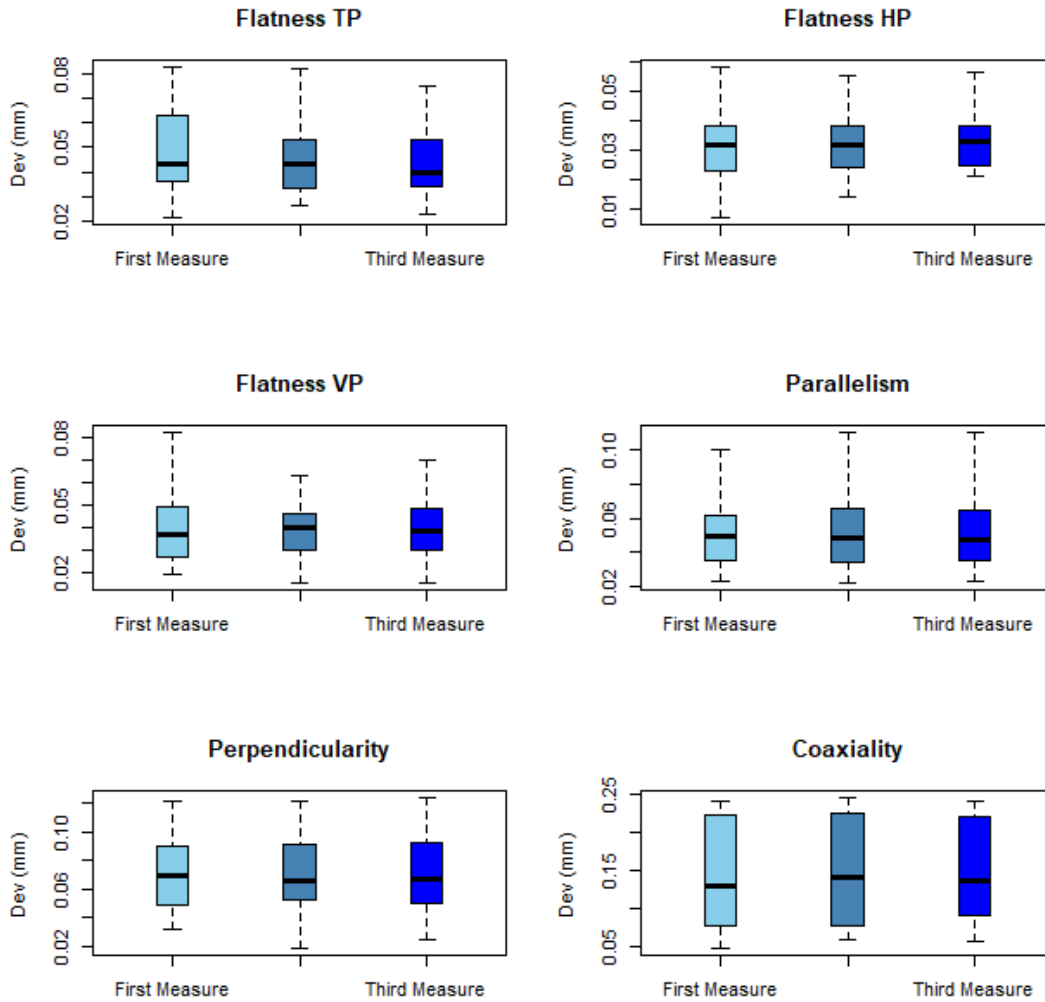


Figure 39. Comparison between the 3 measurements of sample V7 in terms of flatness, parallelism, perpendicularity and coaxiality versus its deviation without outliers.

3.2.8 Comparison between bottom vertical samples V1, V3 and V5

Samples V1, V3 and V5 were printed at the same height inside the building chamber, but they were placed in different positions. From V1 frontally, and V3 and V5 on the laterals. Thanks to: Figure 40 about the sphericity error, it can be seen that samples V1 and V3 share most of the values, while V5 is usually greater, so has higher deviations to the ideal spherical shape. However, it is not possible to distinguish whether the frontal position is better than the lateral one.

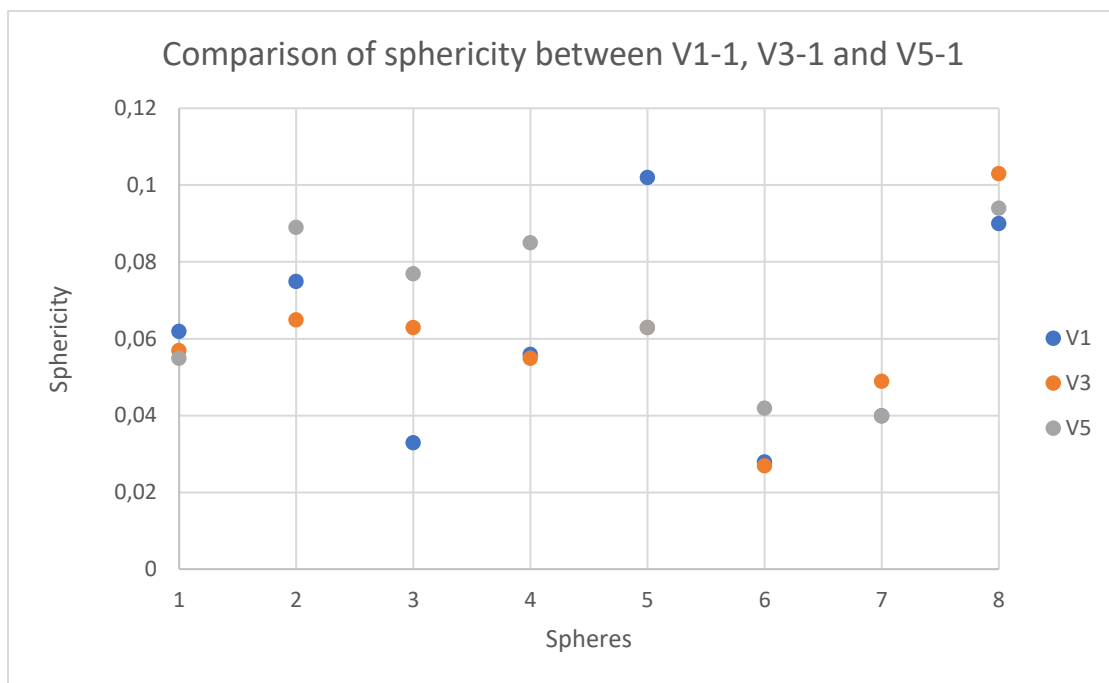


Figure 40. Comparison of sphericity between samples V1, V3 and V5, first measurement for all three.

Figure 41 shows the same outlier shown on Figure 18 present on cylinder 16. This result confirms that there is not a systematic error in the measurement of cylinder 16 with the CMM machine, but the geometry is fabricated with higher deviations to the nominal geometry because of the heat concentration due to the presence of surrounding cylinders of larger size in the cross section. On all the other cylinders the behavior is quite similar, so the lateral or frontal positioning of the sample doesn't influence the results of the cylindricity.

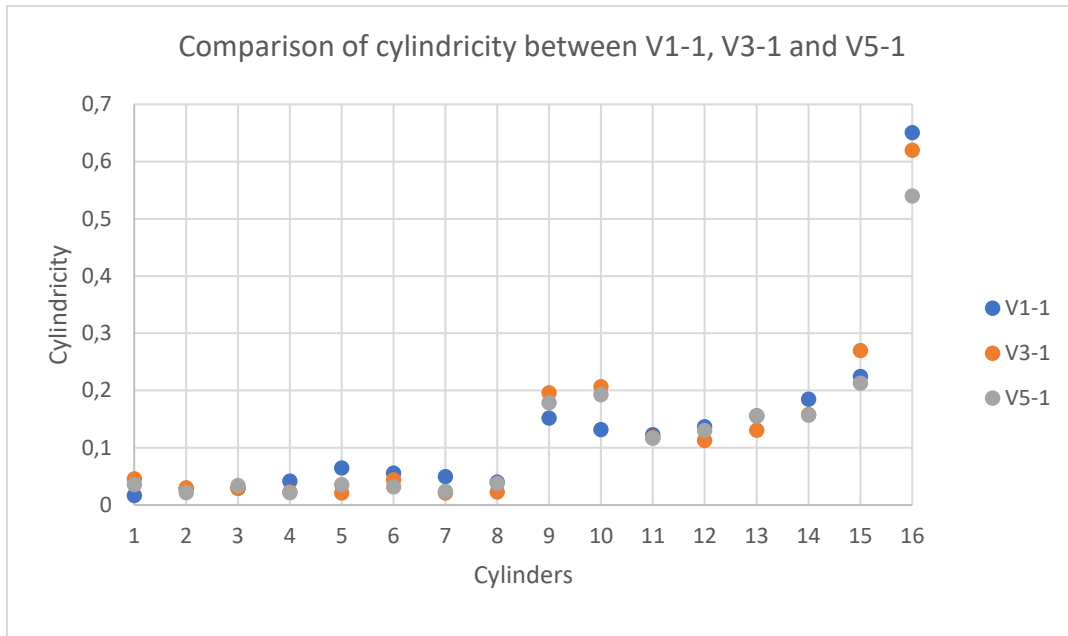


Figure 41. Comparison of cylindricity between samples V1, V3 and V5, first measurement for all three.

Higher errors are measured for the conicity tolerance with higher deviations (Figure 42), and no markable difference is noted among the three vertical samples V1, V3 and V5 meaning that there is no preferential positioning between the front are and the side areas of the build volume.

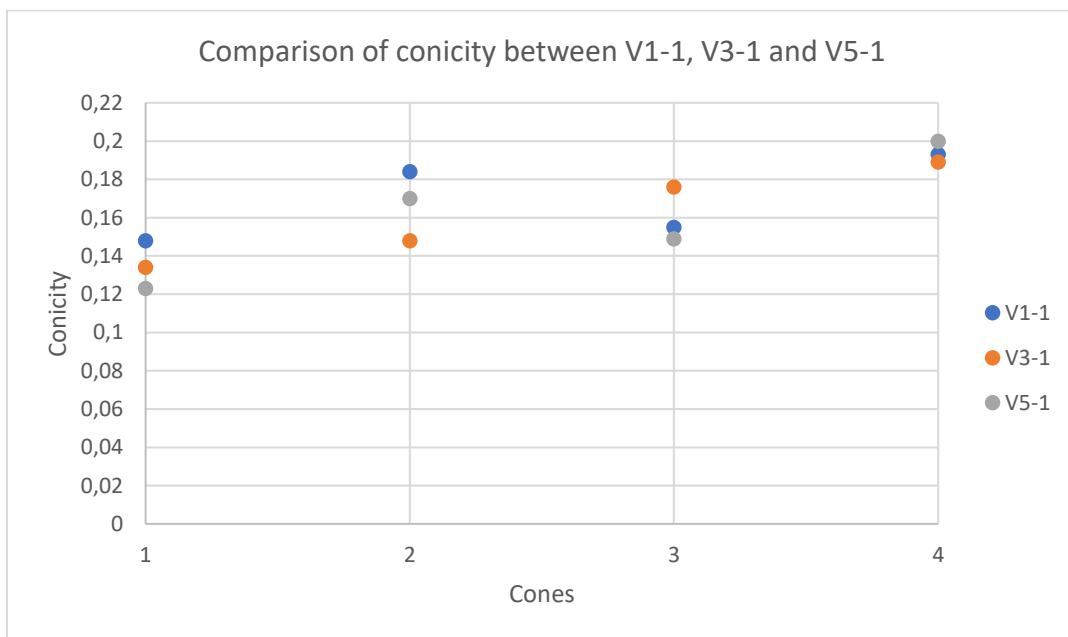


Figure 42. Comparison of conicity between samples V1, V3 and V5, first measurement for all three.

To deepen the analysis of the results, the errors of the concave shapes will be compared to those of the convex ones. Once again, the vertical concave cylinders are the geometry with the highest deviation in all the samples, with a maximum of 0.6 mm in V1-1. Cones for V1-1 vary their deviation in a lower range than samples V3-1 and V5-1, as illustrated in the Figures 43, 44 and 45, even though the absolute accuracy most of the cones it's better for sample V3-1 (Figure 42).

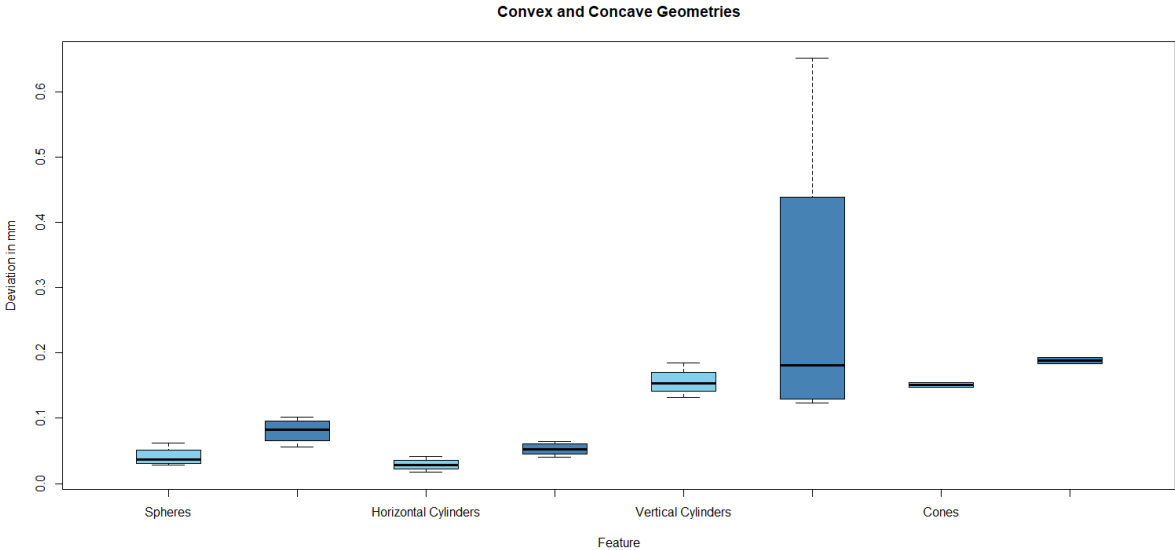


Figure 43. Convex (light blue) and Concave (dark blue) geometries for sample V1-1.

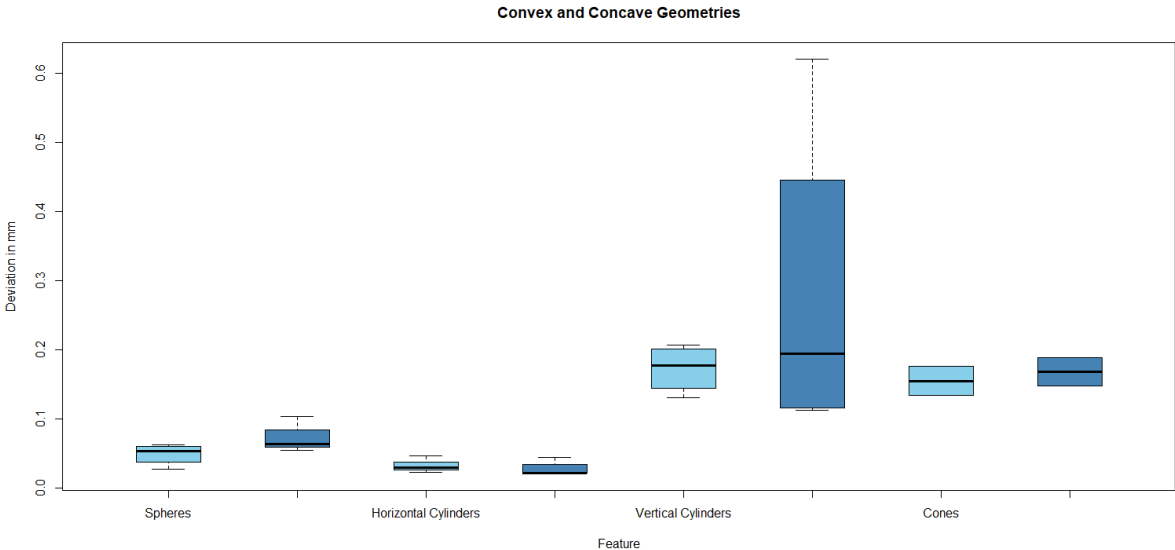


Figure 44. Convex (light blue) and Concave (dark blue) geometries for sample V3-1.

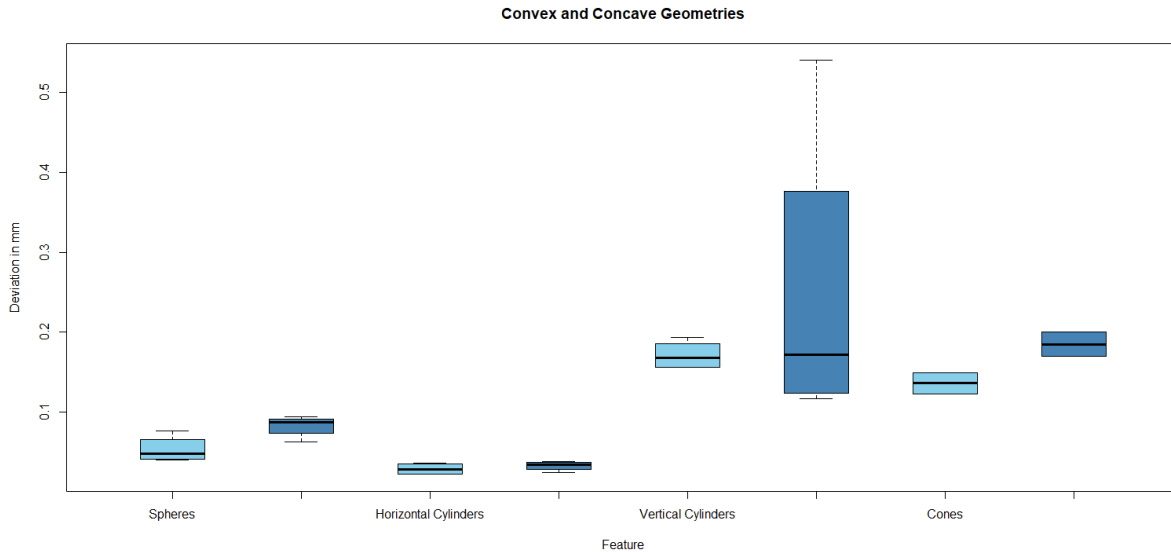


Figure 45. Convex (light blue) and Concave (dark blue) geometries for sample V5-1.

As stated before, the vertical concave cylinders have an average deviation that can't be ignored, with a maximum of 0.30 mm on V1-1 (Figure 46). Convex and concave spheres (Figure 46, 47 and 48) have an average deviation of 0.05 mm and 0.09 mm respectively in all three samples. The errors of concave and convex horizontal cylinders are very similar. Only for sample V1-1 there is a small increment of the deviation of concave horizontal cylinders, with an average deviation of 0.06 mm.

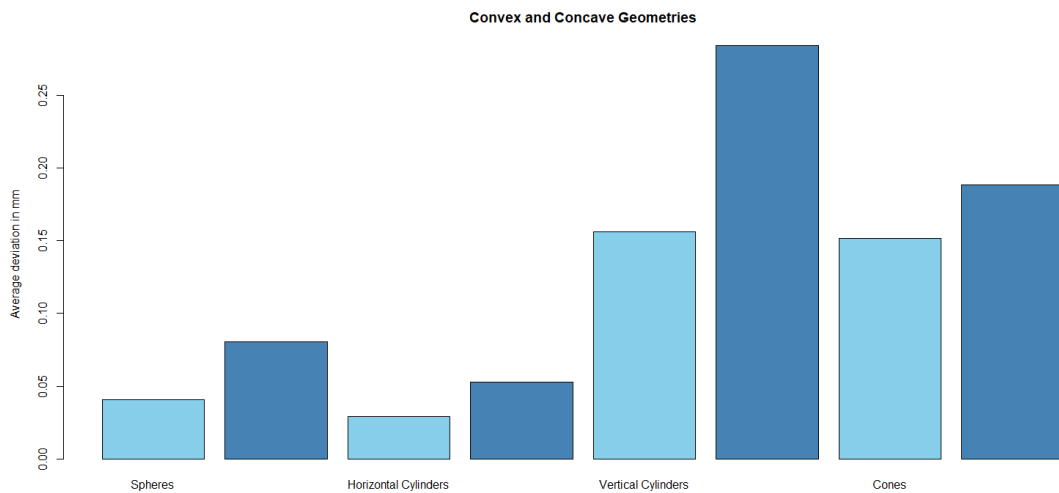


Figure 46. Average deviation of Convex (light blue) and Concave (dark blue) geometries for V1-1.

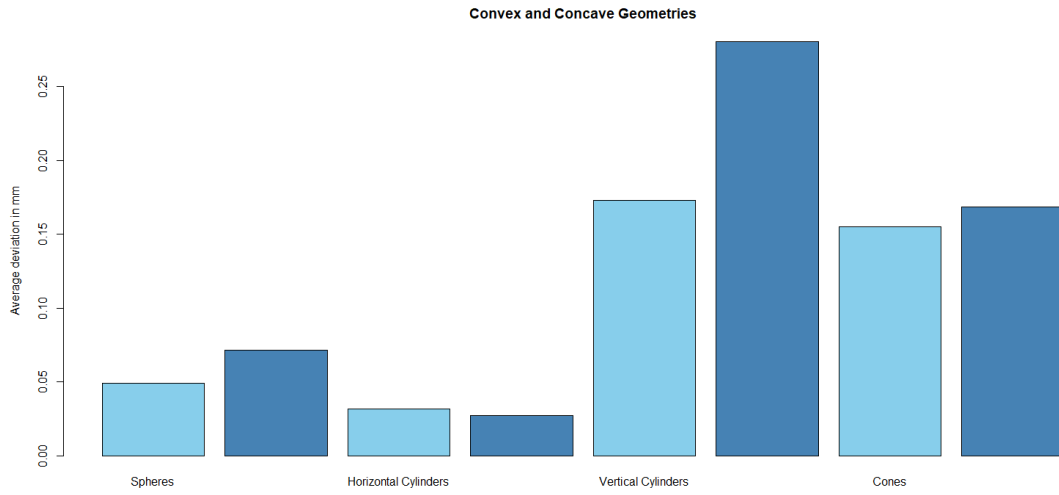


Figure 47. Average deviation of Convex (light blue) and Concave (dark blue) geometries for V3-1.

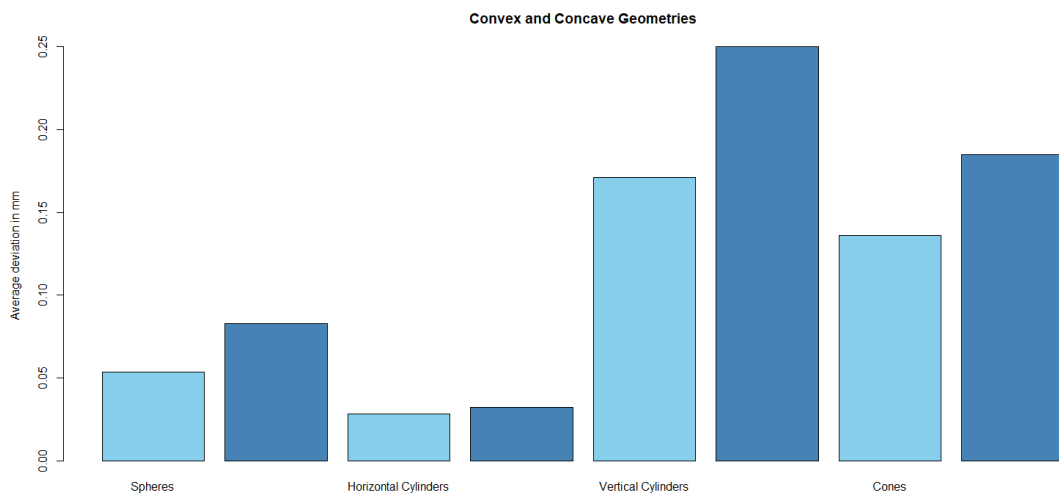


Figure 48. Average deviation of Convex (light blue) and Concave (dark blue) geometries for V5-1.

3.2.9 Comparison between vertical samples at the top V4, V2 and V6

In order to investigate the best positioning at the top of the building volume, the results of the shape errors are analyzed for samples V2, V4 and V6. As shown in Figure 49, the first five spheres, showed a very similar error for the three samples. However, sample V2 has a difference of 0.1 mm on sphere 3 and 0.2 mm on sphere 4 with respect to the other samples. There is a value considered as an outlier on sphere 6 for sample V4, because the difference to the values of the other two samples is 0.65 mm.

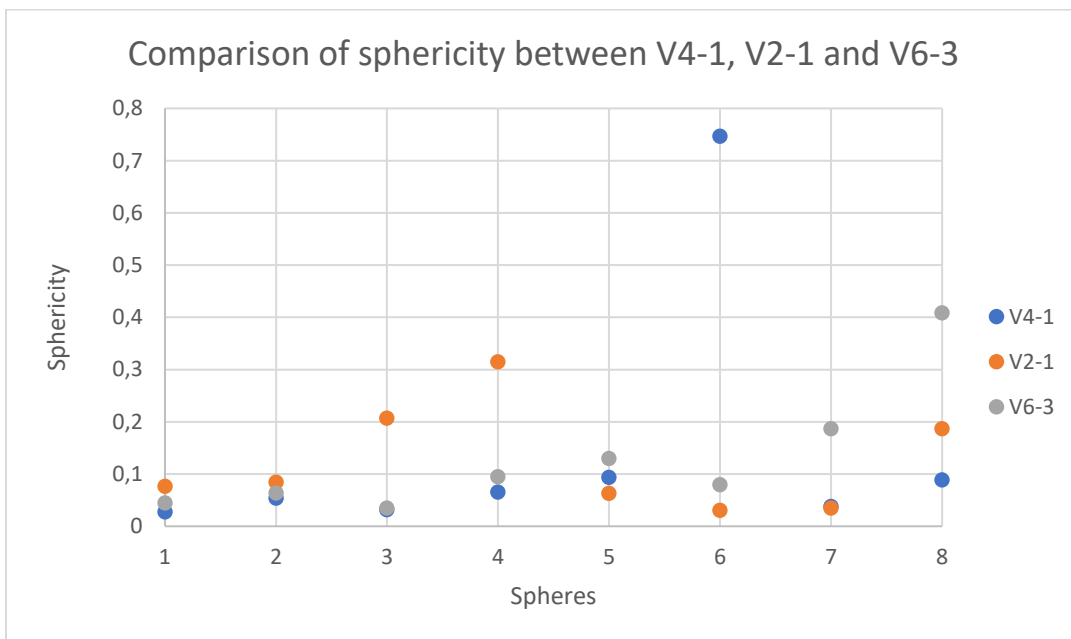


Figure 49. Comparison of sphericity between samples V4, V2 and V6.

When looking at cylindricity (Figure 50), the smallest deviations are registered for sample V6, and the largest ones for sample V2. All the three samples in the cylinders showed a deviation between their values not greater than 0.1 mm. However, the difference among the samples are higher for cylinders 5, 13 and 15, with sample V4 showing an outlier in by an amount of 0.4 mm, 0.35 mm and 0.3 mm respectively.

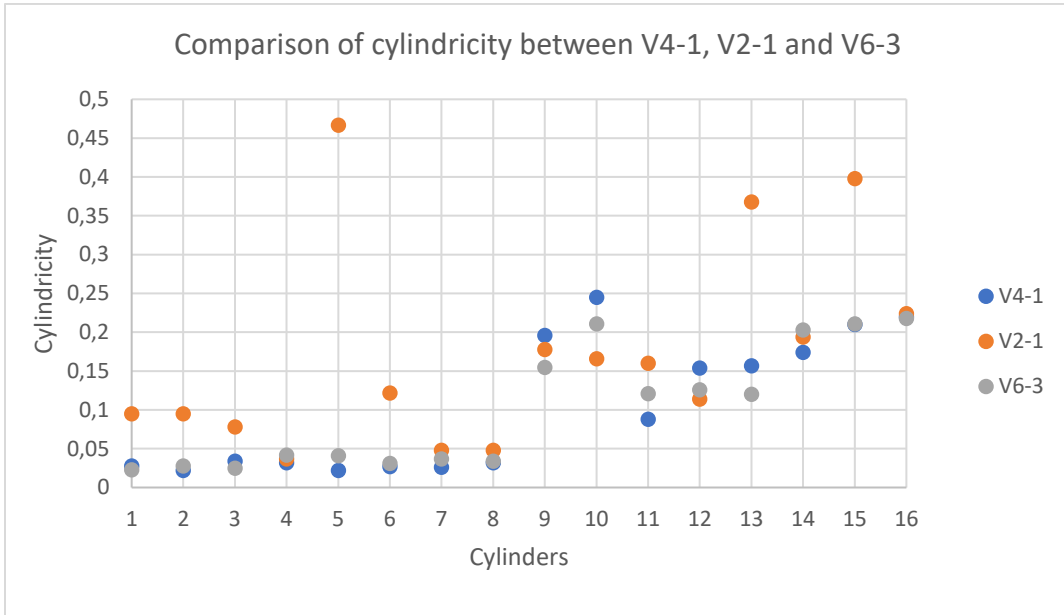


Figure 50. Comparison of cylindricity between samples V4, V2 and V6.

As for the cones (Figure 51), the first cone in sample V4 showed a deviation of 0.37 mm, while 0.1 mm are registered for the same geometry of the other samples. The second cone, which is concave, had a deviation of 0.17 mm very similar for all the three samples. The conicity of the third cone was better on sample V4 with a value of 0.15 mm, while samples V2 and V6 achieved 0.21 mm.

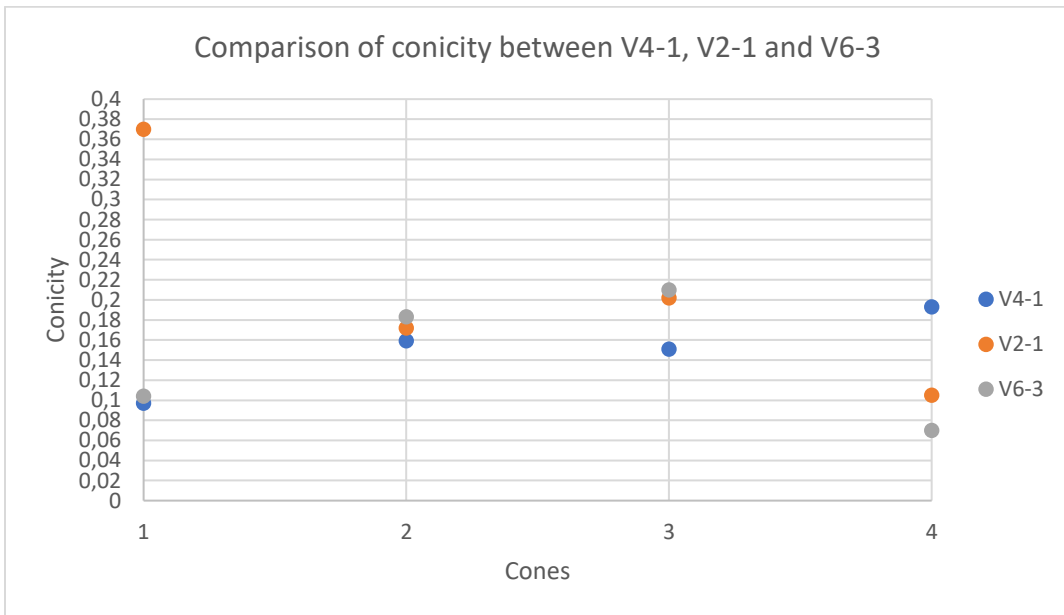


Figure 51. Comparison of conicity between samples V4, V2 and V6.

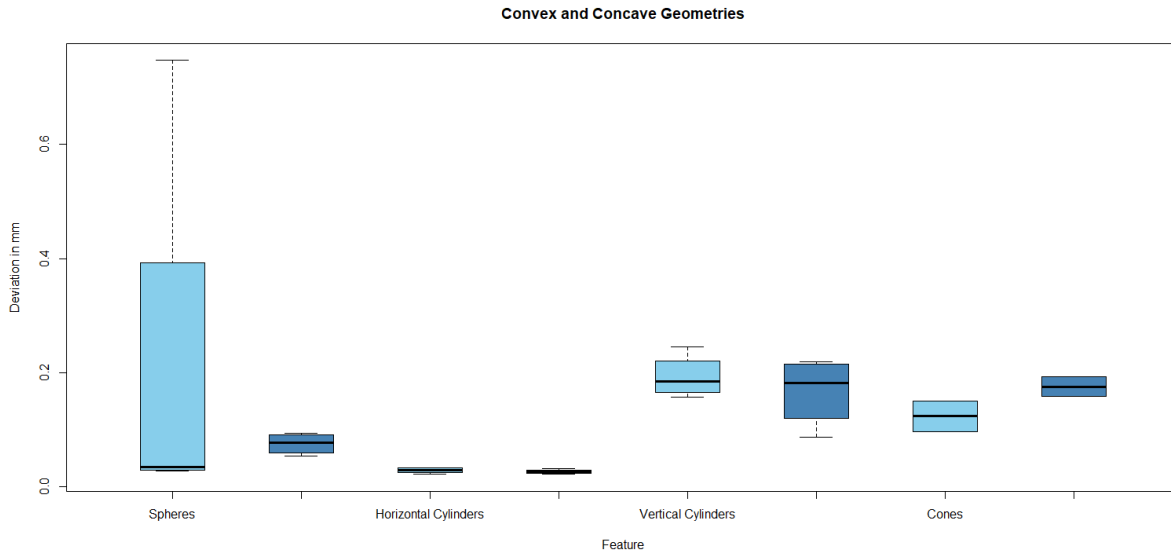


Figure 52. Co Convex (light blue) and Concave (dark blue) geometries for sample V4-1.

Figures 52 and 53 confirm that the horizontal cylinders had the best outcome in terms of minimum deviation on sample V4, with 0.025 mm of average deviation. From Figure 55 it can be observed that sample V2 had an average deviation of 0.05 mm for the horizontal convex cylinders and 0.16 mm for the concave ones, while for sample V6 (Figure 57) the medium value is 0.03 mm for both types of cylinders.

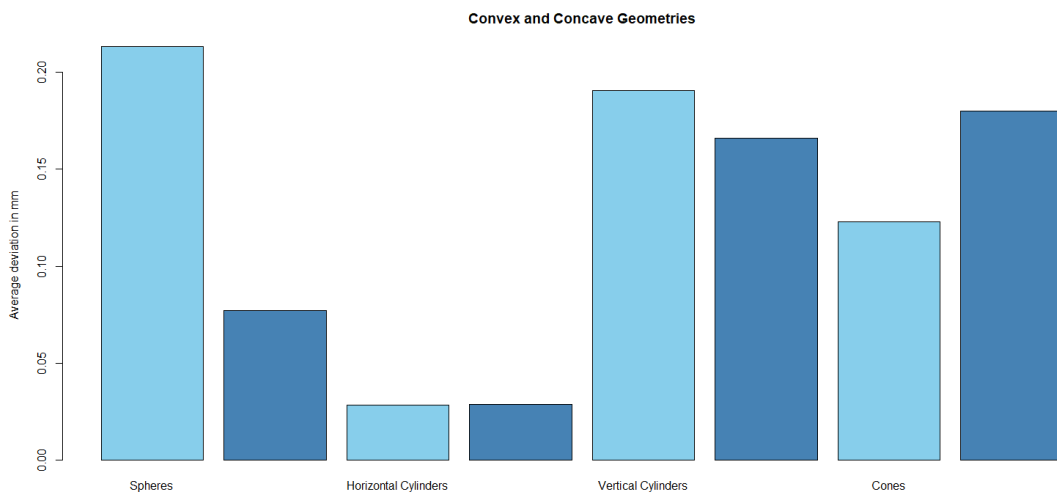


Figure 53. Average deviation of Convex (light blue) and Concave (dark blue) geometries for V4-1

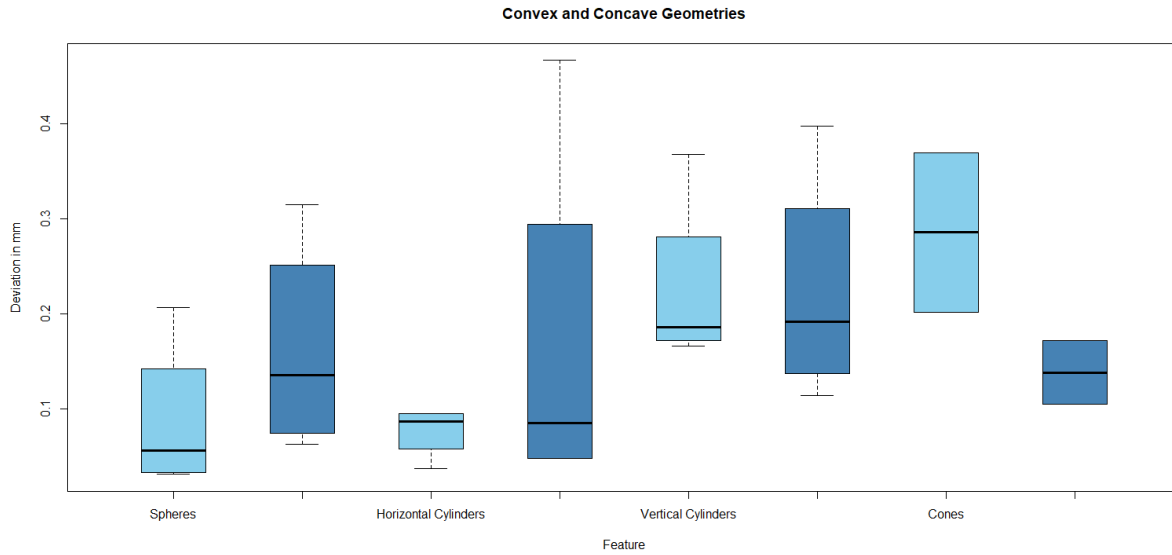


Figure 54. Convex (light blue) and Concave (dark blue) geometries for sample V2-1.

As already noted in Figure 49, the convex spheres 1, 3, 6 and 7 were printed with higher accuracy on sample V2. This result is also confirmed in Figure 54, as the lowest average value of 0.05 mm is registered for the deviation of the convex spheres when compared to the same results for samples V4 (Figure 52) and V6 (Figure 57).

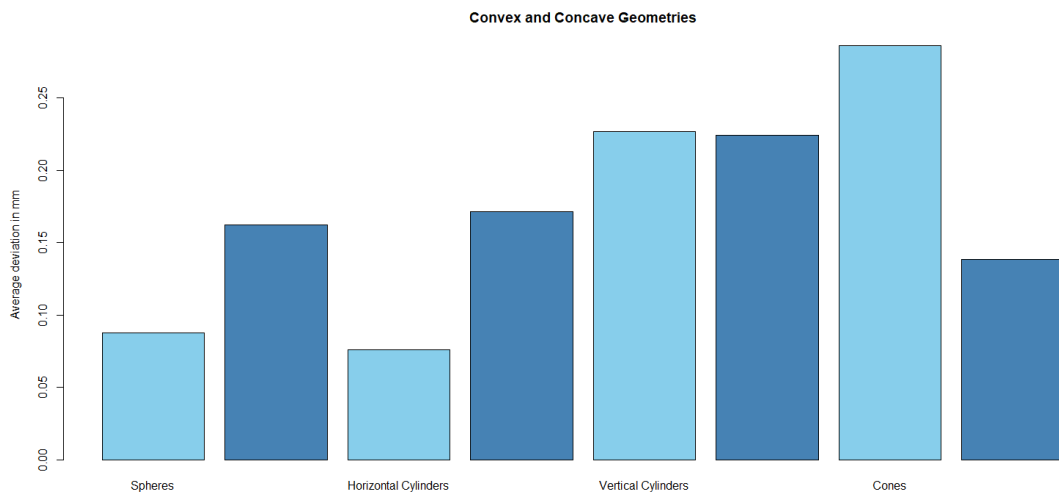


Figure 55. Average deviation of Convex (light blue) and Concave (dark blue) geometries for V2-1

Concave cones 2 and 4, were most accurate on sample V2 with 0.12 mm of average deviation, while the same type of geometry on sample V4 had a deviation of 0.2 mm as seen on Figure 51 and 52.

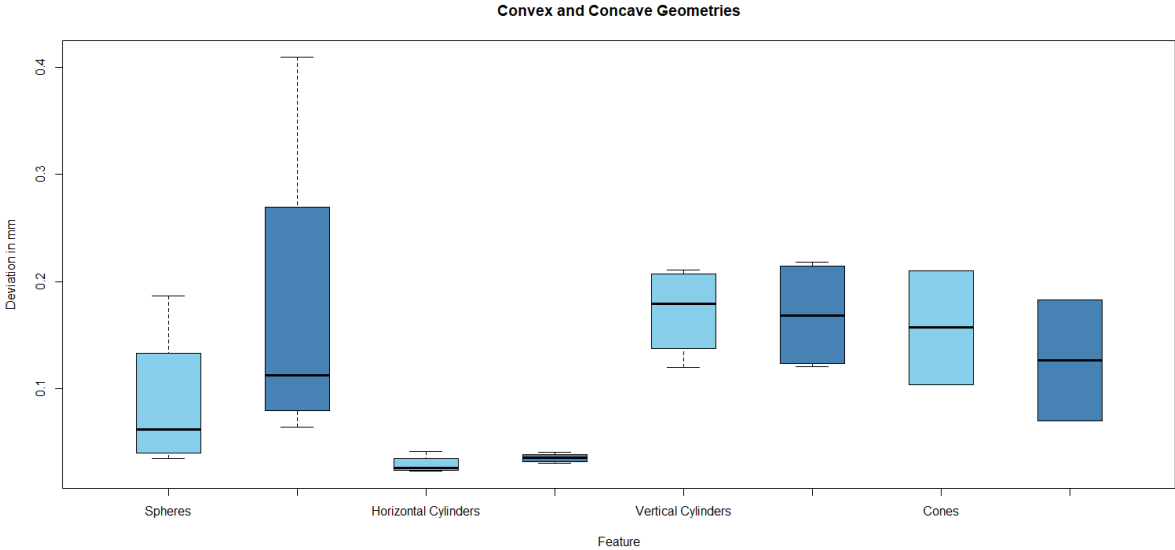


Figure 56. Convex (light blue) and Concave (dark blue) geometries for sample V6-3

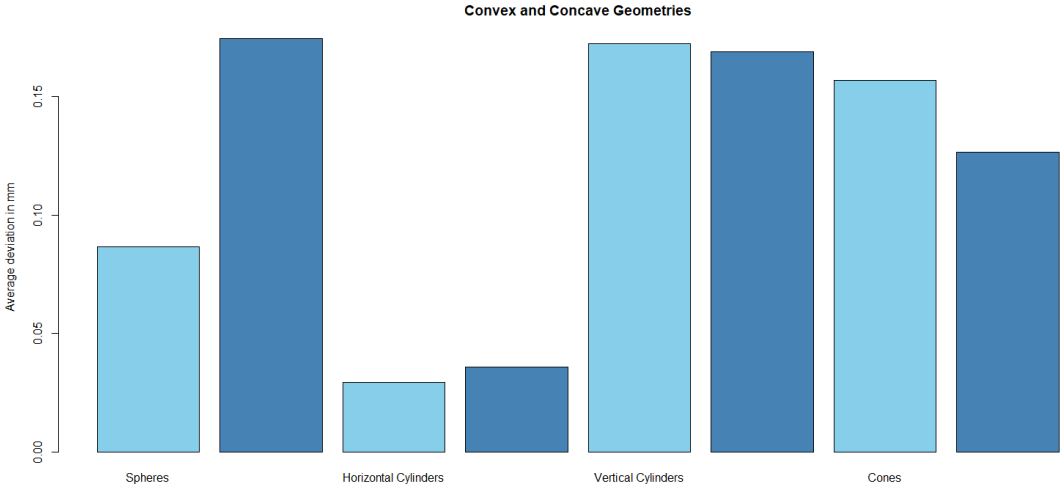


Figure 57. Average deviation of Convex (light blue) and Concave (dark blue) geometries for V6-3

Concave spheres had an average deviation of 0.18 mm on sample V6 (Figure 57), that is the lowest accuracy with respect to the values of 0.08 mm and 0.15 mm for samples V4 (Figures 53) and V2 respectively (Figures 55).

3.2.10 Comparison between vertical samples V1 (bottom) and V7 (middle)

Picking sample V1 as the most representative vertical sample for the bottom of the chamber, it will be compared to sample V7, the vertical sample printed in the middle of the building volume. The first measurement will be considered as the most representative measure of both samples, because as shown in the bar graphs (Figure 11 and Figure 38) it fits in the middle of the three measurements for all the groups of ISO basic sizes. It is very important to remark that the difference is only in the position inside the printer, because they are both printed vertically, V7 in the middle and V1 in the bottom of the printing volume.

By looking at Figure 58 it can be noticed that there is an outlier in the sphere 6 of sample V7. For all the other values, without distinguishing between the convex or concave shape, the sphericity errors for both sample V7 and V1 are very similar, even though sample V1 shows slightly better results.

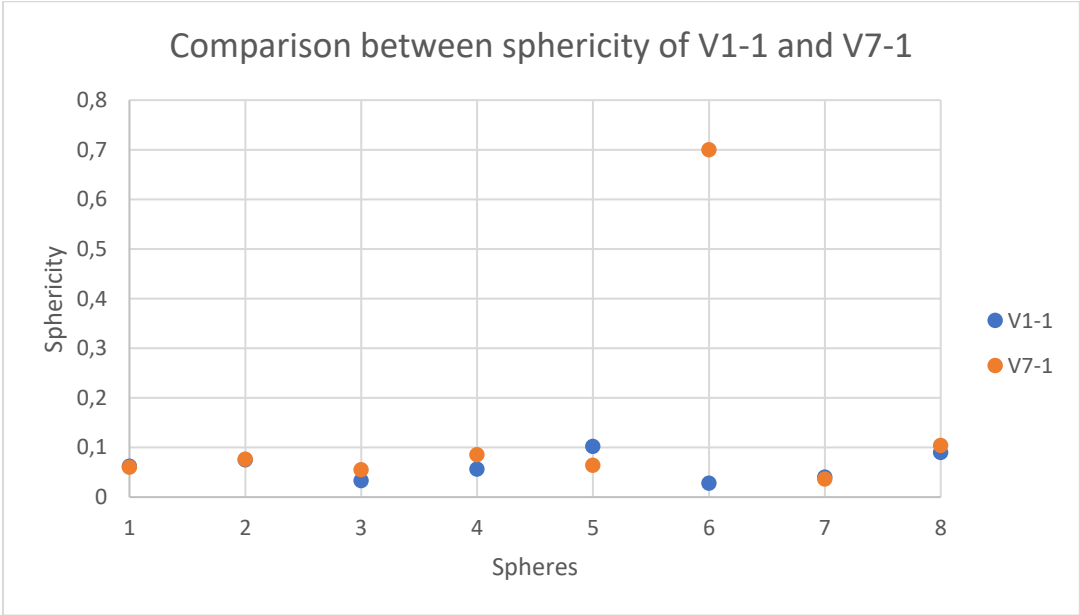


Figure 58. Comparison of sphericity between samples V1 and V7, first measurement for both.

When considering the cylindricity, sample V7 achieves better results mainly for the first 8 cylinder (4 convex and 4 concave). From cylinder 9 on, sample V1 appears slightly better. Once again there's the presence of an outlier on the cylinder 16 (Figure 59), with a value of around 0.6 mm. Thus, considering the cylinders only is better to position the vertical sample in the middle of the build volume, but if the cylinder will be surrounded by other cylinders or geometries, it's better to place the part in the bottom.

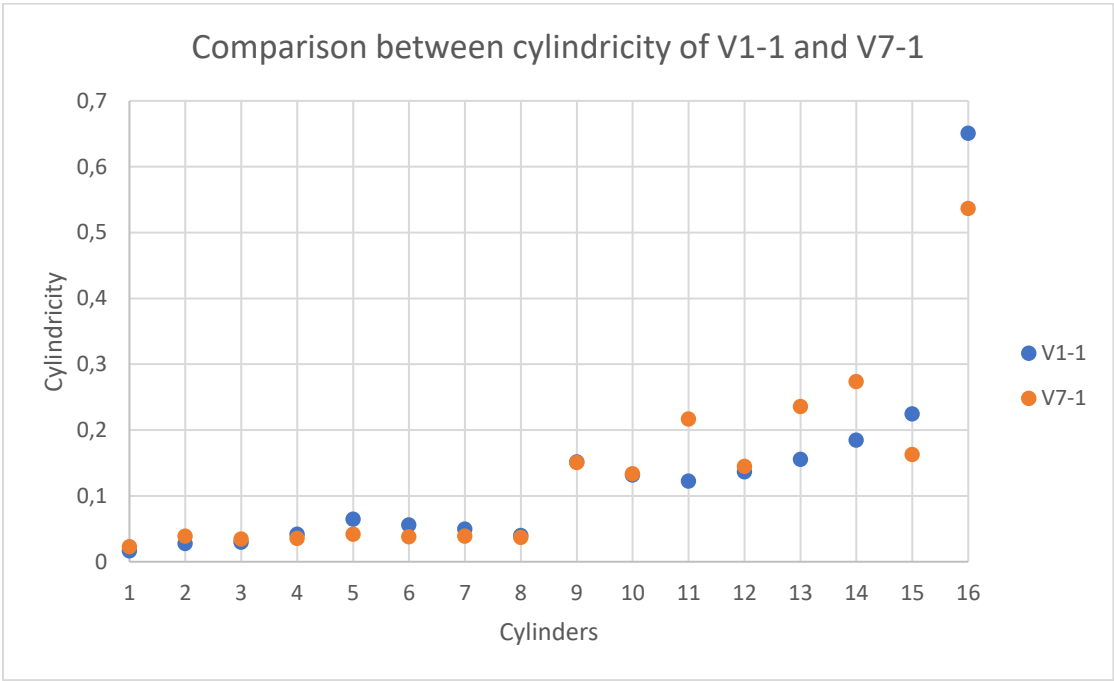


Figure 59. Comparison of cylindricity between samples V1 and V7, first measurement for both.

The bigger concave cone 2 and convex cone 1 (Figure 3) have better conicity on sample V7, while the smallest concave cone 4 and convex cone 3 have lower shape errors on sample V1. However, the values are almost equal in Figure 60, so cones can be printed in both positions with good results. No outliers are present.

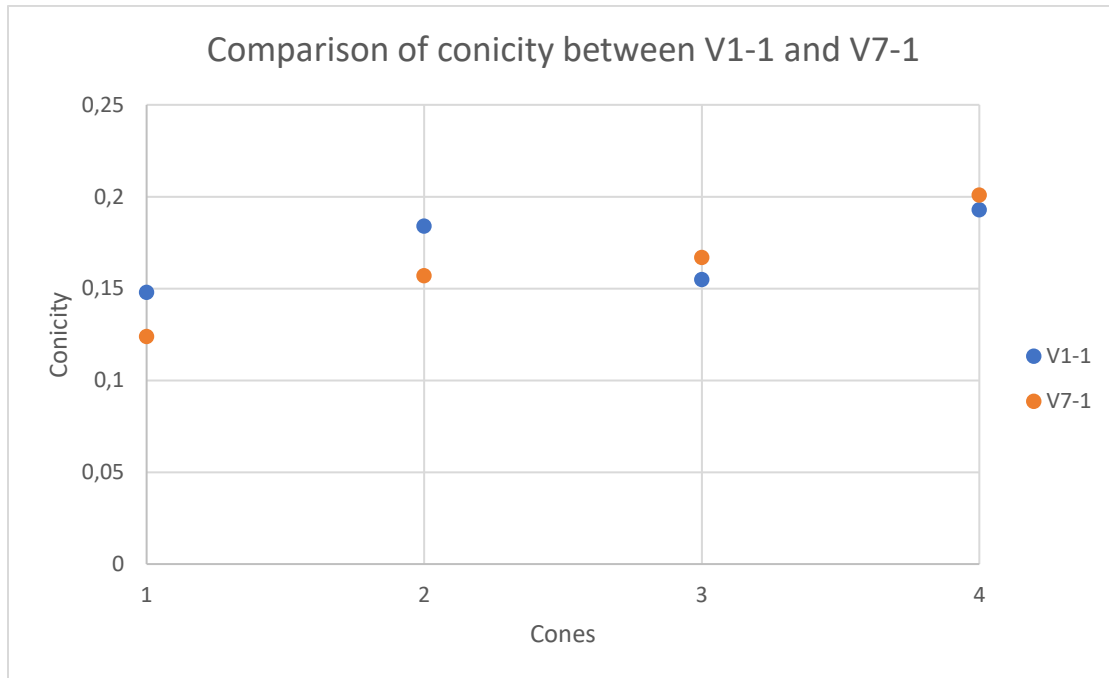


Figure 60. Comparison of conicity between samples V1 and V7, first measurement for all three.

The graphs for V1-1 (Figures 43 and Figure 46) will be compared with the ones for V7-1 (Figures 61 and 62) to assess the validity of the first results.

As noted in Figure 58, it is also observed in Figure 43 and 59 that the convex spheres have lower deviation on sample V1-1 with a maximum of 0.1 mm. The same geometries have a maximum error of 0.7 mm on sample V7-1, due to the presence of the outlier on sphere 6. The same analysis is performed for the average values in Figures 46 and 62. All the concave spheres have an average deviation around 0.05 mm.

As indicated in Figures 59 and 61, horizontal cylinders are very similar in terms of shape accuracy.

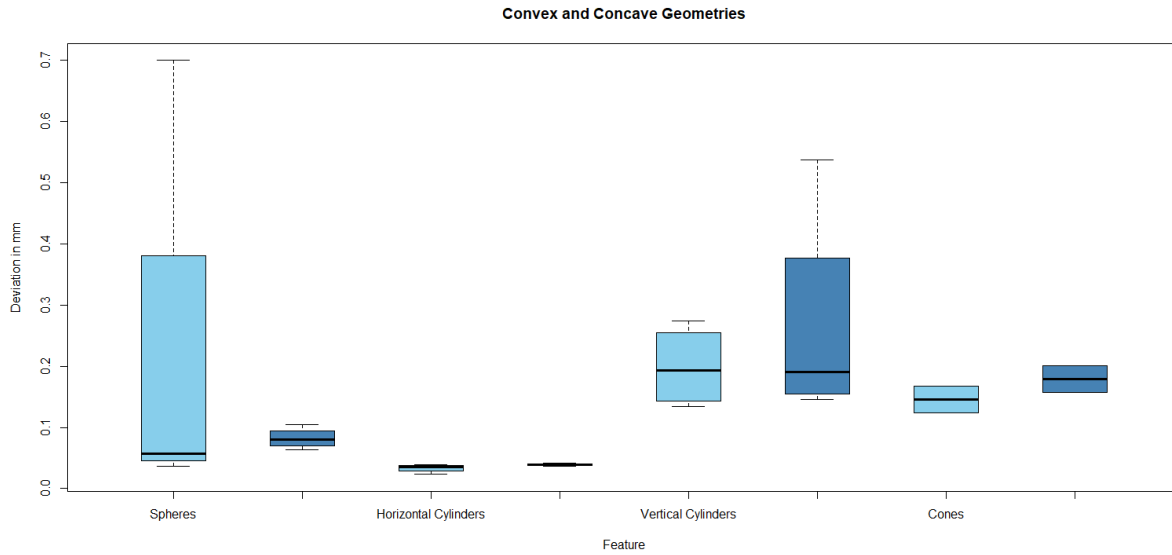


Figure 61. Convex (light blue) and Concave (dark blue) geometries for sample V7-1.

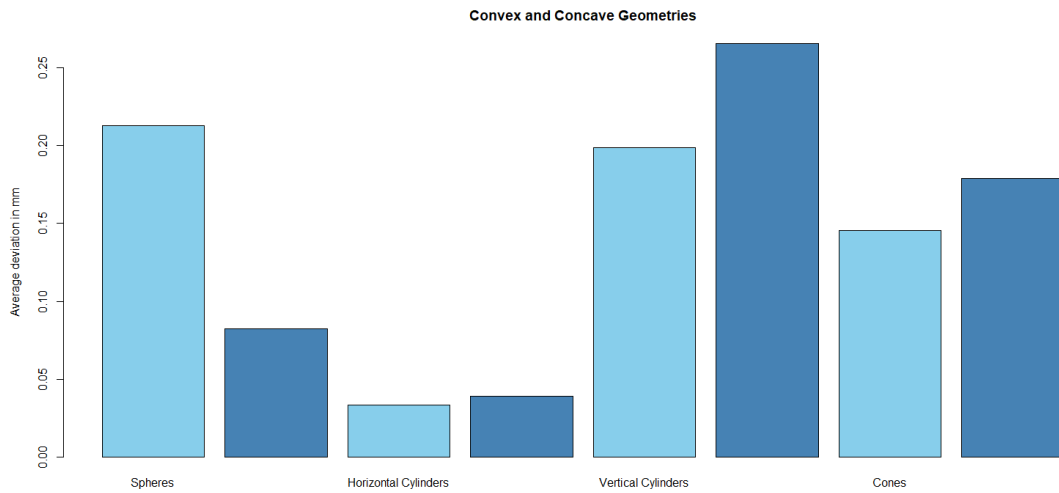


Figure 62. Average deviation of Convex (light blue) and Concave (dark blue) geometries for V7-1

3.3 Comparison between vertical sample V3 (bottom) and horizontal sample O1 (bottom).

In order to know if at the bottom is better for the samples to be positioned vertically or horizontally, comparison is made between sample V3 and sample O1 in terms of sphericity, cylindricity and conicity.

Trying to compare the best possible outcome from Figures 11 and 30, the second replication of the measurement is chosen for sample O1, while the third replication is used for sample V3 because both measurements achieve the best results in terms of the ISO IT grades.

Figure 63 shows that the sample O1 has better sphericity overall, but the two convex spheres 6 and 7 have better sphericity on sample V3. On sphere 8 there is an outlier present only for sample V3. This can be assumed as a problem in the measurement due to the great similarity between both samples in all other cases. In order to achieve better results in terms of sphericity, it can be concluded the sample should be oriented horizontally when located at the bottom. Nevertheless, the difference between the horizontal or vertical orientation of the sample is small, as evidenced in the Figures 66 and 67.

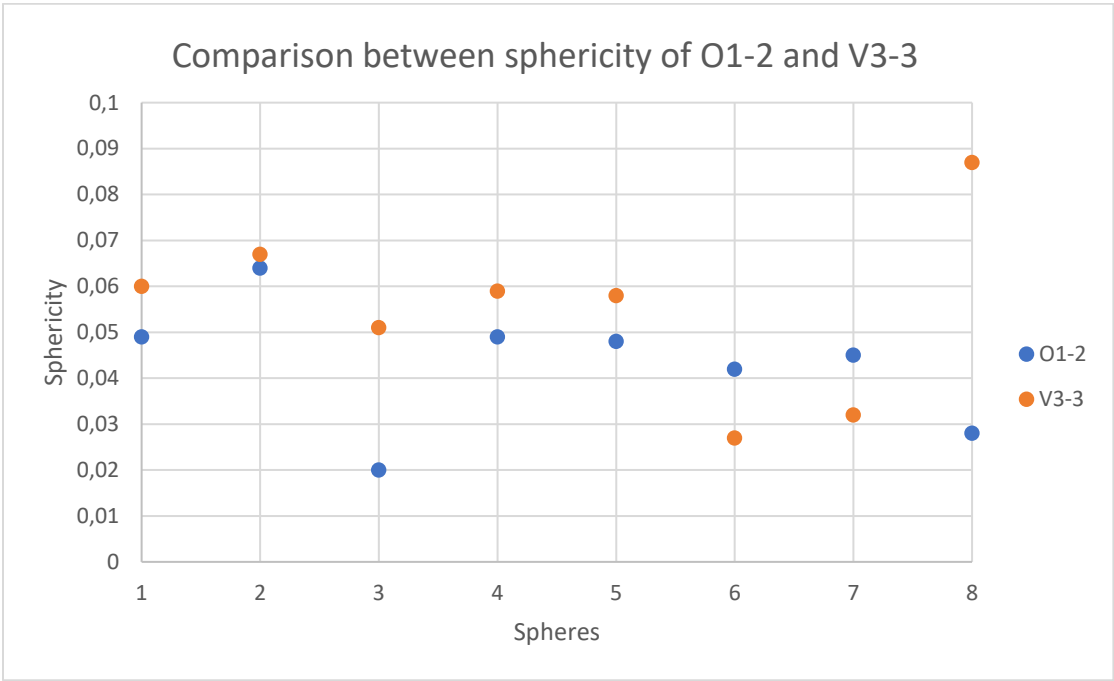


Figure 63. Comparison of sphericity between samples O1 and V3, second and third measurement respectively.

As regards the cylindricity (Figure 64), from cylinder 1 to 8 lower errors are achieved on sample V3, while sample O1 is better for the other cylinders. Convex and concave shapes are represented by cylinders 1 to 4 and by cylinders 5 to 8, respectively. These cylinders are hemicylinders and there is not a big difference in printing them with the horizontal orientation of the sample or the vertical one. Cylinders from 9 to 15 are coaxial geometries. To achieve

higher accuracy, heat concentration for them should be avoided. For this kind of shapes, results show that is better to place the sample horizontally. Convex vertical cylinders are much better on O1-2 than on V3-3, as noted in the Figures 66 and 67.

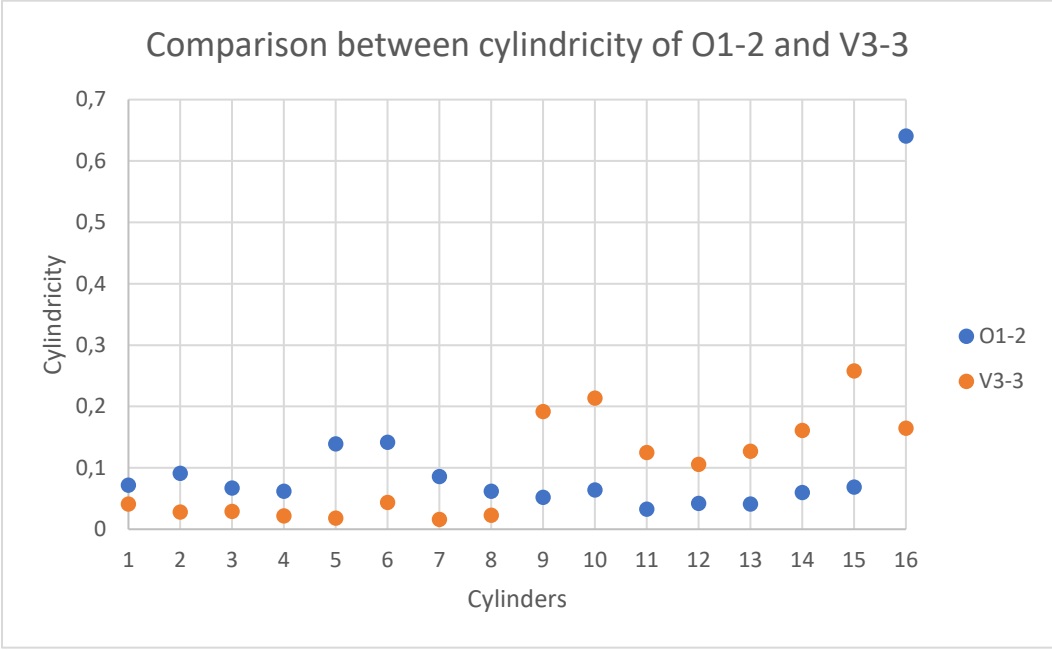


Figure 64. Comparison of cylindricity between samples O1 and V3, second and third measurement respectively.

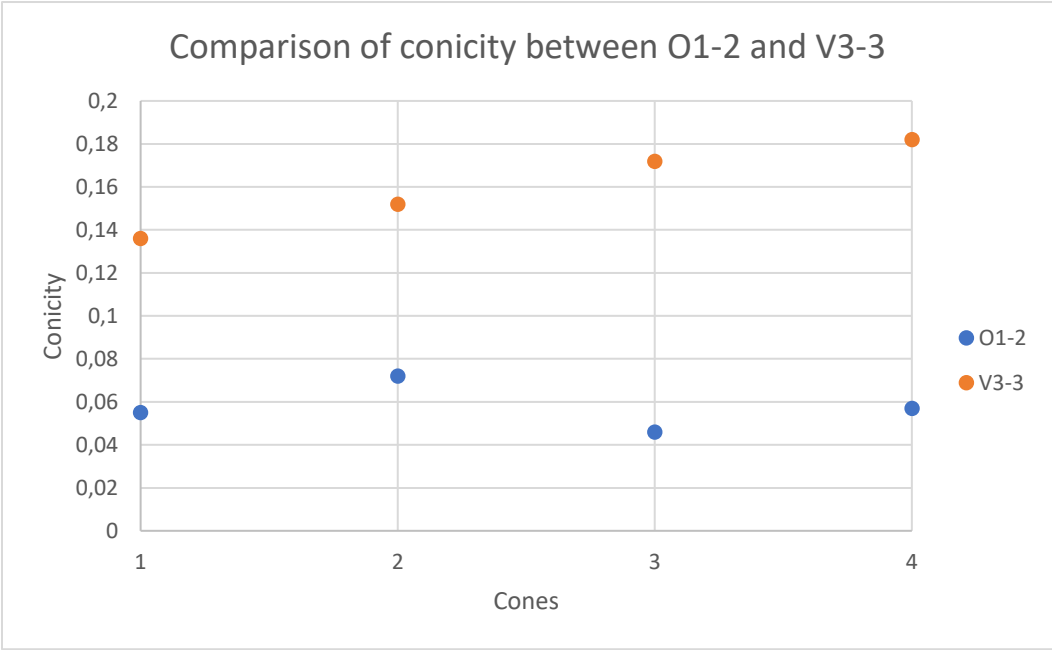


Figure 65. Comparison of conicity between samples O1 and V3, second and third measurement respectively.

Conicity is better when the cone is printed horizontally, with differences of even 0.126 mm with respect to the vertical sample, as observed on Figure 65, no matter if the cone is concave or convex. This is observable as well on Figure 66 and 67.

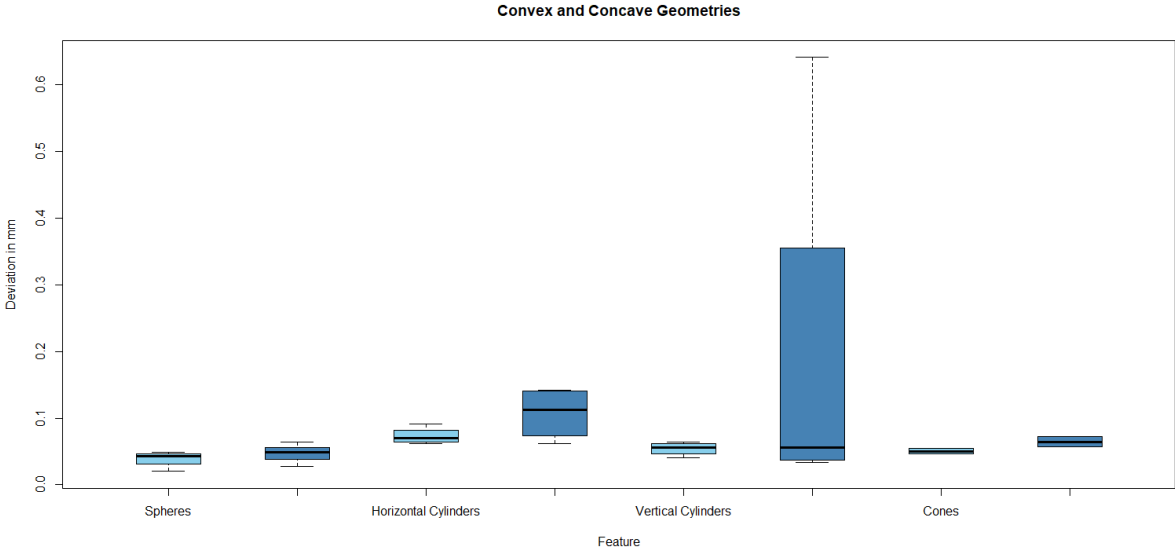


Figure 66. Convex (light blue) and Concave (dark blue) geometries for sample O1-2.

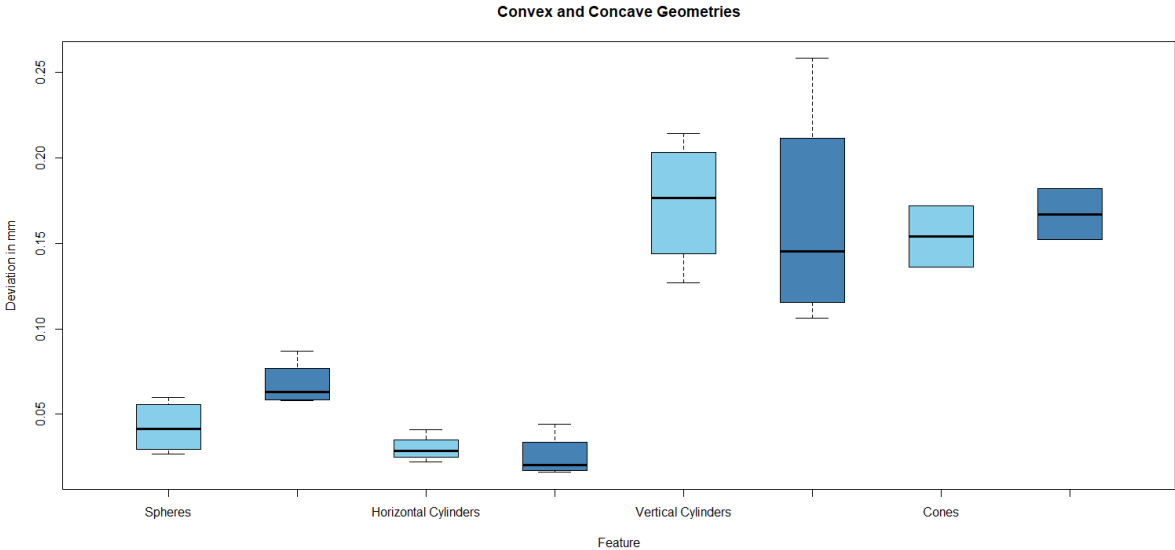


Figure 67. Convex (light blue) and Concave (dark blue) geometries for sample V3-3.

In general (Figure 68), the convex features had a lower deviation in comparison to the concave ones for sample O1-2. For the vertical cylinders the difference is more evident since an average deviation of 0.05 mm is registered for convex cylinders versus 0.20 mm for concave ones. Since the layers are sliced and deposited with respect to the vertical axis of the cylinders, any change in the nature of the part geometry with respect to this axis will result in a staircase effect.

For the sample V3-3 instead, the deviation is high for vertical cylinders and cones no matter their nature, but it's worth noting that the vertical concave ones have a mean deviation of 0.15 mm, that is smaller the previous 0.20 mm for the sample O1-2. Horizontal cylinders both convex and concave are better on V3-3 and the sphericity of the spheres does not depend on the concave or convex shape (Figures 68 and 69).

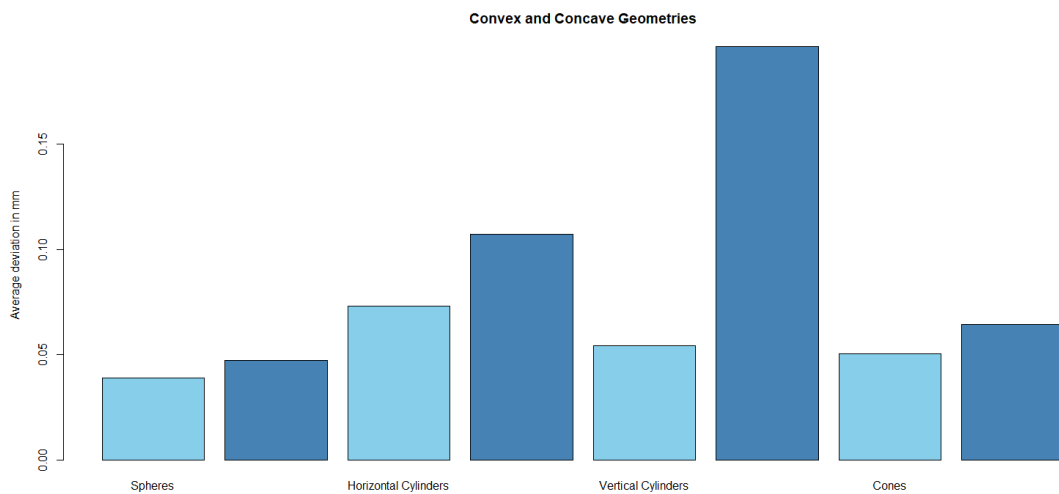


Figure 68. Average deviation of Convex (light blue) and Concave (dark blue) geometries for O1-2.

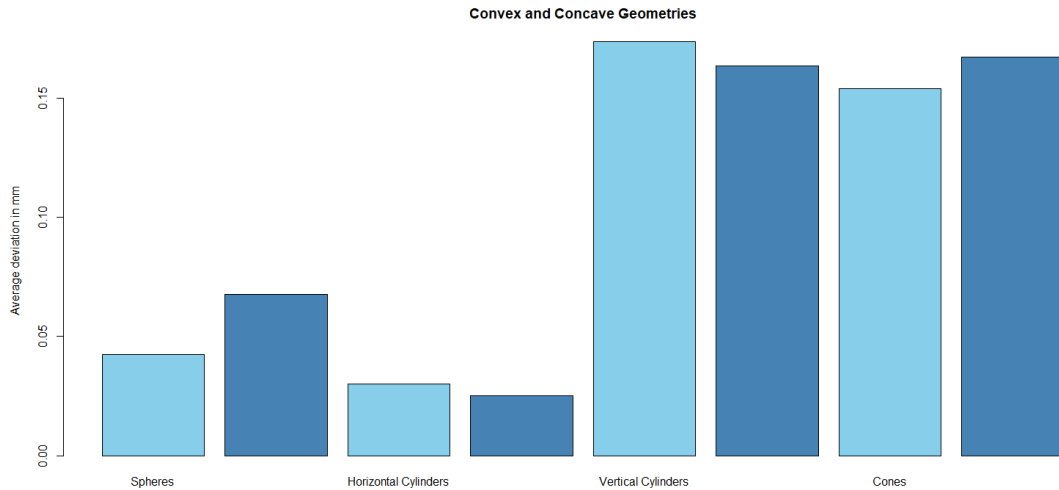


Figure 69. Average deviation of Convex (light blue) and Concave (dark blue) geometries for V3-3.

Now, a set of analyses will be carried out to investigate the distribution of heat, from left to right, and from bottom to top. This study is carried out by comparison of the samples V3 and V5, that are positioned at laterals at the bottom of the build volume. For the top, samples V4 and V6 are considered for their lateral position. Finally, samples V1 and V2 are compared for their frontal position at the bottom and at the top of the build volume respectively.

3.4 Comparison between bottom vertical samples V3 with V5.

Both samples V3 and V5 are located at the bottom of the building volume, and this analysis is aimed at checking if the value of the scaling factor applied for shrinkage compensation by EOS software is correct. According to previous results it seems that value of the factor should not be right, due to the non-homogeneous distribution of heat. Also, thanks to the classification of each feature into different ISO basic sizes, these results will lead to a better understanding of the tolerances with respect to the position of each sample.

ISO Basic sizes	SFERA1	SFERA2	SFERA3	SFERA4	SFERA5	SFERA6	SFERA7	SFERA8
0-3								
3-6							✓	✓
6-10					✓	✓		
10-18			✓	✓				
18-30	✓	✓						
30-50								
50-80								
80-120								
Concavity/Convexity	CX	CV	CX	CV	CV	CX	CX	CV
Deviation on V3-1	0,057	0,065	0,063	0,055	0,063	0,027	0,049	0,103
Deviation on V5-1	0,055	0,089	0,077	0,085	0,063	0,042	0,04	0,094
Absolute difference	0,002	0,024	0,014	0,03	0	0,015	0,009	0,009
Best on	V5	V3	V3	V3	V3-V5	V3	V5	V5

Table 5. Comparison of the characteristics of the spheres on V3-1 and on V5-1.

Table 5 indicates that for ISO basic sizes from 10-18 mm to 18-30 mm, it is better to print the spheres on the lateral side as for sample V3, with a maximum improvement of 0.024 mm. For the ranges smaller than 3-6 mm, the side of sample V5 showed a better accuracy, but with a small difference of 0.009 mm. The accuracy of spheres in the range 6-10 mm was almost equal for both samples.

The dimensional accuracy of the cylinders (table 6) is similar for both samples. For range 18-30, two cylinders out of the four were better on sample V3 and the others on sample V5, even though the smallest difference of 0.001 indicates that V3 was almost the best on all four. When it comes to range 10-18 mm, sample V5 got a lower value of the deviation on three of the four cylinders, while the convex cylinder 13 was better by 0.025mm on sample V3. On range 6-10 mm, the cylinders on sample V3 and sample V5 have similar deviation to their nominal size. As for the spheres, sample V5 is more accurate for the smallest ranges up to 3-6 mm, with a maximum difference of 0.017 mm.

ISO Basic sizes	CIL1	CIL2	CIL3	CIL4	CIL5	CIL6	CIL7	CIL8	CIL9	CIL10	CIL11	CIL12	CIL13	CIL14	CIL15	CIL16
0-3																
3-6				✓				✓	✓							✓
6-10			✓				✓			✓					✓	
10-18		✓				✓					✓		✓			
18-30	✓				✓							✓		✓		
30-50																
50-80																
80-120																
Concavity/Convexity	CX	CX	CX	CX	CV	CV	CV	CV	CV	CV	CV	CV	CX	CX	CX	CX
Horizontal/Vertical	H	H	H	H	H	H	H	H	V	V	V	V	V	V	V	V
Deviation on V3-1	0,05	0,03	0,029	0,023	0,02	0,044	0,021	0,023	0,196	0,21	0,118	0,11	0,131	0,158	0,27	0,62
Deviation on V5-1	0,04	0,02	0,034	0,022	0,04	0,032	0,024	0,038	0,179	0,19	0,117	0,13	0,156	0,157	0,213	0,54
Absolute difference	0,01	0,01	0,005	0,001	0,01	0,012	0,003	0,015	0,017	0,01	0,001	0,02	0,025	0,001	0,057	0,08
Best on	V5	V5	V3	V5	V3	V5	V3	V3	V5	V5	V5	V3	V3	V5	V5	V5

Table 6. Comparison of the characteristics of the cylinders on V3-1 and on V5-1.

3.5 Comparison between lateral vertical samples V4 with V6.

Both samples V4 and V6 are printing at the top of the build volume, so the scale factor is kept constant by the EOS software. Sample V4 achieved the best results for the spheres in all the ranges of ISO basic sizes (table 7). Only the vertical convex sphere number 6 was better on sample V6 by a difference of 0.667 mm, the highest difference present between the spheres in these two samples. However, this can be interpreted as a systematic error on the geometry or of the measurement, because the deviation is much larger than the others. The smaller the range, the higher the difference between the two samples, with 0.32 mm on sphere number 8 belonging to the range 3-6 mm.

ISO Basic sizes	SFERA1	SFERA2	SFERA3	SFERA4	SFERA5	SFERA6	SFERA7	SFERA8
0-3								
3-6							✓	✓
6-10					✓	✓		
10-18			✓	✓				
18-30	✓	✓						
30-50								
50-80								
80-120								
Concavity/Convexity	CX	CV	CX	CV	CV	CX	CX	CV
Deviation on V4-1	0,028	0,054	0,032	0,066	0,094	0,747	0,038	0,089
Deviation on V6-3	0,045	0,064	0,035	0,095	0,13	0,08	0,187	0,409
Absolute difference	0,017	0,01	0,003	0,029	0,036	0,667	0,149	0,32
Best on	V4	V4	V4	V4	V4	V6	V4	V4

Table 7. Comparison of the characteristics of the spheres on V4-1 and on V6-3.

The accuracy of cylinders (table 8) in the range 3-6 mm is similar on both samples, as well as the one for the range 6-10 mm, having small differences between them. In the range 10-18 mm, sample V4 had an average deviation of 0.03 mm. For the biggest range 18-30 mm, again the results for cylinders are similar on both samples, with maximum difference of 0.03 mm.

ISO Basic sizes	CIL1	CIL2	CIL3	CIL4	CIL5	CIL6	CIL7	CIL8	CIL9	CIL10	CIL11	CIL12	CIL13	CIL14	CIL15	CIL16
0-3																
3-6				✓				✓	✓							✓
6-10			✓				✓			✓					✓	
10-18		✓				✓					✓		✓			
18-30	✓				✓							✓		✓		
30-50																
50-80																
80-120																
Concavity/Convexity	CX	CX	CX	CX	CV	CV	CV	CV	CV	CV	CV	CV	CX	CX	CX	CX
Horizontal/Vertical	H	H	H	H	H	H	H	H	V	V	V	V	V	V	V	V
Deviation on V4-1	0,03	0,02	0,034	0,032	0,02	0,027	0,026	0,032	0,196	0,25	0,088	0,15	0,157	0,174	0,21	0,22
Deviation on V6-3	0,02	0,03	0,025	0,042	0,04	0,031	0,037	0,034	0,155	0,21	0,121	0,13	0,12	0,203	0,211	0,218
Absolute difference	0,01	0,01	0,009	0,01	0,02	0,004	0,011	0,002	0,041	0,03	0,033	0,03	0,037	0,029	0,001	0,002
Best on	V6	V4	V6	V4	V4	V4	V4	V4	V6	V6	V4	V6	V6	V4	V4	V6

Table 8. Comparison of the characteristics of the cylinders on V4-1 and on V6-3.

3.6 Comparison between frontal vertical samples V1 with V2

This comparison is carried out to investigate the effect of a different height in the positioning of the parts in the frontal area of the EOS Formiga Velocis machine. Sample V1 is located at the bottom and sample V2 at the top of the build volume, as shown in Figures 7 and 8.

Starting from the biggest range 18-30 mm, spheres (table 9) of sample V1 had a lower deviation of around 0.01 mm. The accuracy of the spheres on sample V1 is again better in the range 10-18 mm, by an average value of 0.022 mm. When analyzing the ranges smaller than 6-10 mm, both samples achieved great accuracy with a very small difference of 0.003 mm in favor of sample V3. For the smaller range 3-6 mm, sample V1 is more accurate with a minimum difference of 0.005 mm. Without distinguishing between convex and concave shapes, the spheres of sample V1 have better accuracy.

ISO Basic sizes	SFERA1	SFERA2	SFERA3	SFERA4	SFERA5	SFERA6	SFERA7	SFERA8
0-3								
3-6							✓	✓
6-10					✓	✓		
10-18			✓	✓				
18-30	✓	✓						
30-50								
50-80								
80-120								
Concavity/Convexity	CX	CV	CX	CV	CV	CX	CX	CV
Deviation on V1-1	0,062	0,075	0,033	0,056	0,102	0,028	0,04	0,09
Deviation on V2-1	0,077	0,085	0,207	0,315	0,063	0,031	0,035	0,187
Absolute difference	0,015	0,01	0,174	0,259	0,039	0,003	0,005	0,097
Best on	V1	V1	V1	V1	V2	V1	V2	V1

Table 9. Comparison of the characteristics of the spheres on V1-1 and on V2-1.

As regards the cylinders (table 10), in the range 3-6 mm, there is a small preference for sample V2 that has a lower average deviation of 0.12 mm with respect to sample V1. Instead, for the range 6-10 mm, sample V1 has a better accuracy with an average deviation of 0.11 mm. In the range 10-18 mm, the cylinders of sample V1 are more accurate and the highest difference with the cylinders of sample V2 is 0.212 mm. In the biggest range 18-30 mm, the cylinders of sample V1 are again more accurate than those of sample V2 with a maximum difference of 0.4 mm.

ISO Basic sizes	CIL1	CIL2	CIL3	CIL4	CIL5	CIL6	CIL7	CIL8	CIL9	CIL10	CIL11	CIL12	CIL13	CIL14	CIL15	CIL16
0-3																
3-6				✓				✓	✓							✓
6-10			✓				✓			✓					✓	
10-18		✓				✓					✓		✓			
18-30	✓				✓							✓		✓		
30-50																
50-80																
80-120																
Concavity/Convexity	CX	CX	CX	CX	CV	CV	CV	CV	CV	CV	CV	CV	CX	CX	CX	CX
Horizontal/Vertical	H	H	H	H	H	H	H	H	V	V	V	V	V	V	V	V
Deviation on V1-1	0,02	0,03	0,03	0,042	0,06	0,056	0,05	0,04	0,152	0,13	0,123	0,14	0,156	0,185	0,225	0,651
Deviation on V2-1	0,09	0,09	0,078	0,037	0,47	0,122	0,048	0,048	0,178	0,17	0,16	0,11	0,368	0,194	0,398	0,224
Absolute difference	0,08	0,07	0,048	0,005	0,4	0,066	0,002	0,008	0,026	0,03	0,037	0,02	0,212	0,009	0,173	0,427
Best on	V1	V1	V1	V2	V1	V1	V2	V1	V1	V1	V1	V2	V1	V1	V1	V2

Table 10. Comparison of the characteristics of the cylinders on V411 and on V2-1.

3.7 Quality of the surface in terms of visible defects

Even when samples V2, V4 and V6 gave very competitive results with all the bottom samples, it's important to also consider that the measurements were done using a CMM machine and a touch probe. The probe tip gets in contact with the specimen surface at fixed points. If a superficial defect is present at that position, it might induce a systematic error in the measurement. If a defect is located in another area of the same geometry of the sample, measurements results will not be affected. A visual inspection is applied to the part surfaces for identifying differences in the superficial or aesthetical quality of the specimens (Figures from 70 to 73).



Figure 70. Sample V3

Sample V3 (figure 70) does not show any specific visible error or defect. All the edges are in line, the geometries look smooth and the holes allow to look inside them as they appear

empty from unsintered powder. This is common for of all the other samples (V1, V5, O2 and V7) printed at the bottom and in the middle of the Formiga volume. Also sample O3, that is positioned in the upper part of the build volume, looks fine.

As shown in figure 71, sample V2 shows many imperfections in three of the four sets of quarters of spheres, in the sets of tilted planes (PL_ANG22 until PL_ANG26), in the cone formed by CON1 and CON2, and on the base. All the errors are present starting from a distance of 25 mm from the upper edge (where the hexagon is present).



Figure 71. Sample V2

The visible errors of sample V4 are less pronounced, figure 72 shows some lines not completed with the correct amount of powder, being the most noticeable the ones on the hexagon. All the other geometries look smooth.

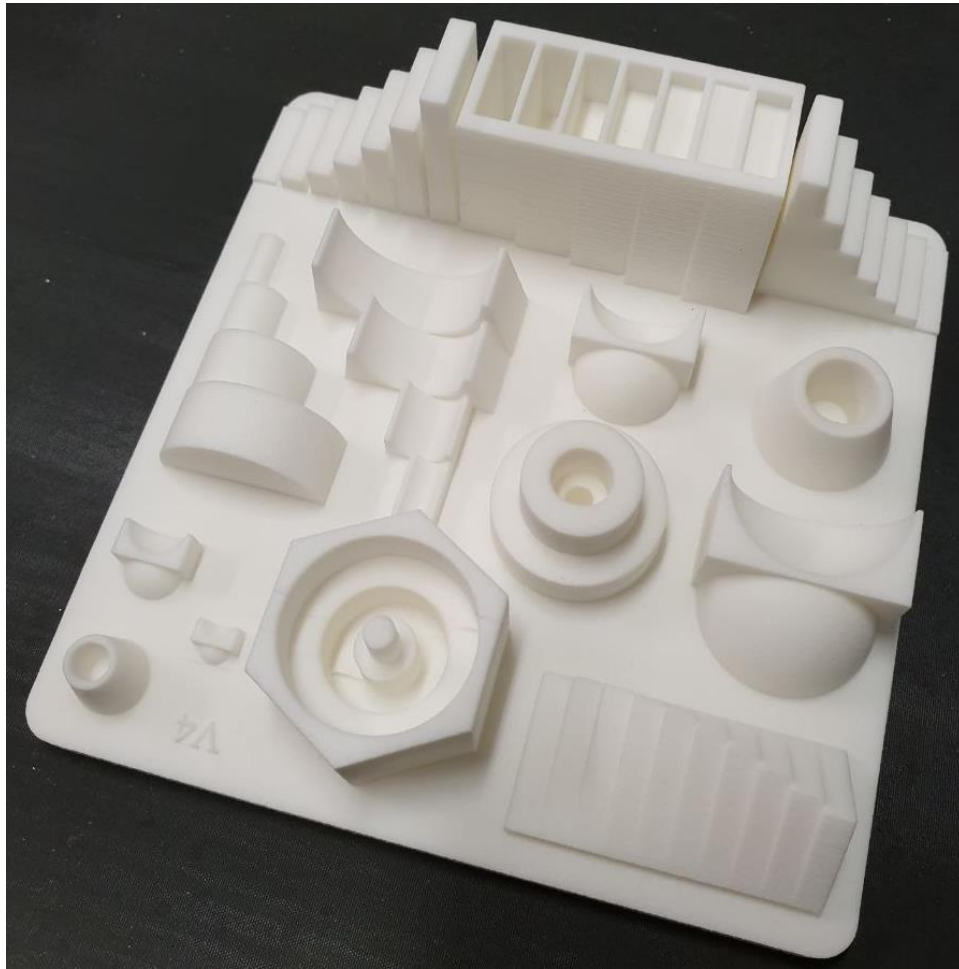


Figure 72. Sample V4

Sample V6 (figure 73), shows complete smoothness on all the geometries, base included, but there is a huge problem on the whole edge. There was a problem with the condenser of the printer while the sample was being produced, so it can't be affirmed that the error is entirely due to the heat, the laser or any specific parameter in general.



Figure 73. Sample V6

Chapter 4

Conclusions

Selective laser sintering, as a 3D printing technique, showed great accuracy and good surface finish (visually) in almost all the samples, as K. Liua and others [32] already suggested in the literature.

It can be observed that the samples of the reference part, which were printed in the vertical direction, showed a lower accuracy when it comes to sphericity and cylindricity. This is because of the stair case effect, but also to the weight of the powder which thanks to gravity, lays in the bottom part of the cylinder or sphere, doing a higher “pressure” than it does in the upper portion of the geometry, because of the fast change from granular to solid state during sintering. In the horizontal samples, the weight is distributed equally alongside the whole part, because the main axis of the geometries is not positioned against gravity. Therefore, the dimensions of the reference part features are closer to the nominal designed value. This statement is also supported by J. Connor et al [33] in the literature.

When it comes to cones, the accuracy is much similar between the samples no matter their position, but they appear to be more accurate when printed horizontally.

When it comes to printing a part with many spheres, the best positioning would be the one used for sample V3, for cylinders the one used for sample V5. The positioning at the top of the build volume should be avoided, because of the low quality it provides.

If the part geometry is mainly composed by spheres and cylinders together, the best placement within the build volume of the Formiga machine is the one of sample O1. For a part with predominant conical shapes, the position of sample O3 should be preferred.

A future research activity to be undertaken could be the use of process simulation to account for the heat distribution in the thermal household of the building volume of the Formiga Velocis P110. The simulation results could be employed to identify possible powder

entrapment or partial powder sintering depending on the geometry and heat distribution. Also, a great way to measure the tolerances could be applying the same benchmarking procedure to pieces with the three types of fit: clearance, transition and interference.

References

- [1] Hofmann DC, Roberts S, Otis R, Kolodziejska J, Dillon RP, Suh J, Shapiro AA, Liu Z, Borgonia J. “Developing gradient metal alloys through radial deposition additive manufacturing”. Scientific Reports 5357; 2014.
- [2] Gibson I, Brent S. (2010). “Additive manufacturing technologies rapid prototyping to direct digital manufacturing”. 1st edition. Springer, New York.
- [3] Calignano F, Manfredi D, Ambrosio E, Biamino S, Lombardi M, Atzeni E, Salmi A, Minetola P, Iuliano L, and Fino P. (2016). “Overview on Additive Manufacturing Technologies”. Digital Object Identifier: 10.1109/JPROC.2016.2625098. PP 1.
- [4] Research group of the Loughborough University. (2019). About Additive Manufacturing, Binder Jetting. Available online on: <https://www.lboro.ac.uk/research/amrg/about/the7categoriesofadditivemanufacturing/binderjetting/>
- [5] Bournias A. (2019). “Introduction to Binder Jetting 3D printing”. 3D Hubs. Available online on: <https://www.3dhubs.com/knowledge-base/introduction-binder-jetting-3d-printing/>
- [6] Ashish M, Vinogradov A. (2015). “Directed Energy Deposition”. Power Ultrasonics. Available online on: <https://www.sciencedirect.com/topics/materials-science/directed-energy-deposition/pdf>
- [7] 3D Natives (2019). “The Complete Guide to Directed Energy Deposition (DED) in 3D Printing”. Available online on: <https://www.3dnatives.com/en/directed-energy-deposition-ded-3d-printing-guide-100920194/>
- [8] Research group of the Loughborough University. (2019). “About Additive Manufacturing, Directed Energy Deposition”. Available online on: <https://www.lboro.ac.uk/research/amrg/about/the7categoriesofadditivemanufacturing/directedenergydeposition/>
- [9] Saboori A, Aversa A, Marchese G, Fino P, Biamino S, Lombardi M. (2019). “Application of Directed Energy Deposition-Based Additive Manufacturing in Repair”. Applied Sciences 9(16):3316 DOI: 10.3390/app9163316. PP 1.

- [10] Research group of the Loughborough University. (2019). “About Additive Manufacturing, Material Extrusion”. Available online on: <https://www.lboro.ac.uk/research/amrg/about/the7categoriesofadditivemanufacturing/material-extrusion/>
- [11] (2017). “Material Extrusion. Engineering product design”. Available online on: <https://engineeringproductdesign.com/knowledge-base/material-extrusion/>
- [12] Redwood B. (2019). “Additive Manufacturing Technologies: An Overview”. 3D Hubs. Available online on: <https://www.3dhubs.com/knowledge-base/additive-manufacturing-technologies-overview/#material-extrusion>
- [13] Bournias A. (2019). “Introduction to Material Jetting 3D printing”. 3D Hubs. Available online on: <https://www.3dhubs.com/knowledge-base/introduction-material-jetting-3d-printing/#pros-cons>
- [14] Additively AG (2018). “Material Jetting”. Available online on: <https://www.additively.com/en/learn-about/material-jetting>
- [15] Tuan D, Ngoa T, Kashania A, Imbalzano G, Nguyena K, Huib D. (2018). “Additive manufacturing (3D printing): A review of materials, methods, applications and challenges”. PP 277. Composites Part B 143 (2018) 172–196.
- [16] Research group of the Loughborough University. (2019). “About Additive Manufacturing, Sheet Lamination”. Available online on: <https://www.lboro.ac.uk/research/amrg/about/the7categoriesofadditivemanufacturing/sheetlamination/>
- [17] Dassault Systèmes (2019). “3D Experience Marketplace. 3D Printing Additive. Photopolymerization- VAT, SLA, DLP, CDLP”. Available online on: <https://make.3dexperience.3ds.com/processes/photopolymerization>
- [18] Gu, D.D.; Meiners, W.; Wissenbach, K.; Poprawe, R. “Laser additive manufacturing of metallic components: materials, processes and mechanisms”. Int. Mater. Rev. 2012, 57, 133–164.
- [19] S. Sun, M. Brandt, M. Easton. (2017). “Powder bed fusion processes: an overview 2”. RMIT University, Centre for Additive Manufacturing, Melbourne, VIC, Australia. Pp 1-4

- [20] Amado A, Schmid M, Levy G, Wegener K. (2011). “Advances in SLS powder characterization”. In: 22nd Annu. Int. Solid Free. Fabr. Symp. University of Texas at Austin, Austin, pp 438–452.
- [21] R.Singh, S.Singh and M.S.J.Hashmi. (2016). “Implant Materials and Their Processing Technologies”. At Reference Module in Materials Science and Materials Engineering. Pp 13-14.
- [22] M.Schmida, A. Amadoa and K. Wegenerb, “Polymer Powders for Selective Laser Sintering (SLS)”, AIP Conference Proceeding, 2011.
- [23] J. Williamsa , A. Adewunmib , R. Scheka,c, C. Flanagan , P. Krebsbacha,c, S. Feinbergd, S. Hollistera, S. Dasb,, “Bone tissue engineering using polycaprolactone scaffolds fabricated via selective laser sintering”, Journal of Biomaterials, 26(23), 2004.
- [24] K.R. Bakshi, A. V. Mulay. “A Review on Selective Laser Sintering: A Rapid Prototyping Technology”. Department of Production and Industrial Engineering, College of Engineering, Pune, India. IOSR Journal of Mechanical & Civil Engineering (2016), e-ISSN: 2278-1684, p-ISSN: 2320-334X, PP 53-57.
- [25] M. Saffarzadeh, G. Gillispie and P. Brown. “Selective laser sintering (SLS) rapid prototyping technology: a review of medical applications”, Harvard Medical School (2016).
- [26] Minetola P., Calignano F. and Galati M. “Comparison of international tolerance grades of AM systems for polymers”. Politecnico di Torino, Dept. Management and Production Engineering (DIGEP).
- [27] N. Raghunath, Pulak M. Pandey. “Improving accuracy through shrinkage modelling by using Taguchi method in selective laser sintering”. International Journal of Machine Tools & Manufacture 47 (2007) 985–995.
- [28] URENIO Research Unit. (2001). “Cost, Benefit, Analysis: Technology Benchmarking. Technology evaluation”. Available online on: <https://www.urenio.org/newventurertools/cba/methodology1.html>
- [29] J.-P. Kruth, B. Vandenbroucke, J. Van Vaerenbergh, P. Mercelis. (2015). “Benchmarking of different SLS/SLM processes as rapid manufacturing techniques”. Division PMA, Department of Mechanical Engineering, Katholieke Universiteit Leuven, Belgium.

[30] ISO 286-1:1988 - ISO system of limits and fits - Part 1: Basis of tolerances, deviations and fit. 1988: International Organization for Standardization (ISO).

[31] Minetola P., Iuliano L. and Marchiandi G. “Benchmarking of FDM machines through part quality using IT grades”. 48th CIRP Conference on MANUFACTURING SYSTEMS - CIRP CMS 2015. Procedia CIRP 41 (2016) 1027 – 1032.

[32] K. Liua, Y. Shia, C.i Lia, LiangHaob, J. Liua, Q. Weia, “Indirect selective laser sintering of epoxy resin-Al₂O₃ ceramic powders combined with cold isostatic pressing”, Journal of Ceramics International, 40, 2014.

[33] Connor J, Punch J, Jeffers N and Stafford J. (2019). “A dimensional comparison between embedded 3D-printed and silicon microchannels”. Phys.: Conf. Ser. 525 012009.